University of Washington
Department of Civil and Environmental Engineering

UNDERSTANDING THE HYDROLOGIC EFFECTS OF FROZEN SOIL

Keith Aric Cherkauer

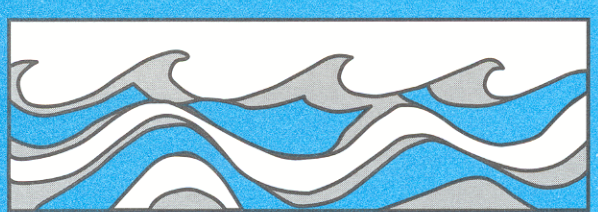

Water Resources Series
Technical Report No. 167
April 2001

Seattle, Washington
98195

Department of Civil Engineering
University of Washington
Seattle, Washington 98195

UNDERSTANDING THE HYDROLOGIC EFFECTS OF FROZEN SOIL

Keith Aric Cherkauer

Water Resources Series
Technical Report No. 167

September 2001

Abstract

Frozen soil plays an important role in the hydrologic cycle of cold regions by increasing the amount of moisture retained in the soil column through the winter and decreasing the infiltration rate of the soil during spring melt. This study investigates how the spatial distribution of snow and frozen soil influence the hydrologic response of a catchment. A field observation program was conducted over three winters (1997-1998, 1998-1999 and 1999-2000) in southeastern Minnesota. Observations of snow depth and soil temperatures were used to identify statistical distributions that can be used to represent their spatial distributions. The statistical distributions of snow and soil temperature were used to represent sub-grid variability of snow and frost within grid cells of the variable infiltration capacity (VIC) macroscale hydrologic model. The influence of the spatial distributions are secondary to the effects of the snow and soil frost algorithms, but they improve the representation of the observed processes. Partial snow cover increases the exchange of sensible heat with the atmosphere during the spring, and the advection of sensible heat from bare to snow covered patches increases the rate of spring melt. The spatial distribution of soil ice increases winter and spring infiltration and soil moisture drainage, while maintaining the increased peak flow response caused by the presence of significantly frozen soil. Discharge records from gauged catchments in the upper Mississippi River basin were used to identify the statistical significance of observed (*e.g.* vegetation type and precipitation) and simulated (*e.g.* soil moisture and snow cover) catchment characteristics on spring runoff response. Ice content was determined to be a significant predictor of both the runoff ratio and peak flow response, indicating that frozen soil plays an important role in spring runoff response in the upper Mississippi basin.

TABLE OF CONTENTS

LIST OF FIGURES

LIST OF TABLES

NOMENCLATURE

α_0	regression intercept
α_i	ith coefficient for regression model
β_i	ith predictor variable for regression model
ΔCC	change in cold content ($W\ m^{-2}$)
ΔH_s	change in energy storage in the surface sir layer ($W\ m^{-2}$)
κ	soil thermal conductivity ($W\ m^{-1}\ K^{-1}$)
ψ_e	air entry potential (m)
ρ_i	density of ice ($kg\ m^{-3}$)
ρ_l	density of liquid water ($kg\ m^{-3}$)
ρ_v	density of water vapor ($kg\ m^{-3}$)
ρ_w	density of liquid water ($kg\ m^{-3}$)
$\rho_w L_e E$	latent heat flux ($W\ m^{-2}$)
θ_i	ice content ($m^3\ m^{-3}$)
$AREA$	gauged area (km^2)
B	baseflow ($mm/(time\ step)$)
B_p	pore-size distribution
C_s	volumetric heat capacity ($J\ m^{-3}\ K^{-1}$)
c_l	specific heat of liquid water ($J\ kg^{-1}\ C^{-1}$)
$DENS$	snow density ($kg\ m^{-3}$)
E	evaporation (mm)
F_s	fraction of the snow-free area that is advected
G	ground heat flux ($W\ m^{-2}$)
G_b	ground heat flux over bare ground ($W\ m^{-2}$)
G_s	ground heat flux over snow ($W\ m^{-2}$)

g	acceleration due to gravity ($m\ s^{-2}$)
H	sensible heat flux ($W\ m^{-2}$)
H_A	advected sensible heat flux ($W\ m^{-2}$)
H_b	sensible heat flux over bare ground ($W\ m^{-2}$)
H_s	sensible heat flux over snow ($W\ m^{-2}$)
ICE	ice content (mm)
i	amount of infiltration (mm)
L_b	latent heat flux over bare ground ($W\ m^{-2}$)
L_e	latent heat of vaporization ($J\ kg^{-1}$)
L_f	latent heat of fusion ($J\ kg^{-1}$)
L_s	latent heat flux over snow ($W\ m^{-2}$)
MAP	mean annual precipitation (mm)
ME	energy available to melt snow ($W\ m^{-2}$)
$OVER$	overstory fraction (fract)
P_s	partial snow cover
PFR	peak flow response (mm)
PMR	peak melt rate (mm/day)
$PREC$	cumulative precipitation (mm)
$Q_{i(i+1)}$	soil moisture drainage from layer i to layer $i+1$ (mm)
q_l	liquid water flux ($kg\ m^{-2}\ s$)
q_v	water vapor flux ($kg\ m^{-2}\ s$)
R	runoff ($mm/(time\ step)$)
R	regression response variable
R_n	net radiation ($W\ m{-}2$)
R_{nb}	net radiation over bare ground ($W\ m^{-2}$)
R_{ns}	net radiation over snow ($W\ m^{-2}$)
$R_{unshielded}$	correction factor for unshielded precipitation gauge
ROR	runoff ratio response (mm/mm)

S	a source/sink term
$\overline{SD}$	mean snow depth
SD_{min}	minimum snow depth for full snow coverage (m)
SD_s	slope of the uniform distribution used to describe partial snow
$SILT$	percent silt content (%)
T	temperature (^oC)
t	time (s)
W_i	soil moisture for layer i (mm)
W_i^c	maximum water content of layer i (mm)
Ws	wind speed ($m\ s^{-1}$)
z	depth (m)

LIST OF ABBREVIATIONS

DAAC	Distributed Active Archive Center
DEM	Digital Elevation Map
EOSDIS	Earth Observing System Data and Information System
GCIP	GEWEX Continental Scale - International Project
GCM	General Circulation Models
GEWEX	Global Energy and Water Balance Experiment
NCAR	National Center for Atmospheric Research
NCDC	National Climatic Data Center
NCEP	National Centers for Environmental Protection
NOAA	National Oceanic and Atmospheric Administration
NSIDC	National Snow and Ice Data Center
SAST	Scientific Assessment and Strategy Team
SWQ	Snow water equivalent
USGS	United States Geological Survey
VIC	Variable Infiltration Capacity

ACKNOWLEDGMENTS

The research described in this report is based on the Ph.D. dissertation of the author, funding for which was provided by the Joint Institute for the Study of Atmosphere and Ocean at the University of Washington, funded under NOAA Cooperative Agreement Number NA67RJ0155, and by NOAA Grant No. NA56GP0198 under the GEWEX Continental-scale International Program (GCIP). Field data discussed in Chapter 3 and used to develop the spatial algorithms in Chapter 4 was collected from the University of Minnesota's Rosemount Agricultural Experiment Station with permission and assistance from Dr. John M. Baker and his staff, including William Breiter and Egbert Spaans. Their help is gratefully acknowledged.

Chapter 1

INTRODUCTION

Frozen soil plays an important role in the hydrologic cycle of cold regions but has been largely ignored in large-scale modeling efforts until recently. Soil freezing affects both the thermal and moisture fluxes of the soil-water system. Ice in the soil increases its thermal conductivity, reduces its volumetric heat capacity, and requires a large influx of thermal energy for transformation to the liquid phase. These effects combine to dampen changes in the soil temperature, strengthening temperature gradients between the ground surface and the atmosphere. Frost contributes to the desiccation of the surface soil layer, while ice in the soil column reduces the soil moisture available for drainage to streams and rivers after thaw. In fine-textured soils, liquid water migrates towards the freezing front, forming ice lenses which displace the surrounding soil [*Marshall et al.*, 1996]. Soils with a high ice content, whether or not there are ice lenses present, have reduced infiltration rates. During melt events, water is forced either to pond on top of the frozen soil, delaying infiltration, or to run off as surface flow, decreasing the response time and increasing peak flows.

The extent and penetration of soil frost is highly dependent on the timing and thickness of the overlying snow cover. Snow acts as an insulator keeping the soil surface warmer and reducing the depth of soil frost formation. If snow accumulates late in the season after an extended period of freezing temperatures, significant freezing may have already occurred, which retards melting of the snow cover. However, if snow accumulation occurs early it will prevent deep frost.

Soil frost also changes the interaction of surface energy fluxes with the atmosphere. In summer, the daily ground surface temperature in vegetated regions is very strongly tied to the diurnal cycle of the near surface air temperature. This relationship is even closer when

the soil is moisture-stressed. Because of this coupling, sensible heat is a minor component of the energy balance. When the soil freezes, the formation of ice changes the surface thermal characteristics, damping the daily surface temperature cycle so that sensible heat flux becomes more important.

Concerns about climate change have grown in importance in recent years, with increased public awareness due to coverage in the popular press [*Wheeler*, 2001; *Brennan*, 2001; *Williams*, 2001]. Predictions of future climate are based largely on global general circulation models (GCMs), which nonetheless can be in considerable error due to incomplete physical knowledge. One of the key areas of uncertainty in GCMs is in their ability to represent the atmosphere-land surface interface [*Halldin et al.*, 1998]. The representation of this interface is of prime importance because it controls the transformation of radiative fluxes (long and shortwave radiation) into latent and sensible heat [*Avissar*, 1998]. Global simulations [*Betts et al.*, 1996] and field observations in the Arctic [*Marsh and Woo*, 1987] and Canadian boreal forests [*Betts et al.*, 1996] have shown that frozen soil can play an important role in this transformation of fluxes. Frozen soil also impacts the hydrologic response of a region by decreasing infiltration [*Kane and Chacho*, 1990; *Marshall et al.*, 1996].

Despite their importance to the hydrology of cold regions, frozen soils have largely been ignored both in land surface schemes and hydrology models. Land surface schemes focus on simulating surface energy and water fluxes, while hydrology models are designed primarily to predict streamflow [*Stewart et al.*, 1998; *Gusev and Nasonova*, 2000]. Macroscale hydrologic models, like the variable infiltration capacity (VIC) model [*Liang et al.*, 1994], attempt to do both by including a physically based representation of the surface. Models for frozen soil have existed for many years, primarily for the study of frost heave as it affects building and road construction [*Hohmann*, 1997; *Shoop and Bigl*, 1997]. These models rely primarily on empirical relationships that predict frost depth based on the number of days that the average temperature is below freezing. Some detailed physically-based point models have been developed, which attempt to account for all of the moisture and thermal fluxes that occur in the soil column during the winter [*Flerchinger and Saxton*, 1989a]. Such physically-based models are consistent with the need to represent the land surface-atmosphere energy exchange in climate and weather applications. They are, however, typically too compu-

tationally intensive for application over large areas. Incorporation of frozen soil effects in macroscale hydrologic models requires a trade-off between the need computational efficiency and accurate physical representation of the impact of frozen soils over large areas.

While many field and model application studies have focused on small-scale frozen soil processes [*Flerchinger and Saxton*, 1989a; *Engelmark and Svensson*, 1993, and others], fewer studies have addressed the effects of these processes at larger watershed scales [*Bathurst and Cooley*, 1996; *Cherkauer and Lettenmaier*, 1999]. This thesis presents the results of a course of research designed to address the following two science questions:

1. How does the spatial distribution of snow and frozen soil influence the hydrologic response of a watershed?

2. How does the hydrologic response to frozen soil change with basin size, climate, vegetation, and other watershed properties?

The first question is addressed through a combination of field work and modeling. A field observational study was used to document the variation of snow and frozen soil, as well as their effects on small scale runoff and infiltration. The observed distribution of snow cover and frost penetration was used to develop a model for simulating the spatial distribution of snow and frozen soil. Once modified, the model was used to assess the impact of spatial distributions at larger scales.

The second question was addressed through the use of observed catchment characteristics and measurements of stream discharge. Model simulations were used to help determine the likelihood of frozen soil events and categorize the observed discharge and precipitation so that the impact of frozen soil could be isolated.

This thesis consists of six chapters. Chapter 2 reviews frozen soil physics, provides an overview of simulation methods and presents the basic frozen soil and snow algorithms developed for and used in this work. Chapter 3 discusses the collection and analysis of data from the field campaign. Chapter 4 describe the development and implementation of spatial snow and frost algorithms based on field observations. Chapter 5 discusses the analysis of sub-catchments within the upper Mississippi River basin, which was conducted to determine

the importance of spring conditions and basin characteristics to the hydrologic response of watersheds during snow melt. Finally, Chapter 6 summarizes the results of the thesis work in terms of the previously posed science questions.

Chapter 2

PHYSICS OF FROZEN SOIL

Frozen soil plays an important role in the hydrologic cycle of cold regions. Figure 2.1 shows the extent of soil freezing in the Northern Hemisphere. Most of this region is influenced by seasonally frozen soils, which form when the air temperature falls below 0°C for several days. These regions have annual average air temperatures that remain above 0°C, but for at least a few days each winter the soil surface freezes. In regions where the annual average air temperature is below 0°C, the soil will remain frozen below a surface active layer which may thaw briefly in the summer. Soil that does not thaw seasonally is called permafrost and forms an impermeable lower bound to the transport of soil moisture. This chapter explores the physics of soil freezing, the interaction of climate and frozen soil, and revisits various approaches that have been used to model frozen soil.

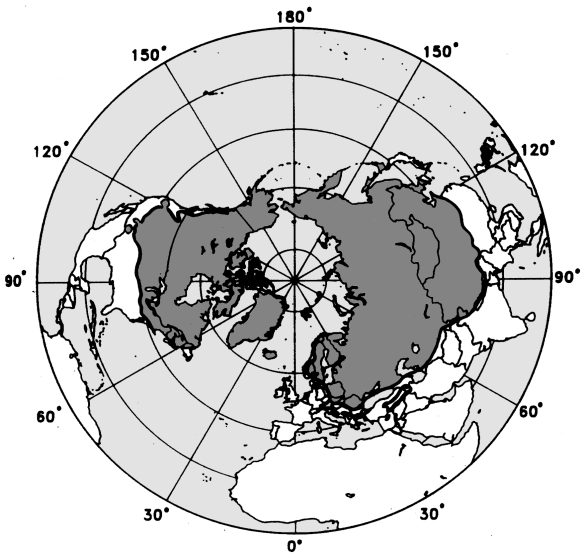

Figure 2.1: Extent of frozen soil in the Northern Hemisphere [*Kane and Chacho*, 1990].

2.1 Physics of Soil Freezing

The depth of seasonal frost penetration is driven by the diurnal freeze-thaw cycle. During the course of a day the soil surface temperature rises, possibly even thawing a thin surface layer, before dropping again at night. If the net daily ground heat flux at the surface is negative (out of the ground) then the freezing front advances; if it is positive then the freezing front retreats. When the surface ground heat flux is strongly positive, a thawing front may form at the surface and advance into the soil. This cycle penetrates only the top few centimeters of exposed soil, but can drive the seasonal freezing front as deep as 2-3 meters [*Williams and Smith*, 1989]. Because of its low thermal conductivity, snow insulates the soil surface and dampens the diurnal flux cycle at the soil surface, thus decreasing the seasonal penetration of frozen soils. Farmers have made use of this property for many years. If fields are left unplowed in the fall, crop residue catches blowing snow through the winter, increasing the retention of snow [*Benoit and Mostaghimi*, 1984, 1985; *Benoit et al.*, 1986]. Timing of snow accumulation and ablation is also critical to the development of frozen soil. An early snow that remains throughout the winter will result in shallower freezing depths than a late snow that falls after many weeks of cold weather.

Frozen soil also changes the dynamics of the snowpack during melt. As the snowpack melts, heat flux at the bottom of the pack will be into the ground, where it causes thaw along the freezing front (the boundary between frozen and unfrozen soil in the soil column). Because the frozen soil restricts the infiltration of melt water from the pack, the combination of this heat flux and lower night time air temperatures causes the melt water to refreeze at the soil surface. This ice layer will remain after the snow has melted and will continue to enhance production of runoff later into the spring [*Gray and Prowse*, 1993].

When the soil column begins to freeze the soil moisture does not solidify instantaneously; rather liquid water coexists with ice within the soil matrix to temperatures well below 0 °C [*Fuchs et al.*, 1978; *Flerchinger and Saxton*, 1989a; *Engelmark and Svensson*, 1993; *Tarnawski and Wagner*, 1996; *Newman and Wilson*, 1997]. *Bouyoucos* [1920] found that some water in a clay-water mixture remained unfrozen to temperatures as low as -78°C. The maximum amount of water that can remain unfrozen is primarily a function of the soil's

specific surface area, the soil temperature, and the presence of any solutes in the soil water [*Flerchinger and Saxton*, 1989a; *Engelmark and Svensson*, 1993]. Soils with finer particles have larger specific surface areas and retain more liquid water to lower temperatures: *e.g.* at the same temperature and water content a clay will contain more unfrozen water then a sand [*Engelmark and Svensson*, 1993; *Marshall et al.*, 1996]. Accurate estimates of the unfrozen water content are crucial to modeling frozen soil because the ice content strongly influences both water and heat fluxes as described below. Various empirical equations have been developed that produce acceptable results [*Fuchs et al.*, 1978; *Engelmark and Svensson*, 1993].

Ice content directly affects both infiltration of melt water into the soil column and the movement of water through the soil column. Ice forms in the soil interstitial spaces as far as possible from the surface of the soil particles, while liquid water remains adhered to surfaces [*Marshall et al.*, 1996]. As freezing progresses, liquid water and water vapor in the soil migrate along the temperature gradient to the freezing front, where they contribute to the growth of ice particles [*Marshall et al.*, 1996; *Hohmann*, 1997; *Shoop and Bigl*, 1997]. Growing ice crystals fill pore spaces, restricting the migration of soil moisture. *Zhao and Gray* [1997] and *Zhao et al.* [1997] showed that the soil moisture content prior to freezing (which determines the initial ice content of the soil) is one of the strongest controls on the amount of water that infiltrates into a frozen soil. Soils with high ice contents have reduced infiltration and hydraulic conductivity, while well-drained soils with low initial ice contents can still allow significant amounts of liquid water movement [*Kane and Chacho*, 1990; *Engelmark and Svensson*, 1993]. *Kane and Chacho* [1990] showed that a 10 cm thick frozen layer is sufficient to severely reduce infiltration. Ice nodes, or pockets of solid ice, may also form in the soil. Infiltration rates through these nodes can be as small as 0.01 mm/day [*Kane and Chacho*, 1990]. However, a continuous frozen layer is hydrologically more important because soil moisture will move laterally to work its way around an ice node [*Stahli et al.*, 1996]. Ice content is also important in the retention of soil moisture through the winter. Because ice does not drain from the soil column, the frozen soil moisture is recovered in the spring when the soil thaws [*Benoit et al.*, 1986; *Marshall et al.*, 1996]. In relatively flat regions, melt water that is unable to infiltrate the frozen ground may pond

in local hollows until the soil thaws enough to allow infiltration [*Marshall et al.*, 1996].

In addition to the hydrologic effects mentioned above, frozen soil has a large impact on the thermal fluxes through the soil column. Heat flux through the soil column is given by:

$$C_s \frac{\partial T}{\partial t} = \frac{\partial}{\partial z}\left(\kappa \frac{\partial T}{\partial z}\right) + \rho_i L_f \frac{\partial \theta_i}{\partial t} + \rho_l c_l \frac{\partial (q_l T)}{\partial z} - L_e \left(\frac{\partial \rho_v}{\partial t} + \frac{\partial q_v}{\partial z}\right) + S \qquad (2.1)$$

where κ is the soil thermal conductivity ($W\ m^{-1}\ K^{-1}$), C_s is the soil volumetric heat capacity ($J\ m^{-3}\ K^{-1}$), T is the soil temperature (°C), ρ_i, ρ_l and ρ_v are the density of ice, liquid water, and water vapor ($kg\ m^{-3}$), L_f and L_e are the latent heat of fusion and vaporization ($J\ kg^{-1}$), θ_i is the ice content ($m^3\ m^{-3}$), q_l is the liquid water flux ($kg\ m^{-2}\ s$), q_v is the water vapor flux ($kg\ m^{-2}\ s$), c_l is the specific heat of liquid water ($J\ kg^{-1}\ C^{-1}$), S is a source/sink term, t is time (s) and z is the depth (m) taken as a positive length downwards from the surface. The six terms in this equation contribute to the local energy balance as follows: the first term describes heat storage in the soil, the second describes the conduction of heat through the soil, the third describes the effects of latent heat as soil moisture freezes and thaws, the fourth describes heat transferred by the migration of liquid water, the fifth describes heat transfer by water vapor, and the final term includes all other energy flux sources and sinks (*e.g.* at the soil surface this could include net shortwave and longwave radiation).

From the presence of heat and water flux components in Eq. 2.1 it can be seen that the migration and phase change of soil water play an integral part in the transfer of heat by the soil column. However, the interaction of soil heat and moisture transfer is complicated by the dependence of soil thermal properties (thermal conductivity and volumetric heat capacity) on soil moisture and ice content. The thermal conductivity of liquid water is $0.57\ W\ m^{-1}\ K^{-1}$, while that of ice is four times larger. Increasing the liquid water content in a soil increases its thermal conductivity, but not as quickly as increasing its ice content. Furthermore, the volumetric heat capacity of water is $4.2\ MJ\ m{-}3\ K^{-1}$, while for ice it is $1.9\ MJ\ m^{-3}\ K^{-1}$, so increasing the soil's ice content decreases its thermal storage capacity. These properties coupled with the dampening effect of the phase change (freezing water releases latent heat, warming the surrounding environment) modify the response of near surface soil temperatures and subsequently affect the surface energy balance. During the

summer, the soil surface temperatures are typically quite similar to surface air temperature (*i.e.* temperature at 2 meters above the ground surface) [*Betts et al.*, 1996; *Betts and Ball*, 1998]. Following the onset of soil freezing, the diurnal soil surface temperature cycle is significantly dampened and no longer tracks the near surface air temperature as closely. This increases the importance of sensible heat flux to the surface energy balance [*Betts et al.*, 1996].

2.2 Modeling Frozen Soil

Models of frozen soil range from simple modifications of soil infiltration parameters based on season [*Sand and Kane*, 1986; *Bathurst and Cooley*, 1996] to degree day methods that estimate frost depth based on the number of days of below freezing temperatures [*Fox*, 1992] to an array of more complex physically-based models that try to solve various simplifications of the coupled heat and moisture flux equations [*Flerchinger and Saxton*, 1989a; *Gel'fan*, 1989; *Lundin*, 1990; *Stadler et al.*, 1996; *Stahli et al.*, 1996; *Tarnawski and Wagner*, 1996; *Newman and Wilson*, 1997; *Shoop and Bigl*, 1997; *Cherkauer and Lettenmaier*, 1999; *Koren et al.*, 1999]. They have been used to predict the effects of frost heave on roads [*Hohmann*, 1997; *Shoop and Bigl*, 1997], to improve understanding of heat and moisture fluxes through frozen soil [*Stahli et al.*, 1996; *Newman and Wilson*, 1997; *Zhao and Gray*, 1997], and to represent the contribution of spring snow melt to basin discharge [*Sand and Kane*, 1986; *Fox*, 1992; *Bathurst and Cooley*, 1996; *Cherkauer and Lettenmaier*, 1999; *Koren et al.*, 1999]. The challenge for macroscale modelers is to develop algorithms that retain enough of the soil freeze-thaw physics to improve the model's representation of thermal and moisture fluxes, while not becoming prohibitively expensive computationally.

Simple methods such as manually reducing the soil infiltration capacity [*Sand and Kane*, 1986; *Bathurst and Cooley*, 1996] show that frozen soils increase spring flows and therefore cannot be neglected when simulating the hydrologic response of large basins in cold climates. However, these methods do not account for seasonal variations in the meteorological forcings that impact the formation of frozen soil. The degree day method employed by *Fox* [1992] makes use of an empirical relationship between the number of days with temperatures below

freezing and frost depth. This allows frost penetration to vary with annual climate forcings, but without a physical representation of soil thermal fluxes it cannot be used to study the land surface-atmosphere interaction.

Detailed physical representations of the coupled heat and moisture transport equations by *Engelmark and Svensson* [1993], *Stahli et al.* [1996], *Zhao and Gray* [1997], *Zhao et al.* [1997], and others have been used to improve the understanding of heat and moisture fluxes within frozen soil. Column models have shown that infiltration into frozen soil is controlled primarily by the saturation of the soil surface during infiltration, the initial saturation of the soil column, and the shape of the freezing point depression curve, while soil temperature has only a minor impact [*Zhao and Gray*, 1997; *Zhao et al.*, 1997]. *Zhao et al.* [1997] established that the effects of phase changes involving water vapor are at least three orders of magnitude smaller than the other components of the heat flux equation, while convective heat can contribute as much as 27% of the heat used to thaw the soil. *Stahli et al.* [1996] demonstrated that infiltration into frozen soil could be better represented by allowing moisture flux through low flow (ice filled pores) and high flow (air filled pores) domains. This method incorporates observations of infiltration occurring in regions where, on average, frozen soil depth is significant. Physical models of frozen soil have also been coupled to snow cover by estimating heat fluxes through observed snow depth [*Gel'fan*, 1989], or by coupling the soil algorithm to a snow accumulation and ablation algorithm [*Flerchinger and Saxton*, 1989a].

Chapter 3

FIELD OBSERVATION PROGRAM

Frozen soil plays an important role in the hydrologic cycle of northern regions. The presence of ice in the soil can significantly retard the infiltration of spring melt water [*Storey*, 1955; *Williams and Smith*, 1989; *Kane and Chacho*, 1990; *Gray and Prowse*, 1993], potentially increasing the peak flow response. An important consideration in determining how frozen soil will affect spring flows is its spatial distribution. Most studies of frozen soil have concentrated on point-scale effects [*Gel'fan*, 1989; *Flerchinger and Saxton*, 1989b; *Engelmark and Svensson*, 1993; *Flerchinger et al.*, 1996]. When observations are made spatially, it has been shown that frozen soil is strongly influenced by vegetation cover [*Stadler et al.*, 1996; *Shanley and Chalmers*, 1999]. It has also been shown that the spatial distribution of frozen soil in a forested environment can have an important effect on the local hydrology [*Stadler et al.*, 1997].

The distribution of soil frost within regions of low relief, like the upper Mississippi River basin, can be very important. Without strong slope gradients to move melt water quickly to a stream channel, it flows to the lowest point. Sometimes infiltration occurs quickly despite extensive frozen soil but sometimes ponding persists in low points until frozen soil thaws [*Baker*, 2000]. If there is enough melt water, ponds will cause localized flooding or breach their constraints and flow further toward the stream network. It has also been shown that tillage practices influence the formation of frozen soil, the timing of spring thaw, and the retention of soil moisture in the spring [*Benoit et al.*, 1986]. *Koren et al.* [1999] made use of a gamma distribution of ice content based on observations of the distribution of frozen soil depth in Russia [*Koren*, 1980] to simulate the effects of frozen soil at the University of Minnesota's Rosemount Agricultural Experiment Station. They showed that frozen soil was very important to their simulations, but no effort was made to assess the applicability of the distributional form of ice content to the region.

The redistribution of snow by wind has also been shown to be an important part of spring melt processes [*Marsh and Pomeroy*, 1996; *Pomeroy et al.*, 1997; *Luce et al.*, 1998]. Deep drifts can remain long after thinner coverage has melted [*Seyfried and Wilcox*, 1995; *Pomeroy et al.*, 1997], while snow-free areas increase the melt of neighboring snow-covered regions through the advection of sensible heat [*Shook et al.*, 1993; *Marsh and Pomeroy*, 1996; *Marsh et al.*, 1997]. Despite these studies, not much is known about the interaction of the spatial distribution of frost and snow.

To increase understanding of these local processes and how they impact streamflow, a field campaign was conducted to investigate the spatial distribution of snow and frozen soil in the upper Mississippi River basin. Observations were made at the University of Minnesota's Rosemount Agricultural Experiment Station (Figure 3.1). During the winters

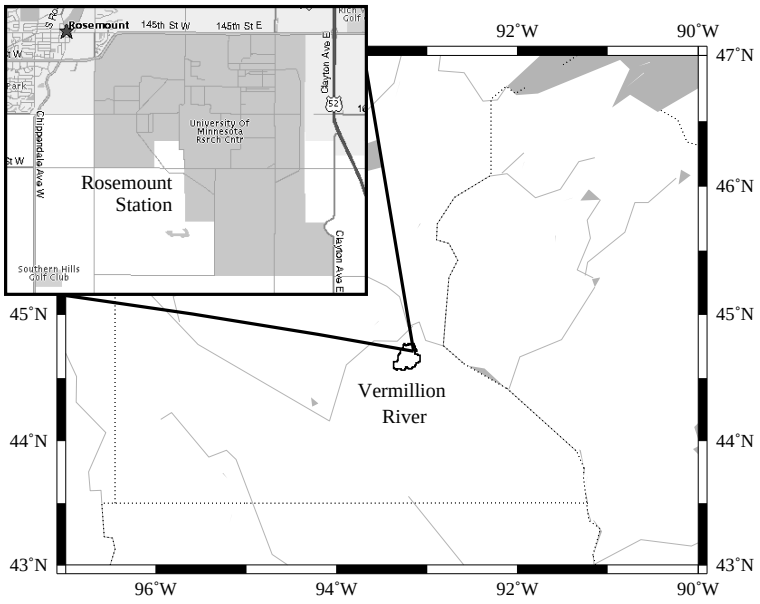

Figure 3.1: Location of the University of Minnesota Rosemount Agricultural Experiment Research Station (shaded area in inset) and the Vermillion River.

of 1997-1998 and 1998-1999 observations of snow depth and soil temperature were collected from the northwest corner of the station ($\sim$10 km^2 in area), where the roads are plowed throughout the winter. Most of this area is cropland, with some pasture to the north and

east, and scattered lines of trees. Observations of snow depth and soil temperatures were made from several sites around the station. The observations were analyzed to determine the impact of land use on soil freezing and the correlation between snow cover and frozen soil and to derive a statistical distribution that can be used to describe the spatial distribution of soil frost and snow cover in the region.

For the winter of 1999-2000 the study was expanded to the entire Vermillion River basin, which drains part of the Rosemount Station. This study was intended to determine if the distributions derived from the field scale experiments applied to a larger basin. Due to equipment problems, this aspect of the observational program had value primarily for the visual characterization of the influence of frozen soil on the Vermillion River basin.

3.1 Field Observations during the Winter of 1997-1998

Since at least 1994, observations of snow depth at the Rosemount Station have been made using a circle of snowsticks (*i.e.* rulers mounted in the ground prior to snow accumulation, from which the depth of snow can be read at a distance) (inset Figure 3.2). A meteorological tower where hourly averaged measurements of wind speed, incoming radiation, and soil temperature and moisture are taken is located in the same field. In October 1997, an effort was undertaken to expand the measurement of snow cover and frozen soil extent throughout the station. In addition to increasing the number of snowsticks used, sixteen new snowsticks were cut so that they extended an extra 60 cm into the ground. Thermocouples were then attached to the longer snowsticks at depths of 30 cm and 60 cm. During a typical spring thaw, frost penetration at the Rosemount site is between those depths, so it was believed that temperature measurements at these depths would allow estimation of the frost depth. Because of the distance between the snowsticks, installation of data loggers was not feasible so measurements were made manually about once a week.

Snowsticks were installed in a circle on the primary field, and in a grid through the accessible portions of the rest of the station (Figure 3.2). Four thermocouple snowsticks were installed in the circle of snowsticks, with one located in a depression, two on the sides of the depression, and one on the side opposite the depression. Three others were used to

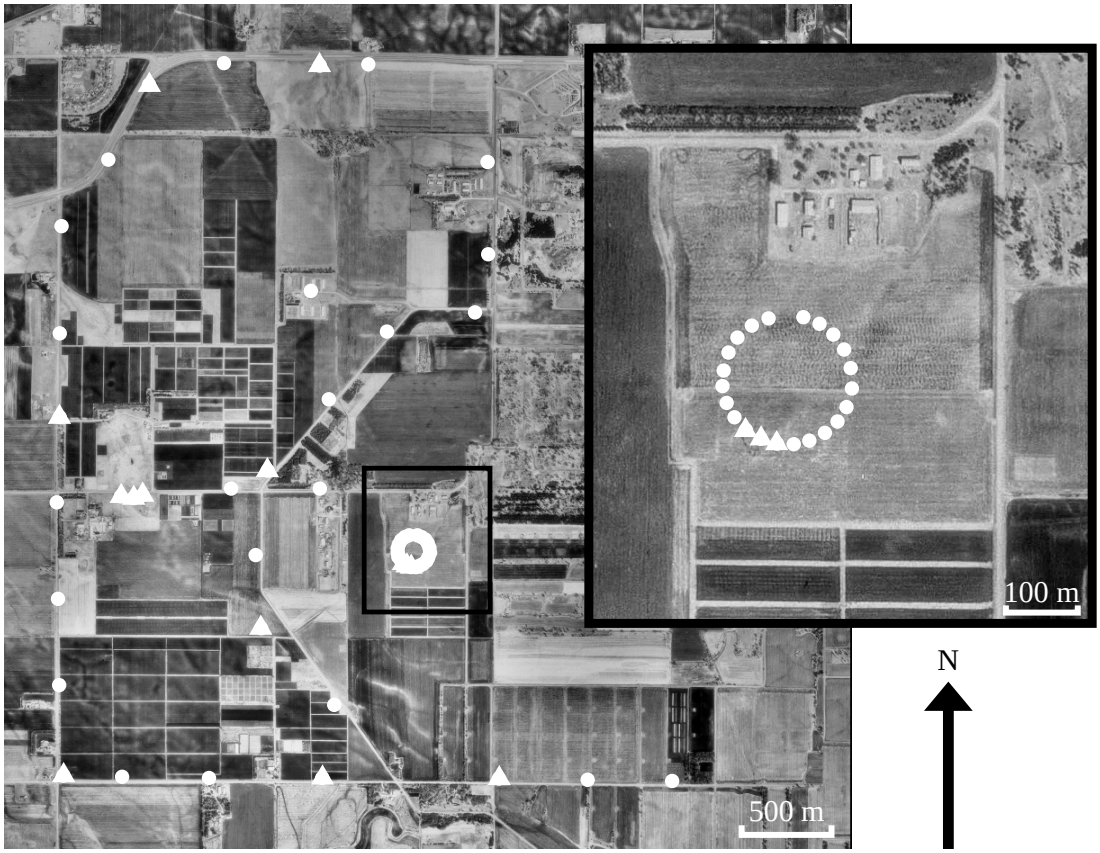

Figure 3.2a: Locations of installed snowsticks (circles) and snowsticks with thermocouples (triangles) at the Rosemount, Minnesota field site for the winter of 1997-1998.

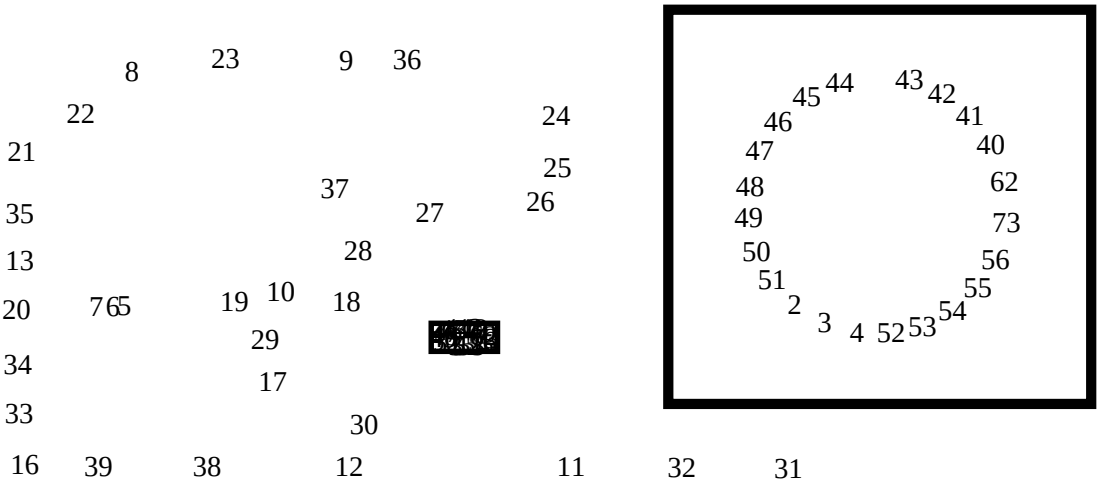

Figure 3.2b: Identification numbers of installed snowsticks, winter 1997-1998.

bracket a large gully on the west side of the station, with one in the depression and one on the high ground to either side.

Most of the fields were harvested and plowed prior to installation of the instrumentation. A few of the selected fields were pastures and a few had been left fallow through the late summer and early fall so these had not been recently plowed. Snowsticks were located within the fields close enough to the road to be read from a car with binoculars, but far enough away to reduce the chance of interference by snowmobile traffic. Nonetheless, several of the snowsticks were lost during the winter due to snowmobiles, while others survived the winter by becoming islands within snowmobile trails. In general, most of the snowsticks survived the winter and were relatively free of disturbances. Thermocouple measurements were taken on 11 days, while only 8 of those days included snowsticks beyond the main field.

3.2 Field Observations during the Winter of 1998-1999

For the winter of 1998-1999 a similar grid of snowsticks was installed around the station (Figure 3.3). In addition to the 30 cm and 60 cm thermocouples, 23 single channel Hobo temperature data loggers were installed to measure the 5 cm soil temperature at 3 hour intervals. Snowsticks were installed farther from the road, again to reduce the likelihood of snowmobile damage. Due to the lack of snow through the winter, the snowmobile season was relatively short and did not impact most of the snowsticks. However, three data loggers were damaged or missing along with one of the thermocouple snowsticks. Two other thermocouple snowsticks had broken wires for at least one depth. One data logger stopped functioning while three others recorded constant minimum temperature values starting a few days after installation. All of the other installed equipment worked as expected. Thermocouple observations were collected on 17 days, including 5 consecutive days of observations while the late season snowfall melted.

3.3 Field Observations during the Winter of 1999-2000

During the final winter of the field campaign the goal was to observe the spatial distribution of snow and frozen soil over a larger region to see if the distributions observed at the

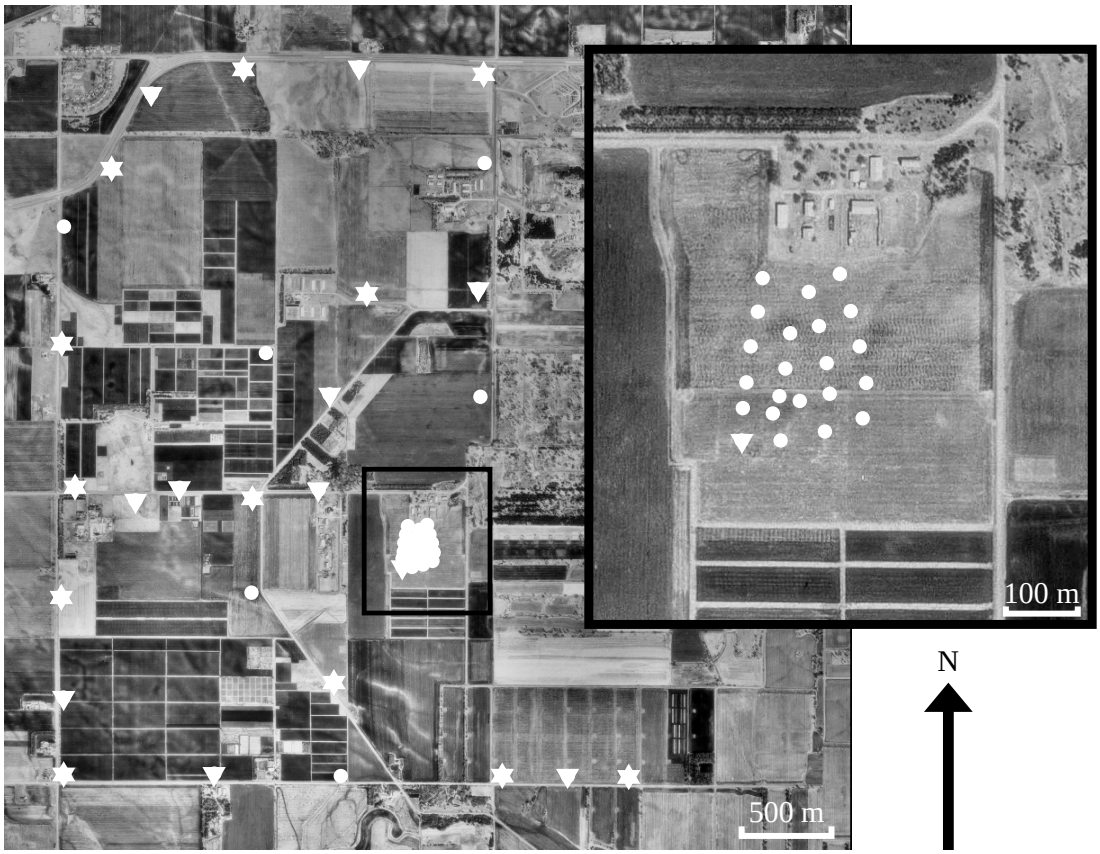

Figure 3.3a: Locations of installed snowsticks (circles), snowsticks with thermocouples (triangles), snowsticks with data loggers (inverted triangles), and snowsticks with thermocouples and dataloggers (stars) at the Rosemount, Minnesota field site for the winter of 1998-1999.

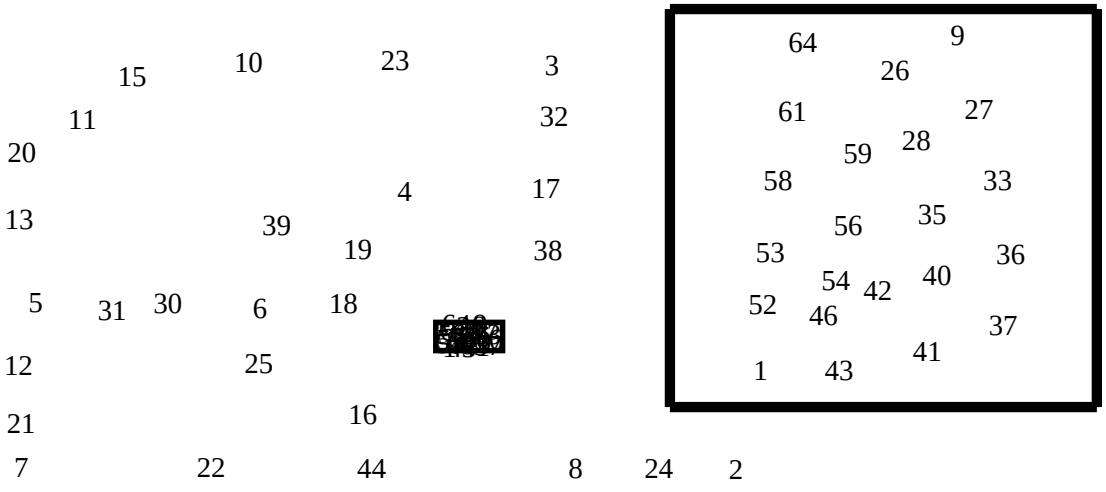

Figure 3.3b: Identification numbers of installed snowsticks, winter 1998-1999

Rosemount station would still be valid. No equipment was installed at Rosemount; instead observations along transects across the Vermillion River basin were planned to coincide with spring melt. The Vermillion River was selected because it drains part of the Rosemount station.

Snow depths and soil temperatures at 10 and 15 cm were observed along the transects (Figure 3.4 and 3.5). Soil temperature were measured by driving a stake into the ground until the attached thermocouples were at the required depths. This method was difficult and time consuming, especially extracting the stake once the measurements were taken. In the end very few observations were taken before the stake broke, and these were questionable as the thermocouples often moved from their mounted locations while the stake was driven into the ground. Most of the information collected came in the form of a visual survey of the basin to observe melt processes and frozen soil effects in action.

Figure 3.6 shows the differences in snow cover between vegetation cover types on February 25, 2000. The forested area has nearly continuous snow cover, the tilled field is almost bare, and the grass covered field still has patches of snow. On the open fields snow cover is most likely to be near the tree cover, where both the accumulation was greatest due to wind redistribution and the snow is shielded at least partially from the incoming radiation. Figure 3.7 shows the formation of fog due to sublimation of the snow on February 25, 2000.

Figure 3.8 shows a tilled corn field well into the melt process on February 25, 2000. Snow is present in the hollows and around rows of corn stalks where accumulation was higher. In Figure 3.9 there is no snow left but the melt water is still present, ponded in the furrows. Without a clear drainage network, melt water remains in the field until it can find a drainage path through the frozen soil. When not completely flooded, the surface thaw layer is muddy.

In Figure 3.10 melt water slowly leaves the area through drain channels next to the roads. Without adequate drainage, water will pond in the low lying areas. There are large melt ponds throughout the region that can persist for several days. If ponding occurs close to a road it may eventually overtop the road as seen in Figure 3.11. This was a fairly common occurrence in the region making some of the roads nearly impassable.

Figure 3.4: Observations of snow melt processes in the Vermillion River basin. Transect observation point in a tilled corn field, February 24, 2000.

Figure 3.5: Transect observations point in a tilled soy field, February 24, 2000.

Figure 3.6: Spatial variation in snow cover caused by differences in vegetation cover, February 25, 2000.

Figure 3.7: Fog developing over snowpack due to sublimation, February 25, 2000.

Figure 3.8: Residual snow cover between tilled ridges, February 25, 2000.

Figure 3.9: Ponding of melt water between tilled ridges, February 25, 2000.

Figure 3.10: High flow through culverts under a side road, February 25, 2000.

Figure 3.11: Ponded melt water flows over the road, February 25, 2000.

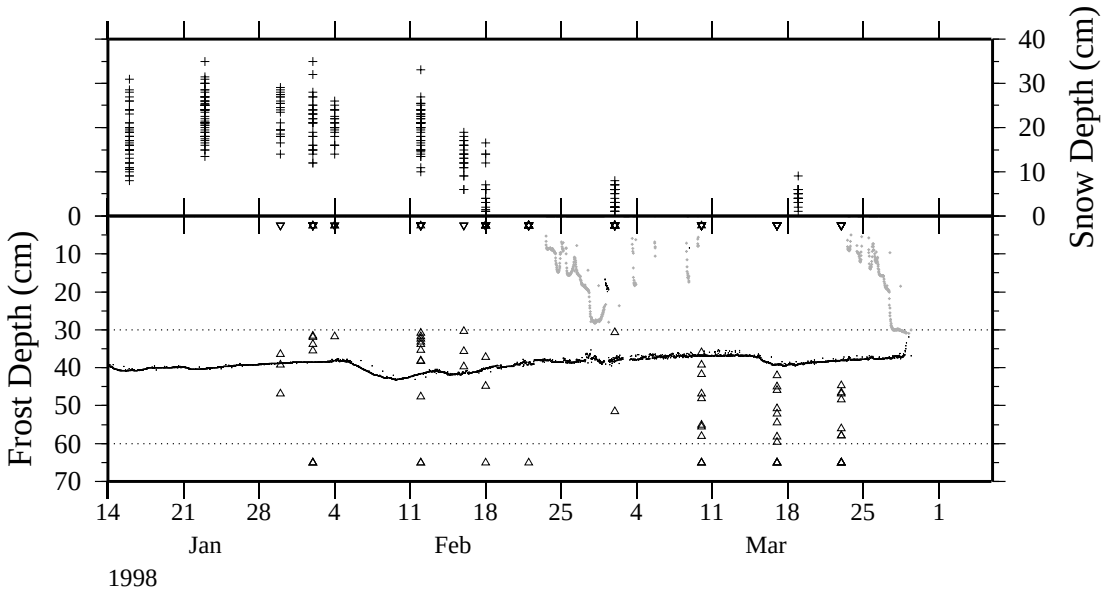

Figure 3.12: Observed snow (top), frost (bottom black) and thaw (bottom gray) depths at Rosemount for the winter of 1997-1998. Pluses indicate the snowstick observations of snow depth, triangles indicate an observed freezing front, inverted triangles indicate an observed thawing front. Black and gray points indicate the freezing and thawing depths observed at the main field. Dotted lines mark the top and bottom of the soil depth interval for which temperature measurements were made. Triangles above or below those lines indicate that a measurement was taken, but from the available observation depths the soil column appears completely frozen or completely thawed. When triangles and inverted triangles overlap they form stars.

3.4 Field Data Analysis

The winter of 1997-1998 was relatively warm with a thinner than average snowpack. For most of the snowsticks frost penetrated to 30 cm only late in the season (Figure 3.12). Snowstick frost depth estimates in Figures 3.12 and 3.13 are interpolated linearly from the thermocouple temperatures. If all thermocouples registered above 0°C, then frost and thaw depths were set to 2.5 cm (to indicate a measurement was taken but no depth could be estimated), while if all thermocouple registered freezing temperatures, frost depth was set to 65 cm. Snow depth through mid-February was between 20 and 30 cm for most of the snowsticks. During this time, most frost depths were less than 40 cm. By March 1 the

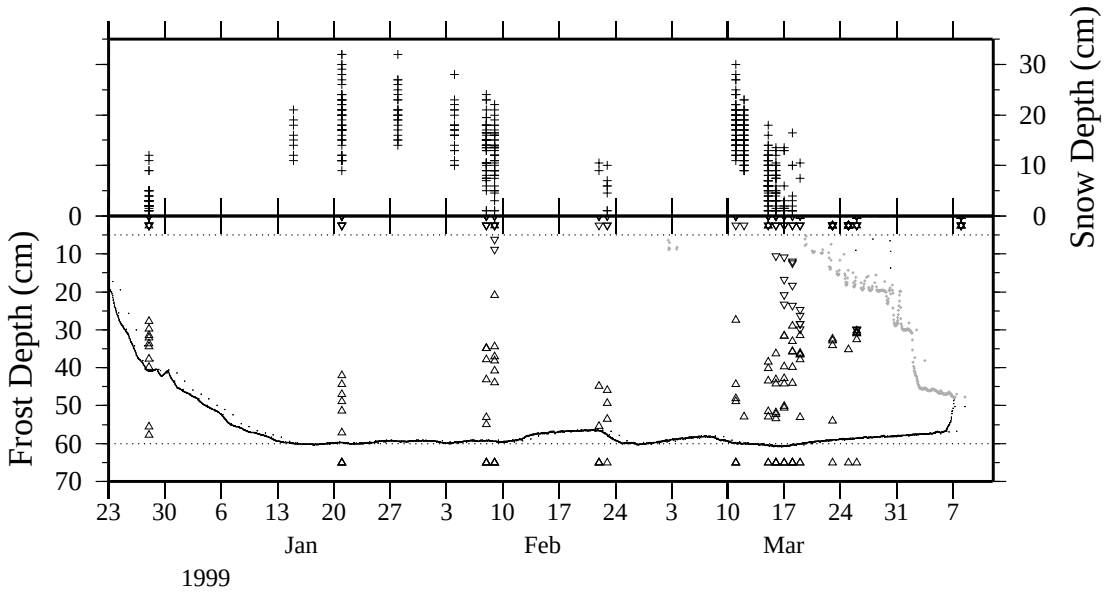

Figure 3.13: Observed snow (top), frost (bottom black) and thaw (bottom gray) depths at Rosemount for the winter of 1998-1999. Symbols described in Figure 3.12.

snowpack had been reduced to less than 10 cm and all but two of the snowsticks showed frost depths of less than 30 cm. Through the rest of March the snowpack remained thin but air temperatures remained at or below freezing, so frost depths became deeper. They also showed more scatter, which is probably related to the patchiness of the snowcover. Only three snowsticks (numbers 2, 3 and 4) showed snowcover in mid-March and these were located on the main field.

Figure 3.13 is similar to Figure 3.12 except that it shows the winter of 1998-1999. Because 5 cm temperatures were available from the dataloggers, Figure 3.13 includes frost and thaw depths between 5 and 60 cm. Because the snowpack developed late, frost depths by mid-January were all greater than 40 cm. By early February the snowpack had begun to melt and the frost had begun to retreat, with some of the snowsticks experiencing surface thaw. A record-setting snowfall in early March allowed for an intensive period of observation as the snow melted, and the soils began to thaw (around March 14 on Figure 3.13). Scatter increased during the thaw, and frost and thaw depths were observed to change by several

centimeters daily. By March 21, most of the snowsticks registered nearly complete thaw.

3.4.1 Time Series Analysis

When instrumentation was installed in the autumn, the land cover type for each field was classified by what type of crop was grown during the previous summer and whether or not the crop residue had been tilled. Table 3.1 shows the cover types for all snowsticks outfitted with data loggers and thermocouples during the winter of 1998-1999 (see Figure 3.3 for spatial distribution). The majority of observed fields were tilled soy and corn. Residue from the corn tends to be taller than either soy or alfalfa even after being plowed. Two of the three grass sites were located in pastures with grass heights of about half a meter. The third, snowstick 18, was located in the mowed grass field next to the Rosemount Station main office and rain gauge.

Data loggers recorded soil temperatures at a depth of 5 cm every three hours throughout the winter. Figure 3.14 shows the time series of average daily temperature for the five observed vegetation cover classes. The data loggers could not record temperatures below -4.88°C, so actual soil temperatures were probably colder than recorded by those loggers that reached the end of the scale for multiple days. Most of the agricultural fields show similar temperature patterns, cooling off rapidly in late December, experiencing a brief rise in temperature just before the new year and then remaining cold through mid-January. Neither of the working grass sites (snowstick 31 disappeared shortly after installation) cooled as dramatically in December or were as cold as the other sites during the winter. During the winter the grass areas captured and retained more snow, insulating the soil from the surface energy exchange and keeping the soil warmer than the more exposed croplands. Warmer soil temperatures in the fall may be due to higher soil moistures, which would retain more heat as the air temperatures decreased. More soil moisture would also keep soil temperatures higher during the winter because more energy would be used in changing liquid water into ice. The warmer of the two grass sites is snowstick 18, which might have been wetter in the fall if the grass was watered. Also, because its position was sheltered, it maintained a more uniform snowcover much longer than any of the other sites.

Table 3.1: List of snowsticks installed during the winter of 1998-1999 that included temperature data loggers at depth of 5 cm. The profile column indicates whether or not the snowstick also included thermocouples at depths of 30 and 60 cms.

Snowstick Number	Profile	Field Cover Type	Status
1	Yes	tilled corn	FAILED/REPLACED
2	Yes	tilled corn	FAILED
3	Yes	tilled corn	OK
4	Yes	tilled soy	OK
5	Yes	tilled alfalfa	OK
6	Yes	soy residue	OK
7	Yes	tilled corn	FAILED
8	Yes	tilled corn	LOST
10	Yes	tilled soy	FAILED
11	Yes	tilled soy	OK
12	Yes	tilled corn	OK
13	Yes	tilled soy	OK
15	No	tilled soy	OK
16	Yes	tilled alfalfa	OK
17	No	soy residue	FAILED
18	No	grass	OK
19	No	tilled soy	OK
21	No	tilled corn	OK
22	No	tilled corn	OK
23	No	grass	OK
24	No	tilled corn	SENSOR CUT
30	No	tilled soy	OK
31	No	grass	LOST

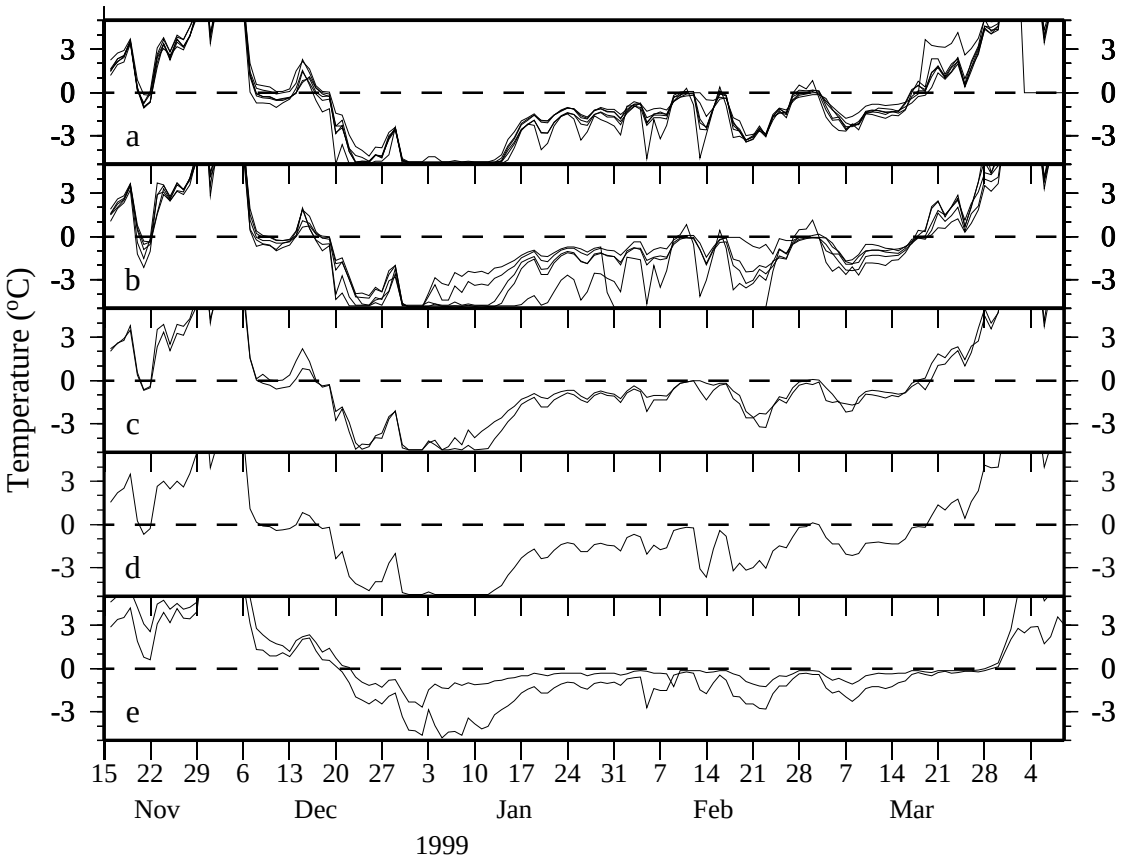

Figure 3.14: Average daily 5 cm soil temperature for the winter of 1998-1999: (a) tilled soy fields (6 sensors), (b) tilled corn fields (5 sensors), (c) tilled alfalfa fields (2 sensors), (d) untilled soy residue field (1 sensor) and (e) grass and pasture fields (2 sensors).

The last day in December when the soil at 5 cm was frozen is shown in Figure 3.15 for all vegetation cover types. Frost appears first in the various crop cover types, while freezing of the grass areas takes several more days. Tilled corn fields appear to freeze the latest of the various crop covers, although all observations fall within the range of observed freeze dates for tilled soy. Tilled soy, with the highest number of observations, also shows the greatest range in freeze dates. The first day of thaw is shown in Figure 3.16. As with the first day of freezing, the first day of thaw for the grass sites is significantly later than for all of the crop types. From the time series in Figure 3.14 it can be seen that the 5 cm soil temperature changes for the agricultural sites are higher in magnitude than those of the grass sites, and many of them thaw for a couple of days around March 1st (day 60 in Figure 3.16). The last snow at the grass sites was observed on March 18, 1999, while snow for the other sites melted off on the 16th and 17th. Despite having no snowcover, the grass sites remained frozen with temperatures around $0°C$ for almost 10 more days.

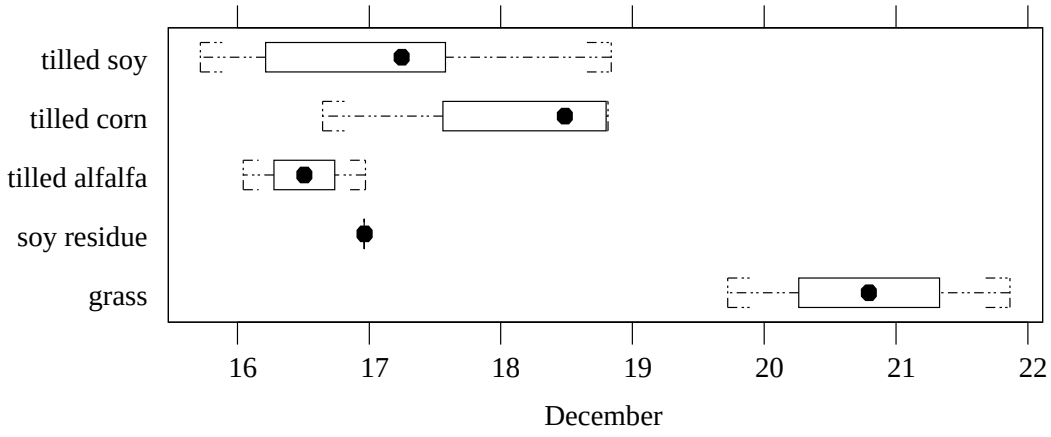

Figure 3.15: Box and whisker plot of date of soil freeze at a depth of 5 cm for the winter of 1998-1999. Freeze is classified by the observed land cover type in late November.

Further analysis of the 5 cm soil temperature data was conducted to determine how closely the time series between and within cover types are related. The sample correlation coefficient between each set of daily average observations was computed and the results for each comparison type are shown in Figure 3.17. Grass, tilled alfalfa, and soy residue classes

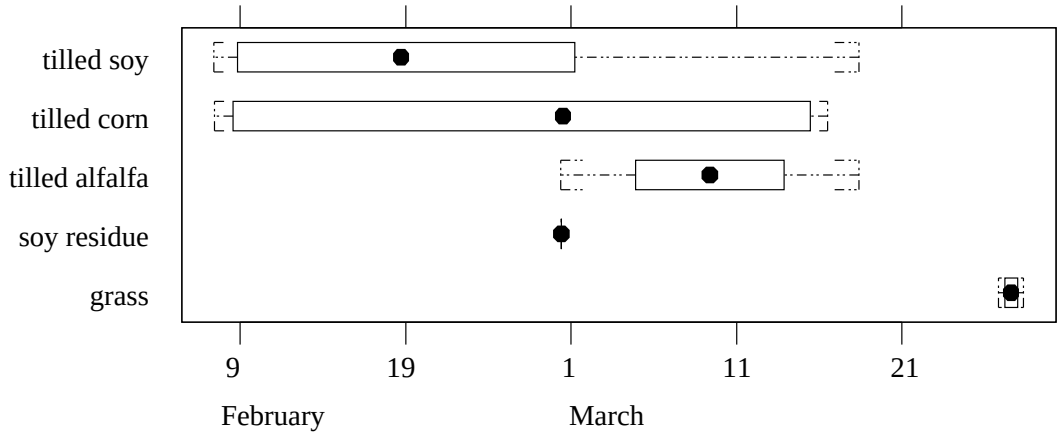

Figure 3.16: Box and whisker plot of date of last freezing temperature at a depth of 5 cm for the winter of 1998-1999.

were not compared because of the limited number of time series. Correlations are high between the various crop classifications, with the median values all over 0.95. Correlations within the tilled soy and tilled corn classes are very similar to each other, though the correlation within tilled corn is slightly lower. From Figure 3.14 it can be seen that there is less agreement between temperature series in the tilled corn fields than those in the tilled soy fields, resulting in the reduced correlation coefficient. As expected, the lowest correlations involve the grass sites.

Observations from the snowsticks with thermocouples (see Table 3.1) were collected less frequently but provide insight into the interaction of snow and frozen soil. Figure 3.18 shows the range of snow depth observations over the winter of 1998-1999. The maximum and median observed depths are very different between the snowsticks. Each set of observations was taken within one to two days, but times between observation sets ranged from one day during melt to over two weeks during in January and February. Efforts were made to observe snow depths shortly after accumulation events, so maximum snow depths should be representative of the actual maximum. Thus differences in the maximum depths between observation sites are most likely related to the redistribution of snow between and during accumulation events.

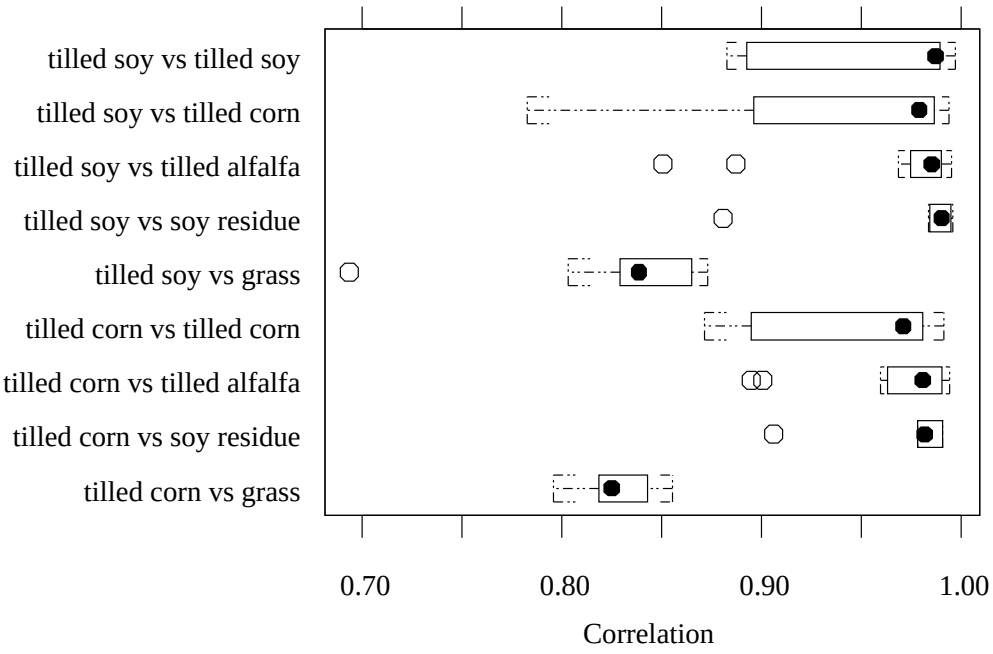

Figure 3.17: Box and whisker plot of observed snow (top), frost (bottom black) and thaw (bottom gray) depths at Rosemount for the winter of 1998-1999.

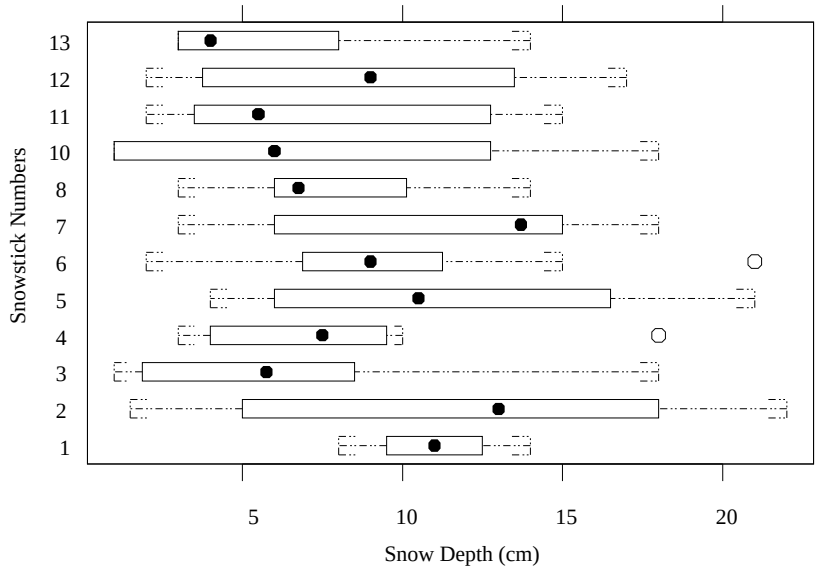

Figure 3.18: Box and whisker plot of snow depth observations for snowsticks with thermocouples for the winter of 1998-1999. Black filled dots represent median observed snow depth, while whiskers and circles indicate the range of observations.

Figures 3.19 and 3.20 are similar to Figure 3.18 except that they show soil temperatures at the depths of 30 and 60 cms. The median values on both plots are near $0°C$ because of the number of observations taken during and just after melt. Temperatures at 60 cm show more variation because soils did not freeze to that depth for most of the snowsticks, while they froze to 30 cm for all cases (see Figure 3.13). Snowsticks 2 and 5, which had some of the deepest snowpacks, also had very small changes in soil temperatures and some of the warmest minimum temperatures, showing that they were well insulated by their respective snowpacks. Snowsticks 3 and 10, which had the lowest minimum temperatures, show no apparent relationship with their respective snowpacks. Observations for snowstick 3 indicate that it tended to have one of the thinnest snowpacks, though it also reported a large maximum. Snowstick 10 had about the same maximum and median snow depths as snowstick 3 but it had a larger range of observed depths.

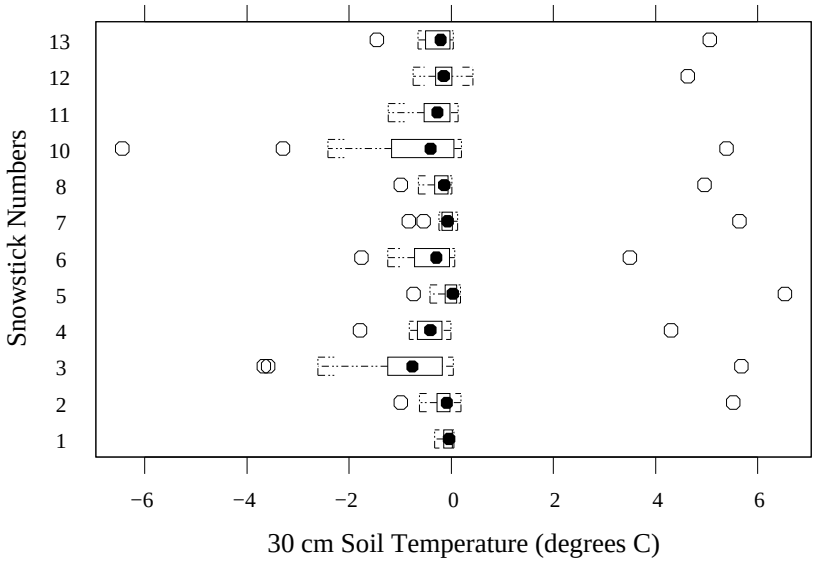

Figure 3.19: Box and whisker plot of soil temperature observations from a depth of 30 cm for snowsticks with thermocouples for the winter of 1998-1999. Black filled dots represent median observed snow depth, while whiskers and circles indicate the range of observations.

Sample correlations between the different observations at each snowstick are shown in Table 3.2. The correlation between the 30 and 60 cm soil temperatures for both winters is

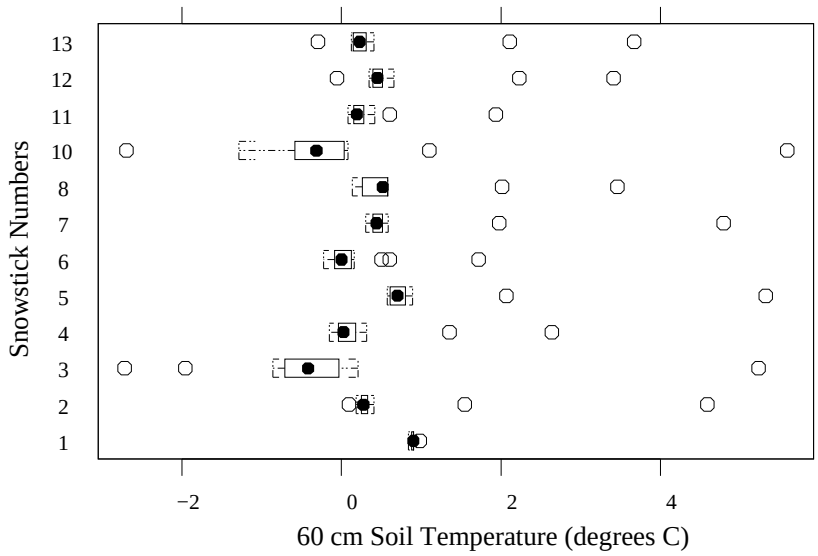

Figure 3.20: Box and whisker plot of soil temperature observations from a depth of 60 cm for snowsticks with thermocouples for the winter of 1998-1999. Black filled dots represent median observed snow depth, while whiskers and circles indicate the range of observations.

high but neither temperature shows a strong correlation with the observed snow depth. The gradient of temperatures through the soil column should be relatively smooth, especially with an insulating cover of snow. However, while the snow reduces the change in soil temperatures, the depth does not control temperature: heat is still transferred through the snowpack but the rate of transfer is smaller. Under a thick snowpack the change in soil temperatures will be small, but the actual temperatures will be determined by the exchange of heat prior to the large accumulation.

3.4.2 Statistical Distribution Analysis

In order to develop spatial algorithms for snow and frozen soil, probability distributions were fitted to the observed data. The first order assessment comes from visually inspecting plots of the probability distributions. Figure 3.21 plots the areal distribution of relative frost depths for each day of measurement during the winter of 1997-1998. Dark bars indicate thermocouple interpolated observations. Since depth estimates could only be made when

Table 3.2: Correlation between observations of snow depth 30 and 60 cm soil temperatures. Values in parenthesis are the t-test p-values.

Winter 1997-1998

Comparison	Winter 1997-1998	Winter 1998-1999
snow depth vs. 30 cm temperature	-0.3029 (0.0645)	-0.0626 (0.6042)
snow depth vs. 60 cm temperature	0.1335 (0.4244)	-0.1555 (0.2055)
30 cm temperature vs. 60 cm temperature	0.7298 (0.0000)	0.8166 (0.0000)
snow depth vs. frost depth	0.3834 (0.0175)	0.0430 (0.7216)
frost depth vs 30 cm temperature	-0.8298 (0.000)	-0.5565 (0.000)
frost depth vs 60 cm temperature	-0.7522 (0.000)	-0.5609 (0.000)

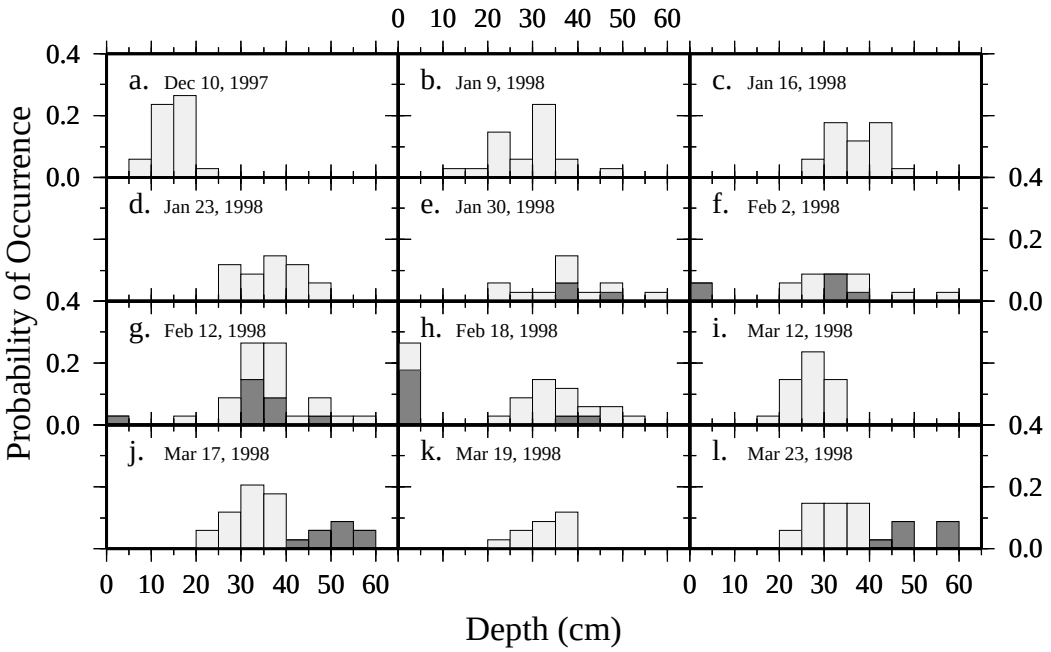

Figure 3.21: Statistical areal distribution of frost depth for given sample days (a-l) for both thermocouple estimated depths (dark) and frost tube observed depths (light).

the frost depth falls between 30 and 60 cm, limited observations were available early in the season when frost depths were shallow, and again later in the winter when frost depths were deeper than 60 cm (see Figure 3.12). As part of an independent project, frost tubes were installed at several of the same locations as the thermocouple snowsticks. Their frost depth observations are included on the plots as light grey bars. Frost tubes are most reliable early in the season; following a partial thaw cycle that occurred in late-February and early-March (Figure 3.12) they were susceptible to the formation of air and ice pockets in the tube. Where observations of the same depth were made using different techniques, the bars are stacked.

The frost tubes show the advance of the freezing front from December through January. By January 30 (Figure 3.21e) the thermocouples began to observe the freezing front. Figure 3.21g shows a strong distribution with most observation points reporting frost depths of 30 to 40 cm. Observations on February 18, 1998 (Figure 3.21h) were taken as most of the snowpack melted and show the frost depth distribution spreading. The thermocouples indicate that the frost depth was advancing (Figures 3.21j and 3.21l), while the frost tubes, many of which experienced a separation within the soil column, indicated very little change until they began to thaw.

Similar plots were made for snow depth (Figure 3.22), 30 cm soil temperature (Figure 3.23), and maximum unfrozen water content (Figure 3.24). During the initial accumulation period (Figures 3.22a-c), there was not much variation among observed depths. As accumulation continued and redistribution of the existing snowpack began to take effect, the observed distribution begins to broaden. As melt began on February 12, 1998 (Figure 3.22h) the distribution shape begins to change, becoming more skewed as some parts of the pack melt faster than others. February 16th and 18th (Figures 3.22i and 3.22j) show the continuation of the melt period with the mean of the distribution decreasing. The distributions on March 2nd and 19th (Figures 3.22k and 3.22l) represent new accumulations later in the season. The observed changes in the snow distribution are similar to those observed by *Luce et al.* [1998] and *Luce and Tarboton* [2000].

Figure 3.23 shows that until snow melt there is very little variation in 30 cm soil temperatures. Once the thickest snowpack is gone, the 30 cm soil temperatures continue to

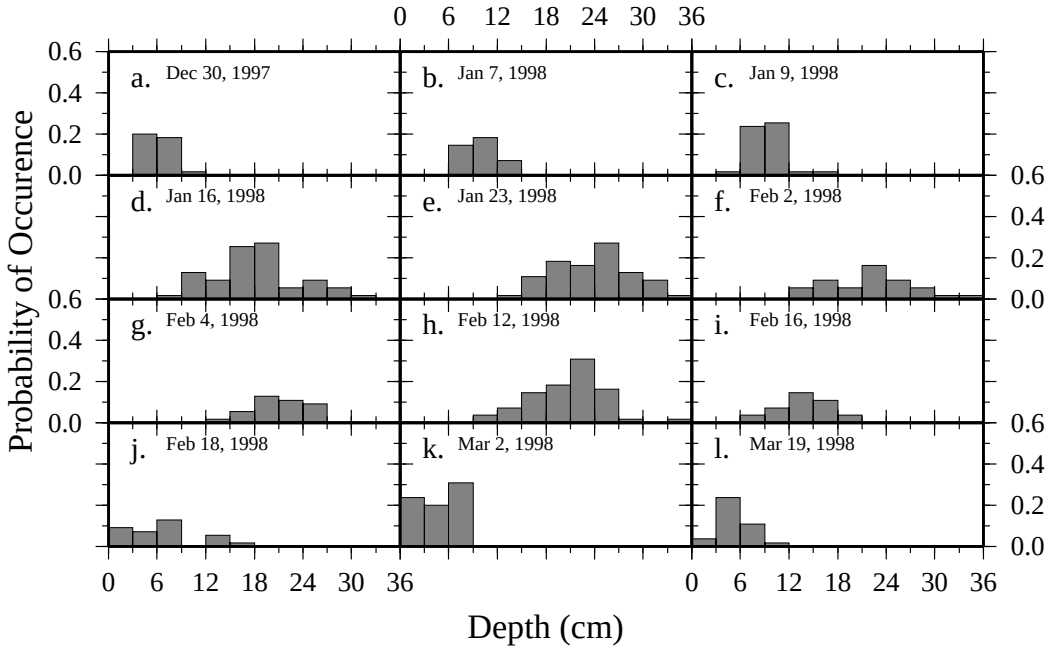

Figure 3.22: Statistical distribution of snow depth for sampled days (a-l).

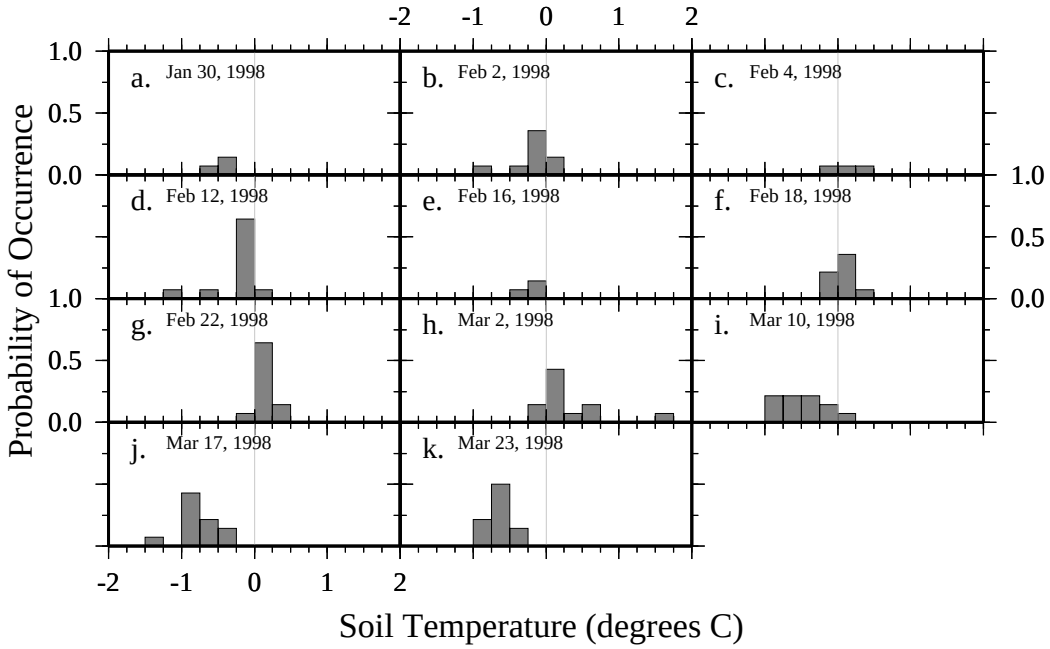

Figure 3.23: Statistical distribution of 30 cm soil temperatures for sample days (a-k).

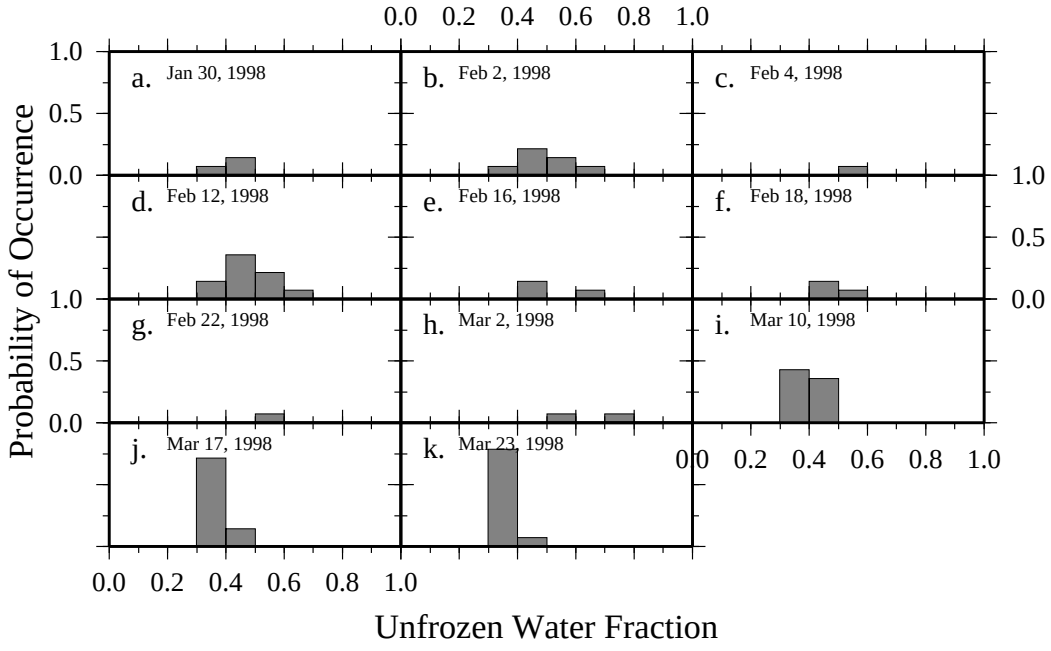

Figure 3.24: Statistical distribution of maximum unfrozen water content at a depth of 30 cm for observed days (a-k). Maximum unfrozen water content is estimated from observed 30 cm soil temperatures (Figure 3.23) using constant soil parameters.

cool and more spread in the values develops. The maximum unfrozen water content in Figure 3.24 is derived from soil temperatures by the method described in *Cherkauer and Lettenmaier* [1999] with constant parameter values: maximum water content of 1, bubbling pressure of 25 cm, and an exponent of 15. The minimal variation in soil temperature shown in Figure 3.23 produces a larger variation in ice content, especially for temperatures near $0°C$ where the maximum unfrozen water content curve changes most quickly.

From Figures 3.22 and 3.23 it is difficult to determine a single distribution for either snow depth or soil temperature. Plotting the cumulative distribution in Figure 3.25 reveals that a uniform distribution could be used to represent most of the variance in both quantities. While the uniform distribution may not describe all of the observed distribution it is

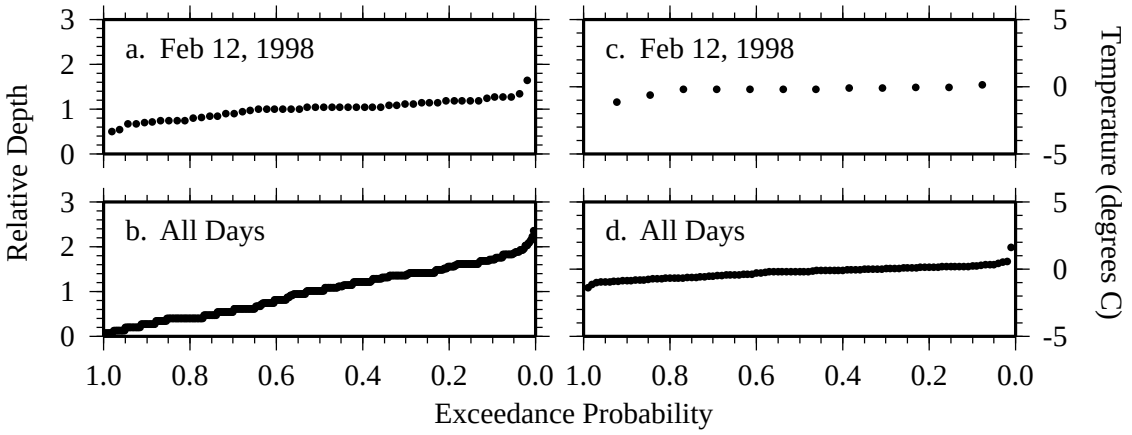

Figure 3.25: Cumulative statistical distribution of: (a) relative snow depth (observed depth divided by mean observed depth) for February 12, 1998, (b) relative snow depth for all days (Winter 1997-1998), (c) 30 cm soil temperature for February 12, 1998 and (d) 30 cm soil temperature for all days of observation (Winter 1997-1998).

relatively straightforward to derive the moments and simple to implement within the VIC model. *Koren* [1980] and *Koren et al.* [1999] made use of a gamma distribution to represent the spatial distribution of frozen soil. *Luce et al.* [1999] and *Luce and Tarboton* [2000] suggested the possibility of using different distributions for the accumulation and ablation phases of the snowpack. Once the spatial algorithms are in place, changing the distributions used should be straightforward.

Table 3.3: Mean, median, and standard deviation of daily observed snow depth linear regression slopes computed for each winter and for all observations.

Winter 1997-1998

	All Depths	Depths > 10 cm
Mean	-11.8	-15.3
Median	-12.3	-15.5
Standard Deviation	5.0	3.0

Winter 1998-1999

	All Depths	Depths > 10 cm
Mean	-14.5	-15.7
Median	-14.5	-15.3
Standard Deviation	3.2	2.5

All Observations

	All Depths	Depths > 10 cm
Mean	-13.2	-15.5
Median	-14.1	-15.5
Standard Deviation	4.3	2.6

The uniform distribution can be described by using the mean depth of the snowpack and its slope. Slopes were derived by fitting a linear regression to the cumulative distributions for each day of observations and averaging. Average slopes along with the median and standard deviations for both years of observations are shown in Tables 3.3 and 3.4.

Snow depth slopes vary on the order of 20% between years when all days of observation are used. If, however, only days with mean snow depths depths greater than 10 cm are used, the difference between years drops to less than 3% and the standard deviations for both years are also reduced. Observations of spatial snow depths across the Rosemount field station indicate that for average snow cover greater than 10 cm, the distribution of snow depths was more uniform. Coverage also tends to be complete (see Tables 3.5 and 3.4.2).

Table 3.4: Mean, median, and standard deviation of daily observed soil temperature linear regression slopes (°C) computed for each winter and for all observations.

Winter 1997-1998

	5 cm Depth	30 cm Depth	60 cm Depth
Mean	N/A	-0.8	-1.9
Median	N/A	-0.8	-1.7
Standard Deviation	N/A	0.3	0.4

Winter 1998-1999

	5 cm Depth	30 cm Depth	60 cm Depth
Mean	-1.7	-1.6	-1.9
Median	-1.5	-1.1	-1.5
Standard Deviation	0.8	1.5	1.3

All Observations

	5 cm Depth	30 cm Depth	60 cm Depth
Mean	-1.7	-1.3	-1.9
Median	-1.5	-0.9	-1.7
Standard Deviation	0.8	1.3	1.0

Table 3.5a: Observation statistics for snow depth during the winter of 1997-1998.

Date	Total Observations	Bare Observations	Mean Snow Depth (cm)
December 30, 1997	21	0	5.7
January 7, 1998	21	0	9.7
January 9, 1998	29	0	8.9
January 16, 1998	53	0	17.9
January 23, 1998	53	0	23.3
January 30, 1998	21	0	23.5
February 2, 1998	29	0	21.6
February 4, 1998	21	0	20.8
February 12, 1998	51	0	20.3
February 16, 1998	21	0	13.5
February 18, 1998	29	9	6.0
March 2, 1998	52	11	4.1
March 19, 1998	21	0	4.7

Thinner average snowpacks are complete in the early accumulation period, but when they are observed in the melt season there will be observed bare patches.

Table 3.4 shows average slopes for all three depths of temperature observations. The average slope of 30 cm temperatures changes by a factor of two between years, while the slope of the 60 cm temperatures remains the same. Standard deviations increase for both depths in the second winter. No temperatures were observed at a depth of 5 cm in the first year, so a comparison between years cannot be made.

3.5 Discussion

Field observations made at the University of Minnesota's Rosemount Agricultural Research Experiment Station from 1997 to 2000 show that even within a small, fairly uniform area frozen soils and snow cover can vary significantly. These distributions affect both the timing and rate of snow melt and timing and rate of infiltration into the locally frozen soil. The

Table 3.5b: Observation statistics for snow depth during the winter of 1998-1999.

Date	Total Observations	Bare Observations	Mean Snow Depth (cm)
December 28, 1998	47	4	3.5
January 15, 1999	8	0	15.8
January 21, 1999	49	0	19.7
January 28, 1999	21	0	21.4
February 4, 1999	21	0	17.5
February 8, 1999	49	0	13.7
February 9, 1999	49	0	12.0
February 22, 1999	11	9	9.8
February 23, 1999	15	8	5.1
March 11, 1999	61	0	18.4
March 12, 1999	53	0	15.1
March 15, 1999	71	8	7.4
March 16, 1999	49	14	5.8
March 17, 1999	49	37	4.9
March 18, 1999	49	39	5.0
March 19, 1999	49	47	9.0

distribution of soil temperatures cannot be completely attributed to the distribution of snow cover and so it must be assumed that soil moisture content and soil physical properties are also important.

The spatial distribution of snow changes through the season as the pack goes through periods of accumulation and ablation. For days when the mean observed snow depth was greater than 10 cm, however, a uniform statistical distribution represents most of the pack variability. The distribution of soil temperatures is more difficult to describe and changes with depth, but the more important control on infiltration is soil ice content, for which a uniform soil temperature distribution may be adequate.

Chapter 4

REPRESENTATION OF SPATIAL VARIABILITY IN SNOW AND FROST

The spatial distribution of frozen soil and snow cover at the start of the spring melt season plays an important role in the generation of spring runoff and in the exchange of energy between the land surface and the atmosphere. Ice in the soil reduces its infiltration capacity, resulting in a higher percentage of snow melt and spring precipitation being partitioned into surface runoff. In order to improve the model's representation of the underlying processes, a frozen soil algorithm was added to the variable infiltration capacity (VIC) macroscale hydrologic model by *Cherkauer and Lettenmaier* [1999]. The algorithm solves for soil ice contents separately within each vegetation type [*Cherkauer and Lettenmaier*, 1999]. This yields different frozen soil characteristics in forested and open areas, as has been documented by field observations [*Kienholz*, 1940; *Pierce et al.*, 1958; *Dingman*, 1975; *Shanley and Chalmers*, 1999]. The algorithm does not, however, simulate the spatial distribution of ice content within each vegetation type. *Stahli et al.* [1996] showed that infiltration into frozen soil is underestimated by models that simulate uniformly frozen soil. Surface water will likely find areas of higher infiltration capacity as it flows across the surface, thus the response to frozen soils is likely to be very different than would be predicted by a spatially unvarying algorithm.

This chapter describes a generalization of the snow accumulation and ablation processes represented within the VIC model [*Cherkauer and Lettenmaier*, 1999]. As with the *Cherkauer and Lettenmaier* [1999] frozen soil algorithm, the snow algorithm does not account for the spatial variation of snow properties within each vegetation type [*Cherkauer and Lettenmaier*, 1999]. While new snow is often fairly uniform in its coverage, drifting and differences in melt caused by topography and local shading can result in highly variable snow coverage by the onset of the melt season [*Gray and Male*, 1981; *Marsh and Pomeroy*,

1996; *Shook and Gray*, 1997; *Luce et al.*, 1998]. The melt rate of partially snow-covered areas has been observed to be significantly higher than that of fully covered regions due to the advection of sensible heat from bare to snow covered areas [*Marsh and Pomeroy*, 1996; *Marsh et al.*, 1997]. Snow-free soil also heats faster than snow-covered regions producing higher sensible heat fluxes. By accounting for a mix of snow-covered and snow-free areas the sensible heat flux exchange between the ground surface and atmosphere does not change abruptly when snow cover disappears.

This chapter describes the development and testing of algorithms representing subgrid spatial variability in snow and frozen soil. The underlying spatial probability distributions were derived from field observations conducted at the University of Minnesota's Rosemount Agricultural Experiment Station (see Chapter 3) during the winters of 1997-1998 and 1998-1999. Added to the VIC model, these algorithms are shown to have improved the representation of cold season processes over the algorithms described by *Cherkauer and Lettenmaier* [1999]. Tests simulations with the new algorithms using data from the Rosemount field site and the St. Croix River, Wisc. are described.

4.1 VIC Model Structure

Liang et al. [1994] describe in detail the formulation of the VIC model with two soil layers; therefore, only a summary is provided here. A third soil layer was added by *Liang et al.* [1996b] who determined that a thin top layer (5-15 cm) significantly improved evapotranspiration predictions in arid climates. A more recent generalization of the model allows the user to change the number of soil layers, although all previous applications have used either two or three layers. The VIC model uses a mosaic-type representation of surface cover, which allows N vegetation types within each grid cell as shown in Figure 4.1. Vegetation can intercept precipitation, or precipitation can reach the ground surface as throughfall. Water can also reach the soil surface as snowmelt.

The amount of infiltration, i, is controlled by a variable infiltration curve, which is based on the available moisture content of the top two layers, $W_0 + W_1$. Water that cannot infiltrate is removed from the cell as runoff, R. Infiltrating water first fills the thin

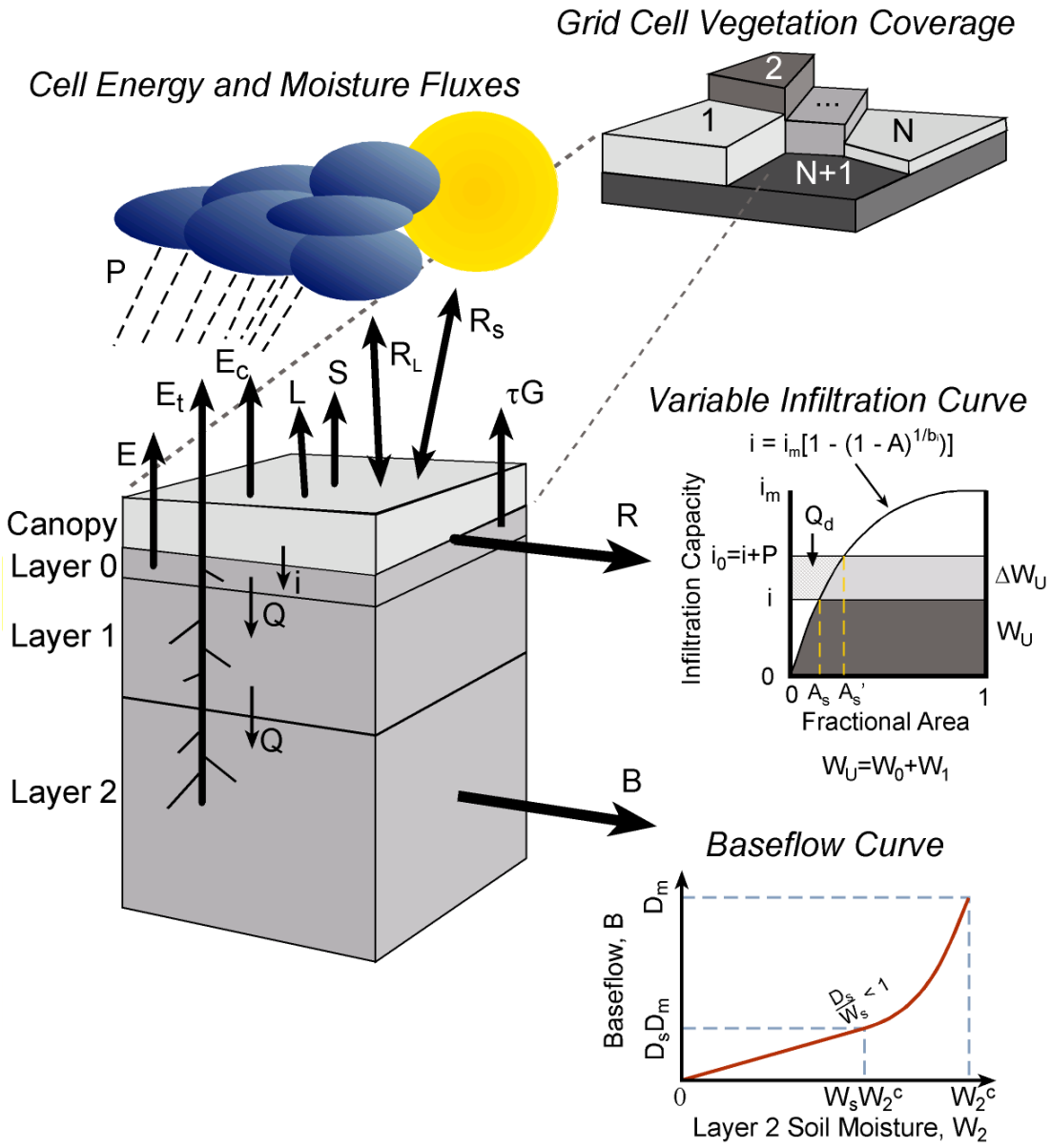

Figure 4.1: Schematic of the variable infiltration capacity (VIC) macroscale hydrologic model with mosaic representation of vegetation coverage and three soil moisture layers.

top layer, which was set to 10 cm here, then the excess infiltration is added to the second layer. Water can leave the top two layers only through evapotranspiration, E_t, or by gravity drainage to the next lower layer, Q_{01} and Q_{12}. The bottom layer loses water through both evapotranspiration and baseflow, B. Baseflow is generated using a non-linear empirical relationship based on the soil moisture of the bottom layer, W_2.

The surface energy balance over bare soil is [*Liang et al.*, 1994]

$$R_n = H + \rho_w L_e E + G + \Delta H_s \tag{4.1}$$

where R_n is the net radiation ($W\ m^{-2}$), H is the sensible heat flux ($W\ m^{-2}$), ρ_w is the density of liquid water ($kg\ m^{-3}$), L_e is the latent heat of vaporization ($J\ kg^{-1}$), E is evaporation (m), $\rho_w L_e E$ is the latent heat flux ($W\ m^{-2}$), G is the ground heat flux ($W\ m^{-2}$), and ΔH_s is the change in energy storage in a layer of air just above the surface ($W\ m^{-2}$). This equation is modified to solve for the surface energy balance above a vegetation canopy, if present, by multiplying the ground heat flux by an attenuation factor, t, which accounts for the reduction of outgoing ground heat flux by vegetation [*Liang et al.*, 1999].

When the model is implemented over a grid mesh (*i.e.* watershed), evaporation, energy fluxes, runoff and baseflow are predicted independently for each grid cell. Streamflow is then simulated at a specified location by routing runoff and baseflow from each grid cell using the method of Lohmann *et al.* [*Lohmann et al.*, 1998a, a].

The VIC model has been implemented at spatial resolutions from 1/8° to 2° to simulate continental scale watersheds in a variety of climates [*Liang et al.*, 1994; *Abdulla et al.*, 1996; *Liang et al.*, 1996a, b; *Nijssen et al.*, 1997; *Liang et al.*, 1998; *Lohmann et al.*, 1998c, b; *Wood et al.*, 1998; *Cherkauer and Lettenmaier*, 1999; *Liang et al.*, 1999], as well as to simulate global soil moisture [*Schnur and Lettenmaier*, 1997]. Recent work in the Upper Mississippi River basin for the GEWEX (Global Energy and Water Balance Experiment) Continental Scale - International Project (GCIP) required that the model be modified for better performance in cold regions with the addition of a new snow accumulation and ablation algorithm, as well as a frozen soil algorithm [*Cherkauer and Lettenmaier*, 1999]. These algorithms are described in the following sections.

4.1.1 Frozen Soil Algorithm

The motivation for development of the frozen soil algorithm was to represent the effects of seasonally frozen ground on surface hydrologic response and the surface energy balance, at a level of complexity consistent with the previously developed VIC algorithms [*Cherkauer and Lettenmaier*, 1999; *Liang et al.*, 1994, 1999]. In this spirit, the VIC soil moisture transport scheme was retained and the thermal and moisture fluxes are solved separately. At each time step, thermal fluxes through the soil column are solved prior to the prediction of soil layer ice content. Subsequently, moisture fluxes are computed using the updated ice contents. Finally, soil thermal properties for the next time step are estimated from the revised distribution of soil moisture and ice. Details of the thermal and moisture flux solutions are discussed in *Cherkauer and Lettenmaier* [1999], which has been included as Appendix B. The research and development of this algorithm serve as the foundation from which an algorithm that represents spatial variability in frozen soil characteristics has been developed.

4.1.2 Snow Accumulation and Ablation Algorithm

The snow algorithm is a minor variation of the two-layer model used in the Distributed Hydrology-Soil-Vegetation Model (DHSVM)[*Storck and Lettenmaier*, 1999]. The DHSVM algorithm employs two snow layers of variable thickness. A thin surface layer is used to solve the surface energy balance, while the bottom or pack layer is used to simulate deeper snowpacks. It also incorporates a snow interception algorithm that allows snow to be retained in an overstory, if present. For use with the frozen soil algorithm in the VIC model, heat exchange with the ground and a snow compaction algorithm were added by *Cherkauer and Lettenmaier* [1999]. The snow surface temperature is propagated through the pack assuming a linear temperature profile and is iteratively balanced with the ground heat flux. Snow depth, required for determining the heat flux through the pack, is estimated by compressing the pack under the weight of new snow and through densification as the snow pack ages.

4.2 Subgrid Variation in Spatial Snow Properties

Field observations show that the maximum rate of snow melt occurs when a basin is partially snow-covered [*Shook et al.*, 1993]. As the snowpack melts and becomes discontinuous, sensible heat becomes a major source of turbulent melt energy at the snowpack edges [*Shook et al.*, 1993], thereby increasing the melt rate relative to that predicted from radiative energy alone. The two-layer snow algorithm implemented in the VIC model assumes that the snow cover is uniform within each vegetation type and elevation band. This implies that the model should underestimate the melt rate of thin, discontinuous snowpacks. Observations of snow melt conditions at Rosemount, Minn., (Chapter 3) clearly show that shallow snow packs in open fields become discontinuous during melt and after redistribution by wind. Runoff and the ponding of melt water was also observed to increase at Rosemount once the snow pack became discontinuous.

To improve the VIC model's simulation of melt events a new algorithm was developed to represent the effects of a partial snowpack. The new algorithm affects the surface energy balance in two ways: (1) it allows for an increasing fraction of snow-free ground to participate in the surface energy balance and (2) it includes the advection of sensible heat from the snow-free fraction in the energy balance of the snowpack. This section describes the development, testing and validation of the partial snow cover algorithm.

4.2.1 Algorithm development

The spatial snow algorithm consists of two parts: one that controls processes when the snow pack no longer covers the entire cell area and another that controls the advection of sensible heat from snow-free areas.

Partial snow cover

During snow accumulation the snowpack is assumed to cover the ground surface completely (Figure 4.2a). Once melt begins the coverage fraction, P_s, is adjusted according to the the depth of the snowpack at the current time step. As long as the pack depth is greater than the minimum depth required for full coverage, SD_{min}, snow cover is continuous (Figure

4.2b). Once the pack depth falls below SD_{min} the coverage fraction is calculated based on the assumption of a uniform distribution (see Chapter 3) (Figure 4.2c), which can be described using the equation:

$$P_s = \frac{2\overline{SD}}{SD_s} \tag{4.2}$$

where $\overline{SD}$ is the mean snow depth for the current time step and SD_s is the negative slope of the distribution with respect to the fractional coverage area (where 1 represents full coverage). Because the distribution is uniform, SD_s is equal to the negative of the maximum snow depth, -SD_{min}, when the snow just covers 100% of the cell.

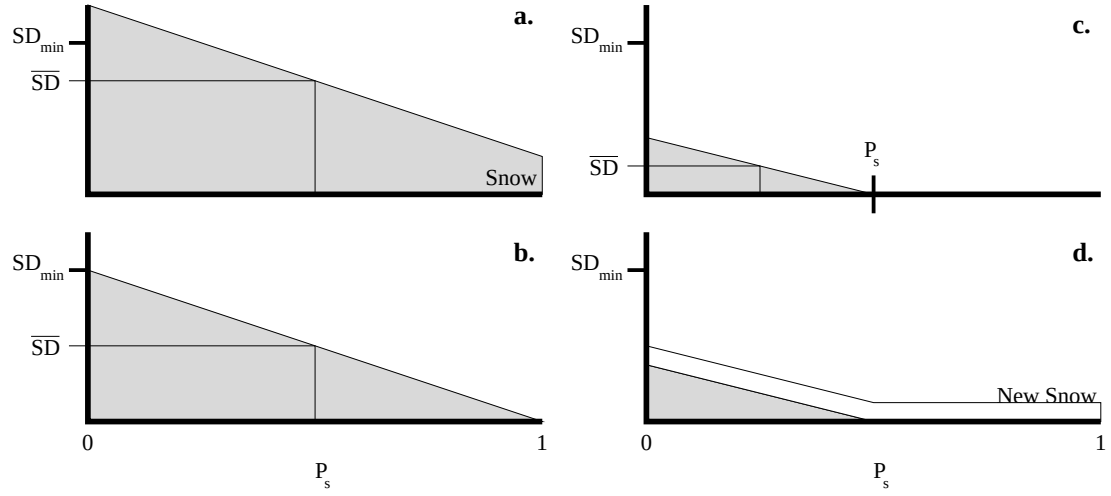

Figure 4.2: Spatial snow algorithm schematic where P_s is the fractional snow coverage, $\overline{SD}$ is the average snow depth and SD_{min} is the minimum snow depth for complete snow cover: (a) deep snowpack that completely covers the area, (b) snowpack depth equal to minimum depth for full coverage, (c) snowpack covers less than the full cell area, and (d) new snow accumulation over an established snowpack distribution.

There are two special cases to account for: (1) the melt of thin accumulating snowpacks and (2) fresh snow on a partially snow free grid cell. If snowpack depth does not exceed SD_{min} prior to a melt event, the algorithm computes a new distribution slope set to the negative of the current maximum snow depth. This reduces the initial change in P_s, which could be quite large for a thin snowpack. The second special case is the accumulation of new snow over a partially covering snowpack. In this case, the depth distribution has

already been established by a previous melt event, but new snow falls evenly across the cell area (Figure 4.2d). If another melt event occurs shortly after this accumulation, it is assumed that the new snow has not been redistributed so the previous spatial distribution of snow cover must be preserved. Therefore the algorithm stores the new snow over the old distribution. If accumulation continues until the mean pack depth exceeds SD_{min}, the old distribution is ignored and the new snow is included when the next melt event requires the calculation of the new distribution. However, if melt occurs before the pack depth exceeds SD_{min}, then the algorithm melts the stored snow before returning to the original distribution.

The snowpack energy balance is found using the energy equation:

$$ME + R_{ns} = H_s + L_s + G_s + (1 - P_s)H_A - \Delta CC \tag{4.3}$$

where ME is the energy available for melt, R_{ns} is the net radiation, H_s is the sensible heat flux, L_s is the latent heat flux, G_s is the ground heat flux, H_A is the advected heat flux and ΔCC is the change in cold content. While snowpack coverage is 100%, Equation 4.3 represents the entire surface energy balance (Figure 4.3a). However, when the pack no longer covers the entire cell area the snow-free region makes use of the standard energy equation:

$$R_{nb} = H_b + L_b + G_b \tag{4.4}$$

where R_{nb} is the net radiation, H_b is the sensible heat flux, L_b is the latent heat flux, and G_b is the ground heat flux (Figure 4.3b).

Average atmospheric energy fluxes are combined using the snow cover fraction resulting in cell area average values. These in turn are used to estimate the ground heat flux:

$$(1 - P_s)R_{nb} = (1 - P_s)(H_b + L_b) + G_s + P_s(H_A - \Delta CC - ME + R_{ns} + H_s + L_s) \tag{4.5}$$

Advection of Sensible Heat

The advection of sensible heat from neighboring snow-free areas plays a major role in the melt of the edges of the remaining snowpack. The snow-free region (Figure 4.3) will be warmer than the snowpack during the day as it absorbs more of the incoming radiation.

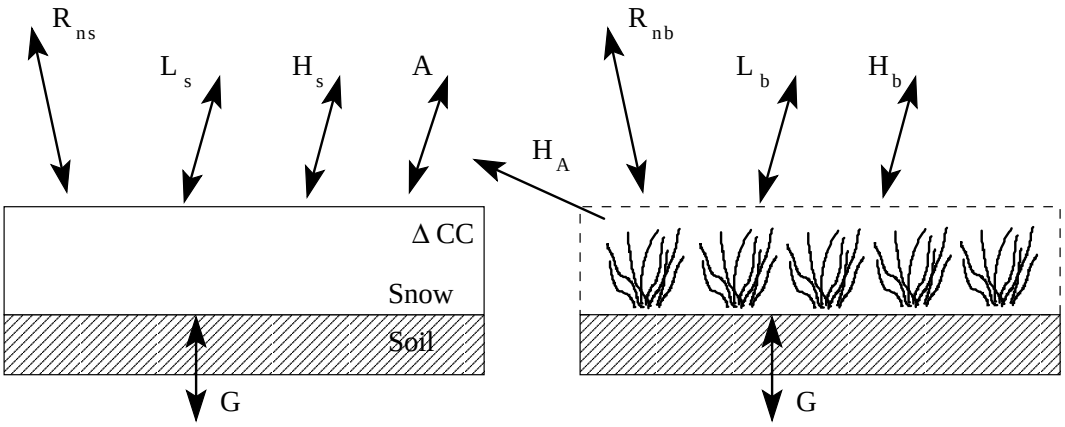

Figure 4.3: Schematic of surface energy fluxes when snow cover is fractional. Turbulent sensible heat H_a increases the melt rate of the pack.

The warm air above the snow-free surface will be transported over the neighboring snow-covered areas by local winds. This process is referred to as the turbulent or advected sensible heat flux.

From observations of the advected sensible heat flux, in the Arctic, during snow melt *Marsh and Pomeroy* [1996] proposed that the portion of the sensible heat flux that is advected to the snow patches (H_A) can be represented as:

$$H_A = \left(\frac{H_b(1 - P_s)}{P_s} \right) (F_s) \tag{4.6}$$

where H_b is the sensible heat from the bare patches and F_s is the fraction of the snow-free area that is advected.

Marsh et al. [1997] observed that the snow melt rate peaks when snow coverage is about 60%, at which time nearly 100% of the sensible heat flux from the bare patches is advected to the snow-covered patches. For larger values of P_s, F_S declines. Between 50% and 20% coverage, F_S appears to decrease exponentially from 0.48 to 0.01 [*Marsh et al.*, 1997]. Values for F_s were not available for coverage fractions less than 20%. These observations were used

to develop an equation for F_s:

$$F_s = \begin{cases} 1.0 & \text{if } P_s > 0.6 \\ \log_{10}^{-1}(3.0P_s - 1.8) & \text{if } P_s > 0.5 \\ \log_{10}^{-1}(5.6667P_s - 3.1333) & \text{if } P_s > 0.2 \\ 0.01 & \text{if } P_s > 0 \end{cases} \tag{4.7}$$

4.2.2 Point Model Tests

Testing for the spatial snow algorithm was conducted using observations from the University of Minnesota's Rosemount Agricultural Experiment Station [*Cherkauer and Lettenmaier*, 1999]. Two simulation cases were run: the first used the original (uniform) snow algorithm and the second used the distributed snow algorithm described above. The slope of the uniform snow distribution was set to the slope of the spatial distribution of snow depth at Rosemount for the winters of 1997-1998 and 1998-1999, 15.5 cm (see Table 3.3). Because the distribution is uniform and the coverage fraction is between 0 and 1, the slope of the distribution is also equal to twice the average snow depth ($2\overline{SD}$).

Calibration

Soil parameters were estimated from several soil surveys conducted at the measurement site and nearby fields. During the winter it was assumed that the field was bare, neglecting the effects of tillage and residue. However, to predict the antecedent soil moisture conditions correctly for each successive winter, summer vegetation cover (corn in this case) was needed. Vegetation type controls evapotranspiration through the summer months, and antecedent soil moisture is very important to the development of early season soil frost. The growth and harvest cycle was simulated by allowing the vegetation height to increase each month starting in April, until a maximum height was reached in August. Harvest (the removal of vegetation) was assumed to take place in October. The LAI was also increased monthly from April to August, and then decreased slightly in the fall as the crop dried out before harvest.

Snow depth was measured in the field using a circle of snow sticks. The number of snow sticks used in the circle varied each winter, as did their location within the field. For

comparison with the model, the mean depth and standard deviation for snow at all snow sticks were computed for each day measurements were collected.

Figures 4.4, 4.5, 4.6 and 4.7 compare simulated snow and frost depths for four winters, 1994-1995, 1995-1996, 1996-1997 and 1997-1998. Simulations for the winter of 1994-1995 (Figure 4.4) were started with initial observed conditions and therefore they show the best early season frost conditions. In the other three winters, the frost front penetrates more rapidly than observed, but by the end of the season it approaches the observed depth more closely. Deviations in initial frost depths may be caused by differences in antecedent soil moisture or by mischaracterizations of early season snow accumulation. However, melt season conditions are more important than early season conditions for predicting the impact of soil frost on spring discharge.

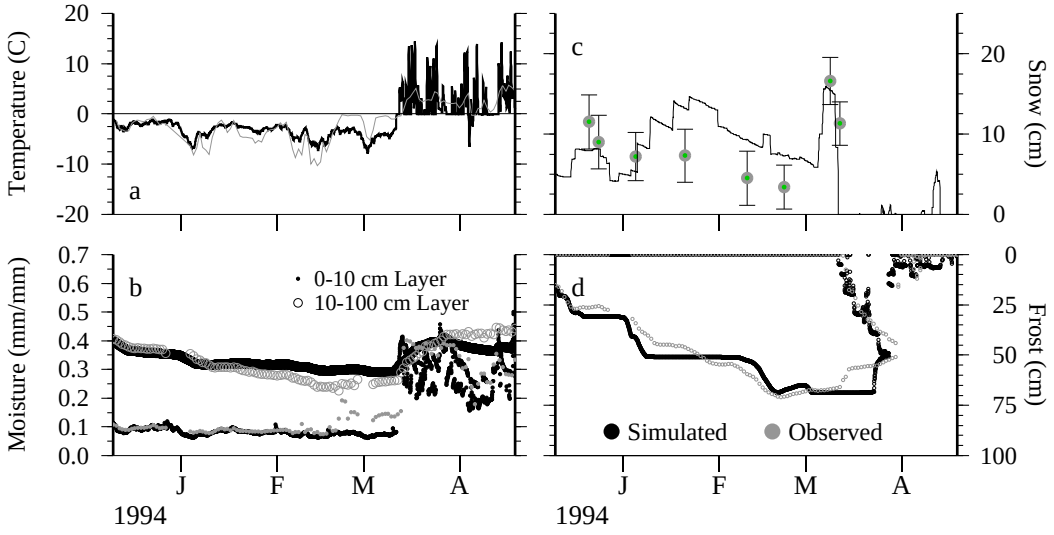

Figure 4.4: Point simulation (black) versus observations (gray) at the Rosemount Agricultural Experiment Station during the winter of 1994-1995 for (a) 5 cm soil temperature, (b) soil moisture content in the top 10 cm (dots) and the next 90 cm (circles), (c) simulated snow depth versus mean (dot) and standard deviation (bars) of observations, and (d) freezing and thawing front depths.

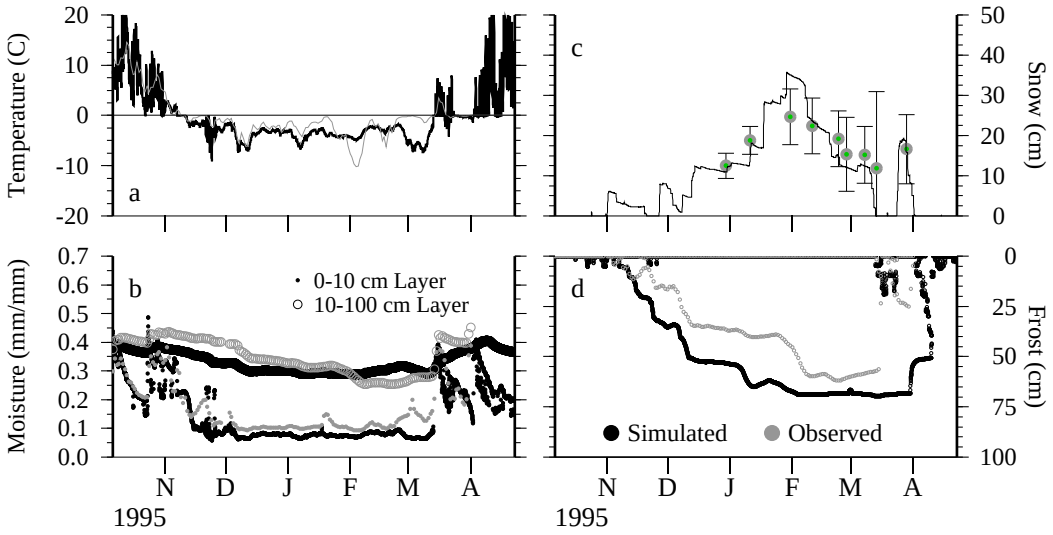

Figure 4.5: Point simulation (black) versus observations (gray) at the Rosemount Experiment Station for the winter of 1995-1996.

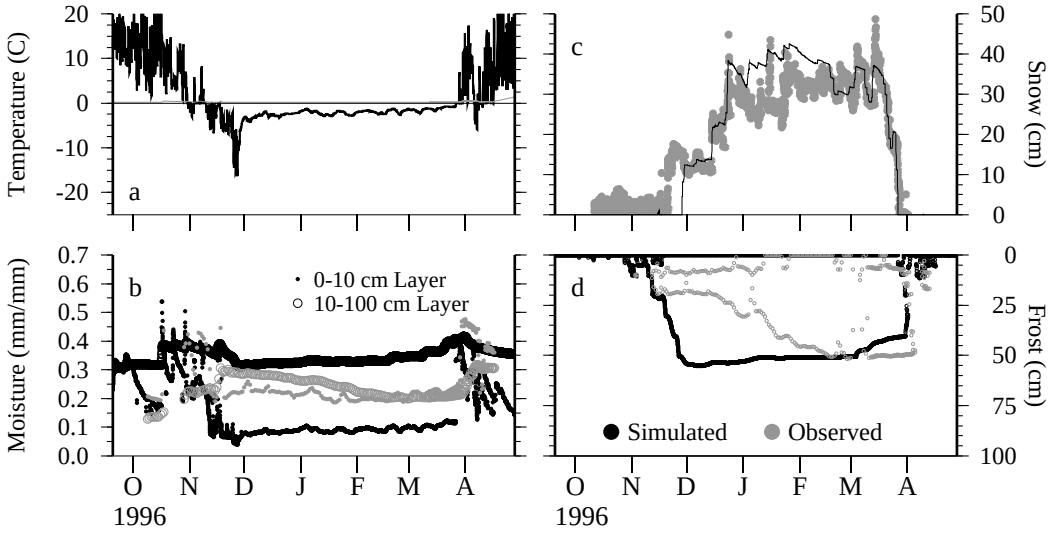

Figure 4.6: Point simulation (black) versus observations (gray) at the Rosemount Experiment Station for the winter of 1995-1996.

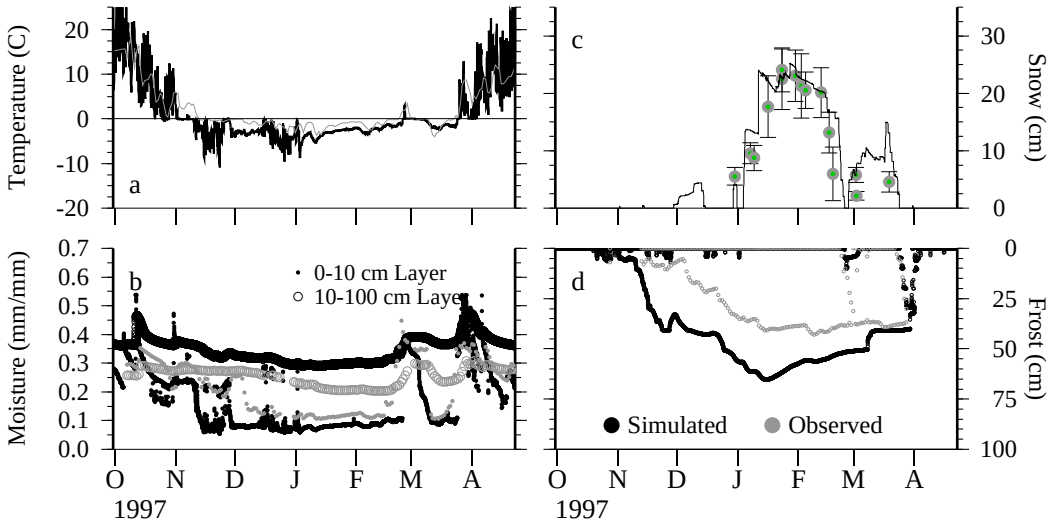

Figure 4.7: Point simulation (black) versus observations (gray) at the Rosemount Experiment Station for the winter of 1995-1996.

Comparisons

Figures 4.8, 4.9, 4.10 and 4.11 compare melt period simulations for the four simulated winters (1994 through 1998). Snowcover during the winter of 1994-1995 is very thin and coverage becomes fractional several times during the winter (Figure 4.8a). When coverage is fractional, the advection of sensible heat flux from the bare fractions (Figure 4.8d) increases the rate of melt (Figure 4.8c). This yields a thinner snowpack for the simulation with fractional snowcover (grey) than for the full cover simulation (black) (Figure 4.8b). It should be noted that there is no visible difference in cumulative melt by the end of the season (cumulative differences due to sublimation are very small). This demonstrates that the spatial snow algorithm does not impact accumulation, only the timing and rate of snow melt.

For both the winter of 1995-1996 (Figure 4.9) and the winter of 1997-1998 (Figure 4.11) the model predicts fractional coverage during the last few days as the snowpack melts. Snow melt rates increase during the period of partial coverage, with the largest differences when the advected sensible heat is strongest. The winter of 1996-1997 (Figure 4.9) has the deepest

snowpack at the time of melt of the four winters simulated. Because the snow cover was deep and melted rapidly there is very little effect from the defined distribution of snowcover.

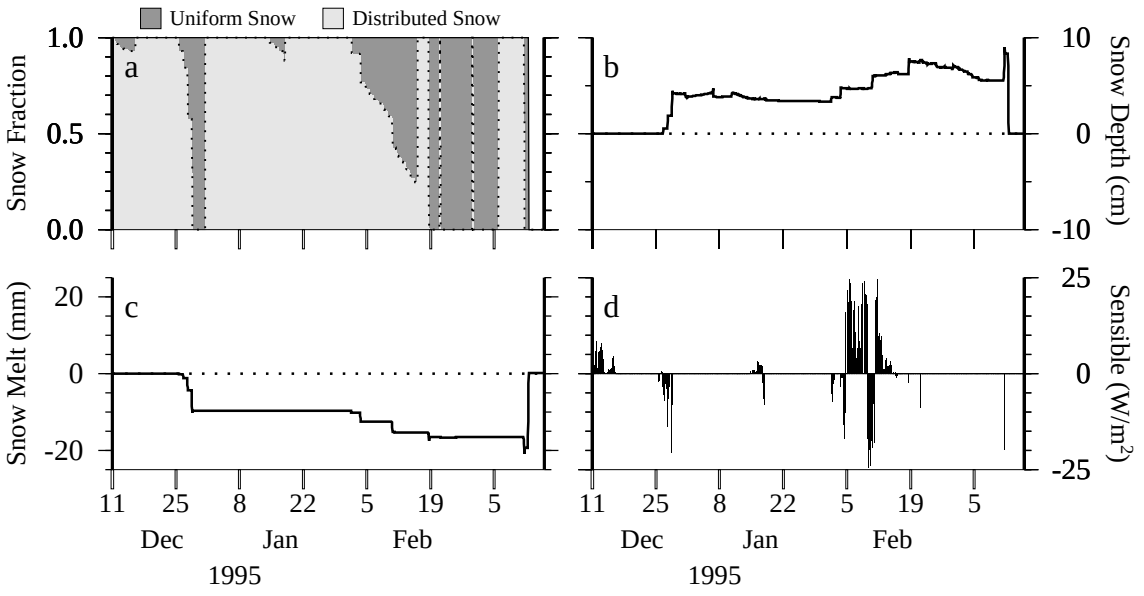

Figure 4.8: Simulated snowpack and energy fluxes for uniformly covering snowpack and uniformly distributed snowpack for the winter of 1994-1995: (a) snow cover fraction: spatially distributed snow cover (light grey) and spatially unvarying snowpack (dark grey), (b) snow depth difference (cm): spatially unvarying snowpack minus spatially distributed snowpack, (c) cumulative snow melt difference (mm): spatially unvarying snowpack minus spatially distributed snowpack, and (d) advected sensible heat (W/m^2) for spatially distributed snowpack. All simulations are at an hourly time step.

4.2.3 Catchment Scale Implementation

To further test the spatial snow algorithm, it was applied to the St. Croix River above St. Croix Falls, Wisc (see Figure 4.12. for the period 1970 to 1990. Weekly flows for the VIC model with spatially unvarying frozen soil and snow cover (*i.e.* the VIC model from *Cherkauer and Lettenmaier* [1999]) are plotted against observations in Figure 4.13. Simulations made use of the daily precipitation data set corrected for wind-induced gauge undercatch as described in Appendix A. In 1972, the peak is overestimated because the

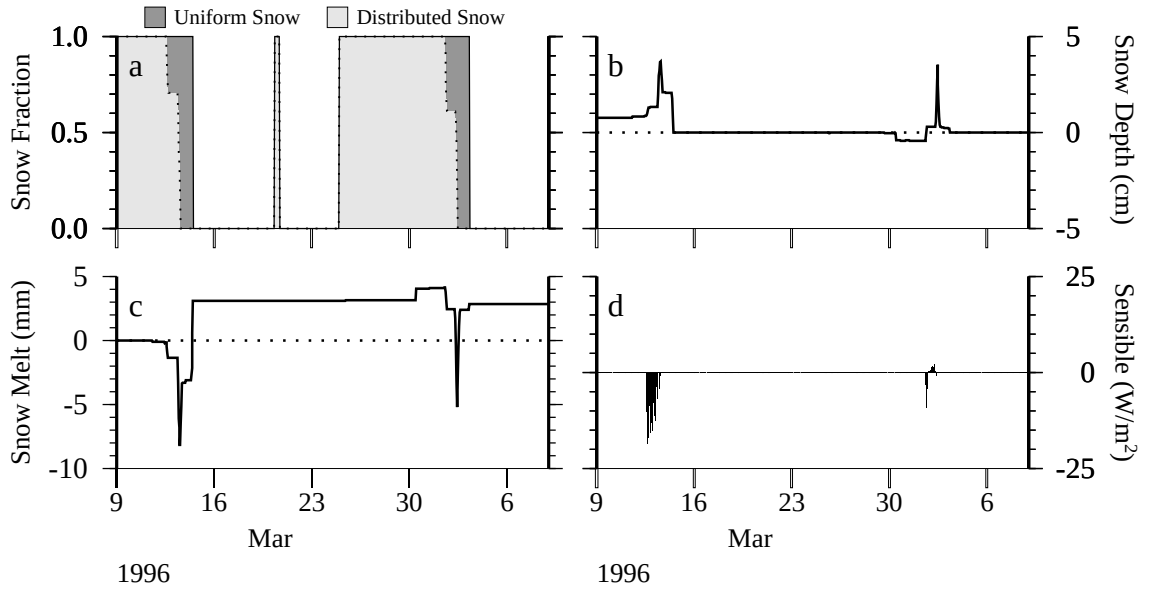

Figure 4.9: Simulated snowpack and energy fluxes for uniformly covering snowpack and uniformly distributed snowpack for the winter of 1995-1996.

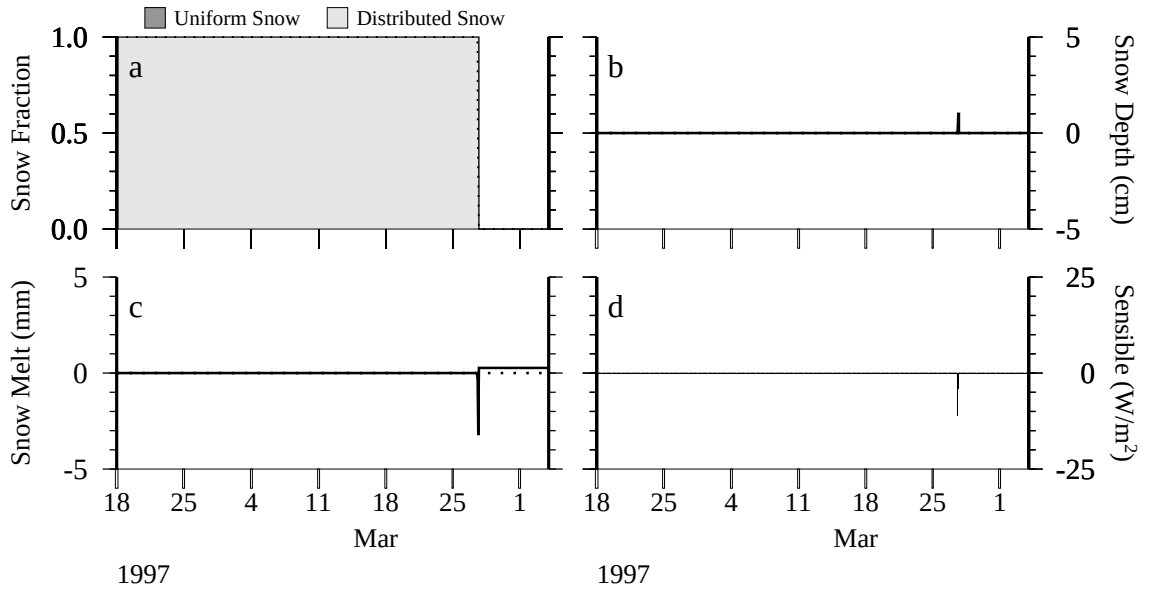

Figure 4.10: Simulated snowpack and energy fluxes for uniformly covering snowpack and uniformly distributed snowpack for the winter of 1996-1997.

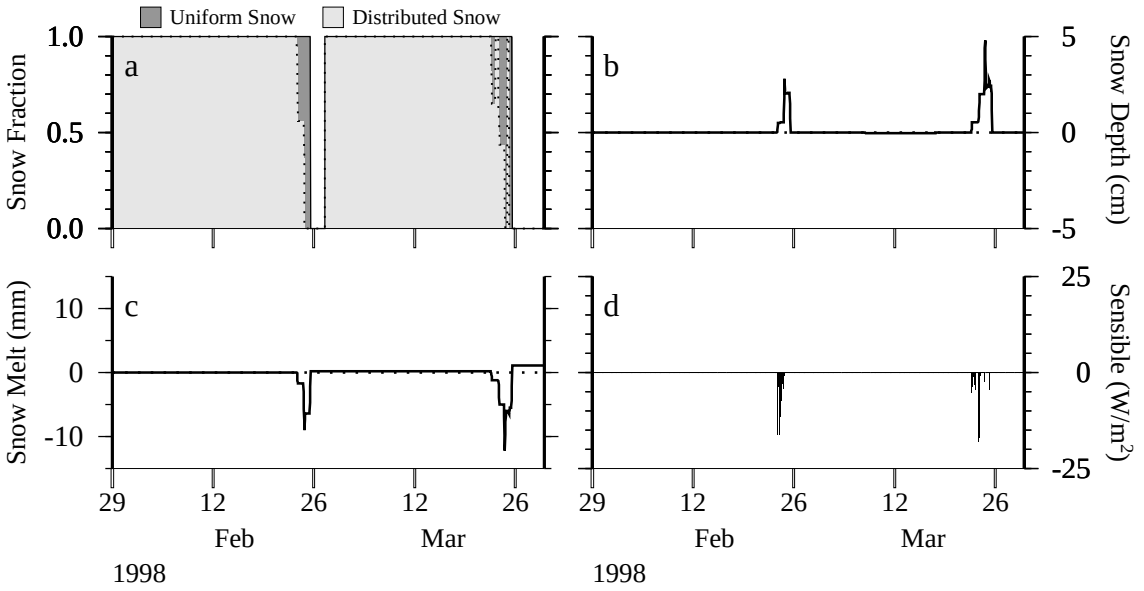

Figure 4.11: Simulated snowpack and energy fluxes for uniformly covering snowpack and uniformly distributed snowpack for the winter of 1997-1998.

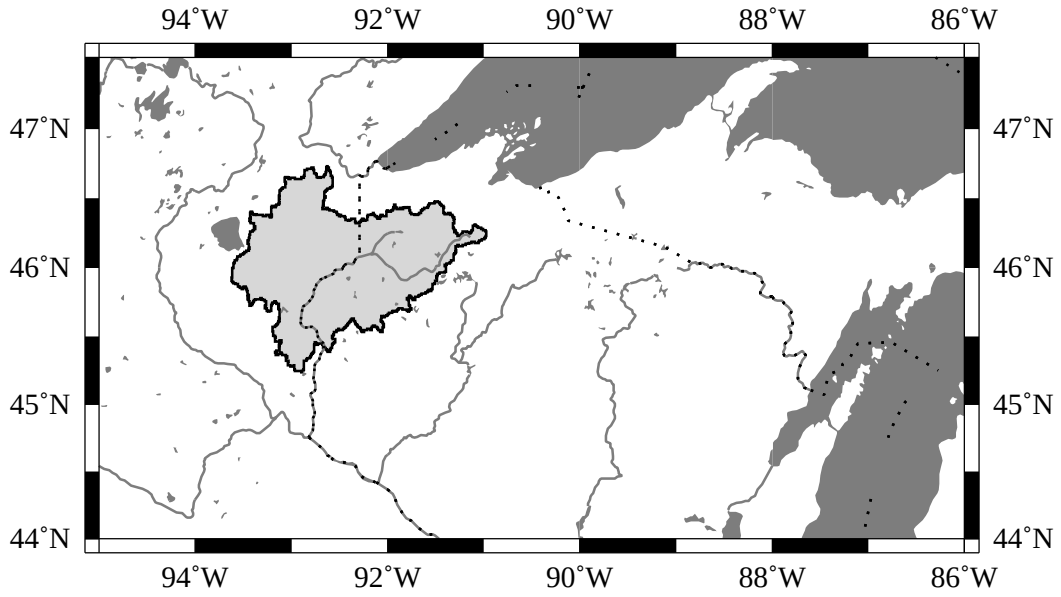

Figure 4.12: Location of the St. Croix River watershed above St. Croix Falls, Wisc. Catchment is shaded light gray.

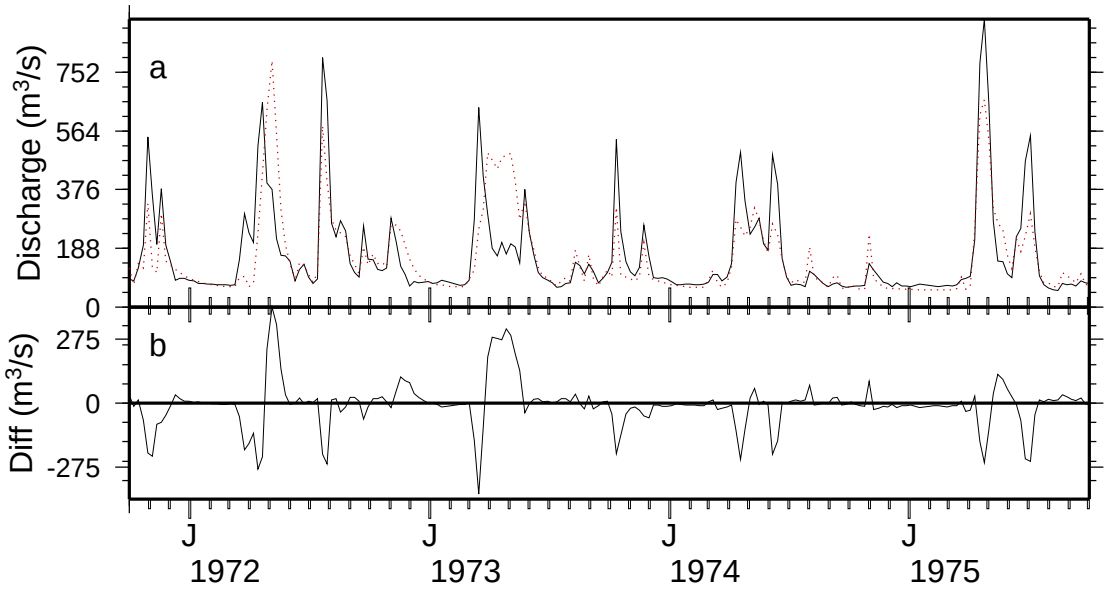

Figure 4.13: Observed (solid) versus simulated (dotted) discharge for the St. Croix River at St. Croix Falls, Wisc. for water years 1971 to 1974: (a) weekly discharge rates and (b) weekly differences (simulated minus observed). Simulated discharge was created using the standard full energy balance VIC model with frozen soil.

simulated snowpack does not experience partial melt in March so the entire pack was present in April. In 1973, snow melt is also late, but the soil contains more ice which lasts longer after snow melt than in 1972. As the ice thaws, soil moisture near the surface remains higher so there is less infiltration and the wetter soils maintain a higher baseflow rate. The winter of 1975 also has a high ice content, but the soil is nearly saturated (including ice content) prior to melt, whereas in 1973 the soil is much drier. In both 1974 and 1975, snow melt occurs at the correct time, so the melt discharge peaks are timed correctly.

Figure 4.14 compares VIC model simulations of the St. Croix basin with and without the spatially distributed snow algorithm. The hydrographs are quite similar in shape (Figure 4.14a), although there are small differences (Figure 4.14b). By the time it reaches St. Croix Falls, the St. Croix River drains 16,162 km^2 and the impact of slight variations in the timing of snow melt caused by the spatial distribution algorithm are mostly obscured.

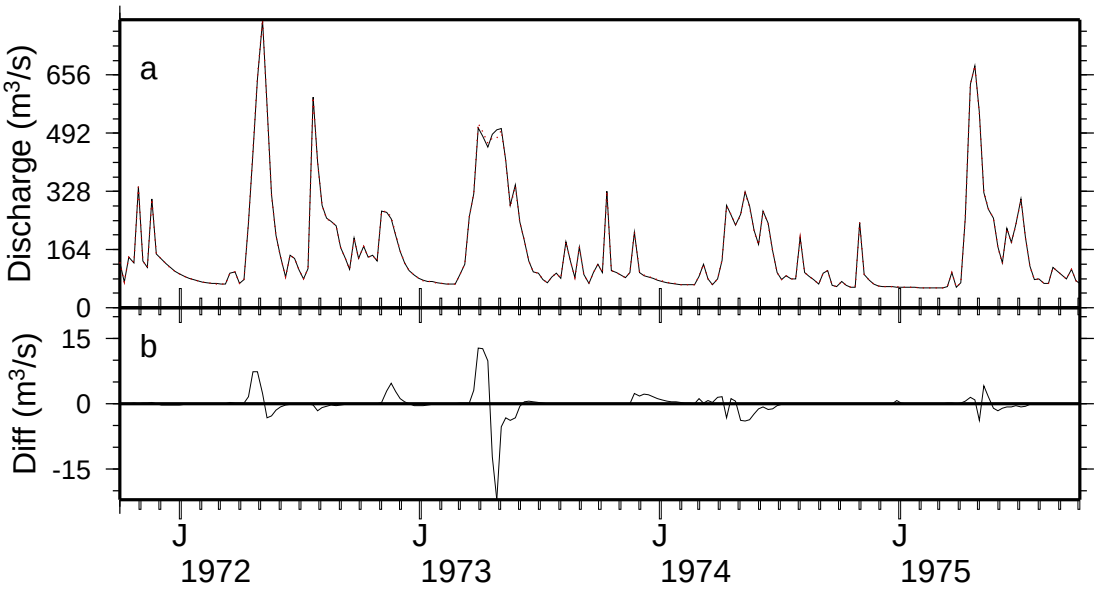

Figure 4.14: Comparison of VIC simulations: (a) full energy balance with frozen soil with no snow distribution (solid) and with spatially distributed snow cover (dotted), (b) differences (with distribution minus without distribution).

The spatial snow algorithm makes a larger difference to the grid cell sensible heat fluxes during melt. As bare ground emerges from under the snowpack, the bare soil surface

is exposed directly to incoming solar radiation. The exposed soil, with its lower albedo, soon becomes warmer than the snowpack surface and increases sensible heat flux exchange with the atmosphere. Figure 4.15 compares model-simulated sensible heat fluxes with and without spatially distributed snow cover. With the spatial distribution, simulated sensible heat fluxes are increased by a maximum of almost 50 W/m^2 on a daily basis during the melt season of February through May 1970 (Figure 4.15a). Average monthly sensible heat fluxes (1971-1975) are increased by the spatial snow algorithm on the order of 2 W/m^2 from February through May (Figure 4.15b). This improved representation of melt season sensible heat fluxes implies that the representation of surface temperatures has also been improved. As noted by *Betts et al.* [1996], improving the representation of surface fluxes during winter seasons is very important for improving global climate simulations.

Figure 4.16 shows the spatial distribution of average April sensible heat fluxes across the St. Croix River basin. Sensible heat increases toward the southern reaches of the basin with and without spatially distributed snow cover (Figures 4.16a and 4.16b respectively). There is, however, no clear pattern in the difference between average April sensible heat values (Figure 4.16c), though they do show that the average sensible heat flux in April is increased using the spatial snow algorithm.

4.3 Spatial Frozen Soil Algorithm

Simulations using the *Cherkauer and Lettenmaier* [1999] frozen soil algorithm had a tendency to overestimate peak flow response to frozen soil. One of the reasons for this is that frozen soils vary spatially. Variations can be caused by differences in the vegetation cover [*Shanley and Chalmers*, 1999] or by the redistribution of snow. The influence of frozen soil can also be affected by the distribution of ice content, either by antecedent precipitation events or by melt or rain inputs once the soil has frozen. In any case, the distribution of ice in the soil has a large effect on infiltration. Water from rain or melting snow will pond or flow off impermeable soil, but over a patch of more permeable soil nearby it will infiltrate. Thus by having a uniform frost layer within each vegetation type, the VIC model algorithm is likely to overestimate the effects of frozen soil on peak flows.

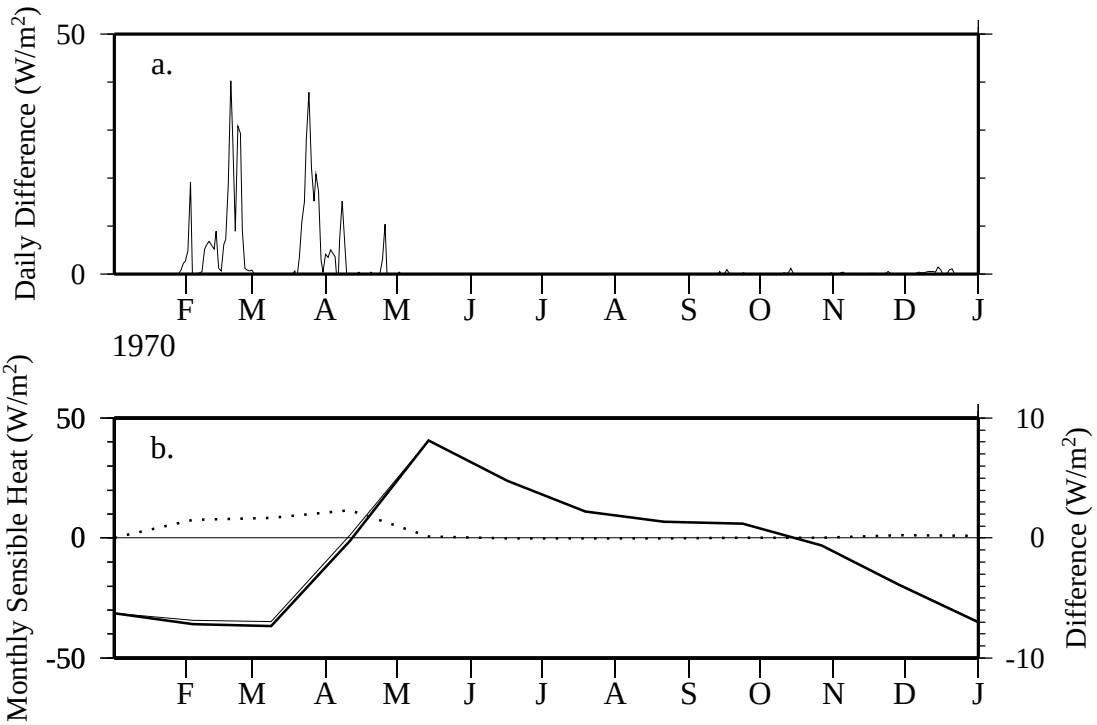

Figure 4.15: Comparison of sensible heat fluxes during spring melt between the model with spatially distributed snow cover and the model with spatially unvarying snow cover: (a) sensible heat flux difference (with spatial distribution minus without spatial distribution) for 1970 and (b) average annual sensible heat fluxes (solid) and sensible heat flux differences (dotted) for the same cell.

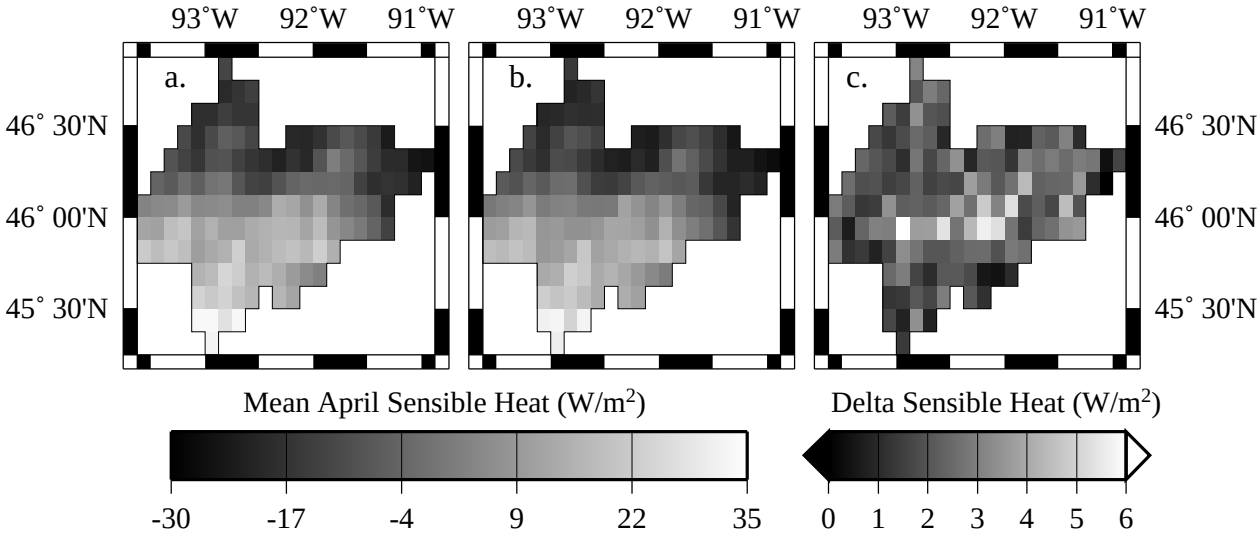

Figure 4.16: Spatial distribution of mean April sensible heat flux for the St. Croix River: (a) with spatially distributed snow cover, (b) without spatially distributed snow cover and (c) difference (with spatially distribution minus without spatial distribution).

4.3.1 Algorithm Development

As with the spatial snow algorithm (see Section 4.2), the spatial frozen soil algorithm makes use of the observed spatial distribution of soil temperatures from the Rosemount field site (see Table 3.4). It is assumed that a uniform distribution with a slope of 1.5 °C is sufficient to represent most of the observed variability. The distribution is then applied to soil temperatures at each soil node (Figure 4.17a) to produce a range of temperatures.

Unfrozen water content for each node is estimated using [*Cherkauer and Lettenmaier*, 1999; *Flerchinger and Saxton*, 1989a]:

$$W_i = W_i^c \left[\left(\frac{1}{g\psi_e} \right) \left(\frac{L_f T}{T + 273.16} \right) \right]^{B_p} \tag{4.8}$$

where W_i is the liquid water content of layer i (mm), W_i^c is the maximum water content of layer i (mm), g is the acceleration due to gravity $(m\ s^{-2})$, L_f if the latent heat of fusion $(J\ kg^{-1})$, T is the soil temperature (°C), ψ_e is the air entry potential (m), and B_p is the pore-size distribution. To account for the spatial variability in soil temperatures, each layer is divided into a series of separate bins that store their own ice content (Figure

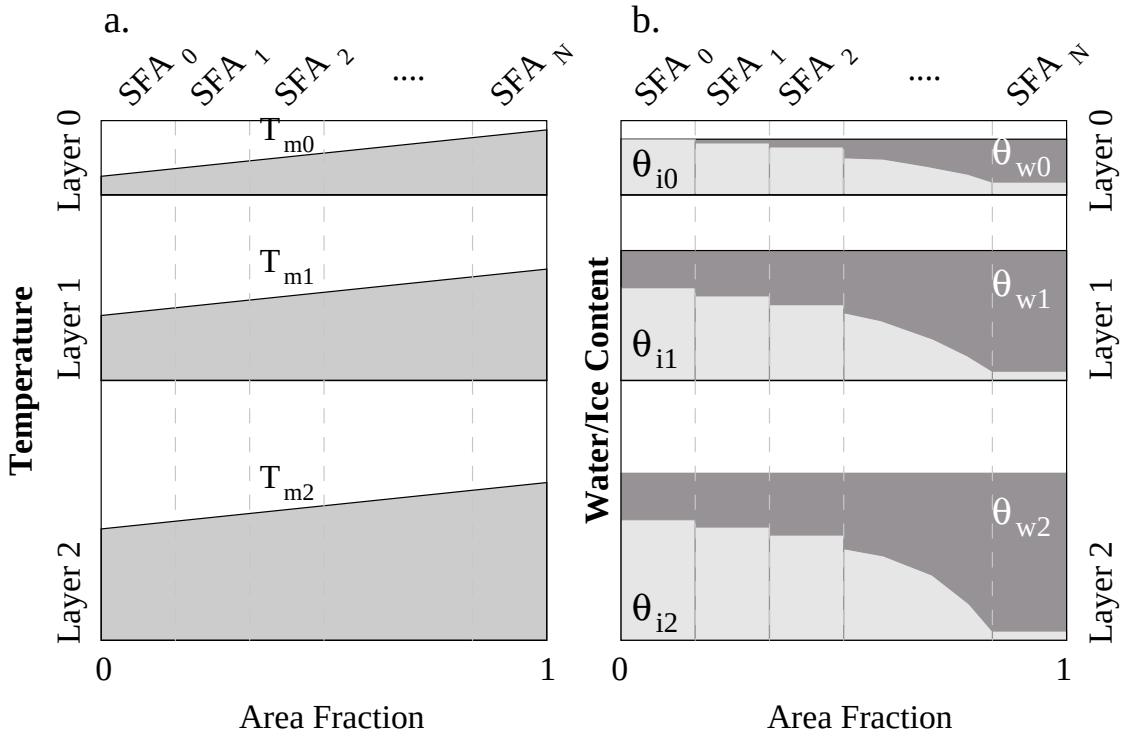

Figure 4.17: Spatial frost algorithm schematic: (a) uniform soil temperature distribution and (b) non-uniform ice content distribution. Layers indicate the three VIC soil moisture layer, T_{mN} is the mean temperature for layer N, θ_{iN} is the ice content for layer N, θ_{wN} is the total moisture content for layer N and SFA_M is the fractional area of bin M.

4.17b). Liquid water is distributed evenly through all of the bins and allowed to drain proportional to the ice content in that bin. Bins with higher ice contents will allow less water to drain, so the total soil moisture drainage for the layer will be reduced. With the spatial distribution of ice content, some bins can restrict almost all drainage, while others can drain virtually unrestricted. The distribution of ice content is also applied to infiltration. Bins with higher ice contents appear to be saturated and restrict infiltration. Because the relationship between temperature and ice content (eqn 4.8) is a nonlinear relationship, the spatial distribution of ice in the soil is not uniform.

4.3.2 Point Model Tests

As with the spatial snow algorithm, the spatial frost algorithm was tested at the Rosemount field site. Two simulations were run with and without the spatially varying frost algorithm. The spatial snow algorithm was not used for either case. Results for the four winters from 1994-1998 are plotted in Figures 4.18, 4.19, 4.20 and 4.21.

There are small differences in the depth of frost, especially in the winters of 1995-1996 (Figure 4.19) and 1996-1997 (Figure 4.20), but these differences have a limited effect on infiltration and runoff. Differences in baseflow are fairly similar between winters, with the spatially distributed model draining 50 mm more soil moisture through the melt period in three of the four winters (Figures 4.18b, 4.19b, 4.20b and 4.21b). Cumulative runoff differences are small in the winters of 1994-1995 (Figure 4.18e) and 1995-1996 (Figure 4.19e). Because the soil is not saturated (Figures 4.18c, 4.19c) during melt, both models can infiltrate the limited amounts of snow melt and precipitation during these years. This means that both models have released nearly the same amount of baseflow within a few weeks of complete thawing of the soil column.

The winter of 1996-1997 shows a decrease of cumulative runoff for the spatially distributed frozen soil algorithm of nearly 50 mm as the deepest snowpack of the four winters melts rapidly over saturated soils in late March (Figure 4.20e). The spatially distributed frost model allows more infiltration, which leaves the site as baseflow. This can be seen in the persistence of the cumulative runoff and baseflow plots in Figures 4.20b and 4.20e.

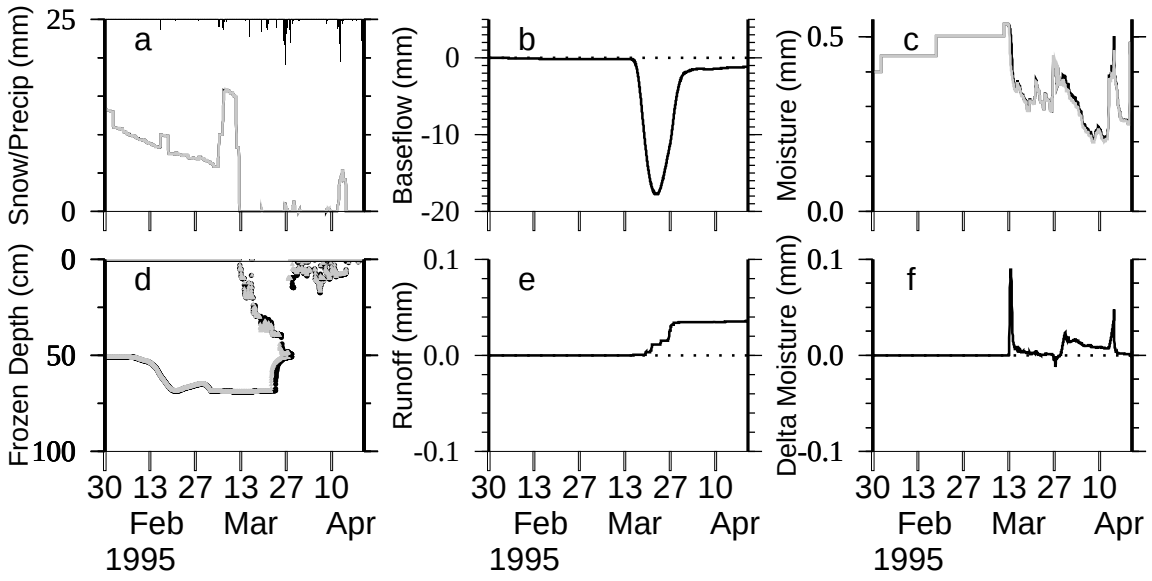

Figure 4.18: Comparison of simulations with spatially unvarying frost (black) and spatially distributed frost (grey) for the Rosemount Experiment Station, winter of 1994-1995: (a) snow depth (cm) and Precipitation (mm), (b) baseflow difference (unvarying frost minus spatially distributed frost) (mm), (c) top layer moisture (mm/mm), (d) frost and thaw depths (cm), (e) runoff difference (unvarying frost minus spatially distributed frost) (mm), and (f) top layer moisture difference (unvarying frost minus spatially distributed frost) (mm/mm). Displayed data represent hourly values.

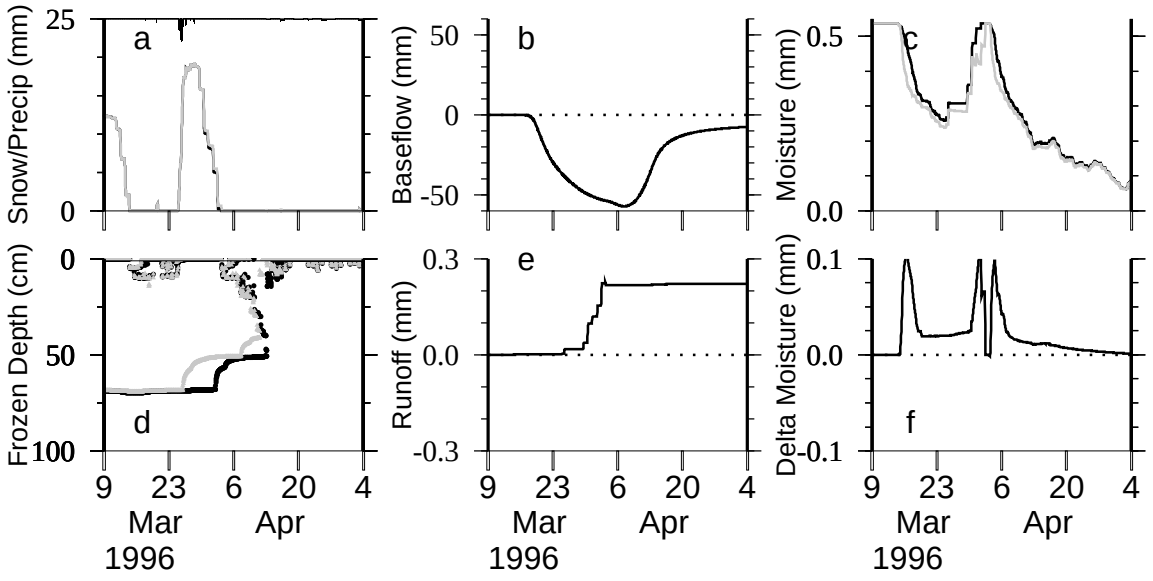

Figure 4.19: Comparison of simulations with spatially unvarying frost (black) and spatially distributed frost (grey) for the winter of 1995-1996.

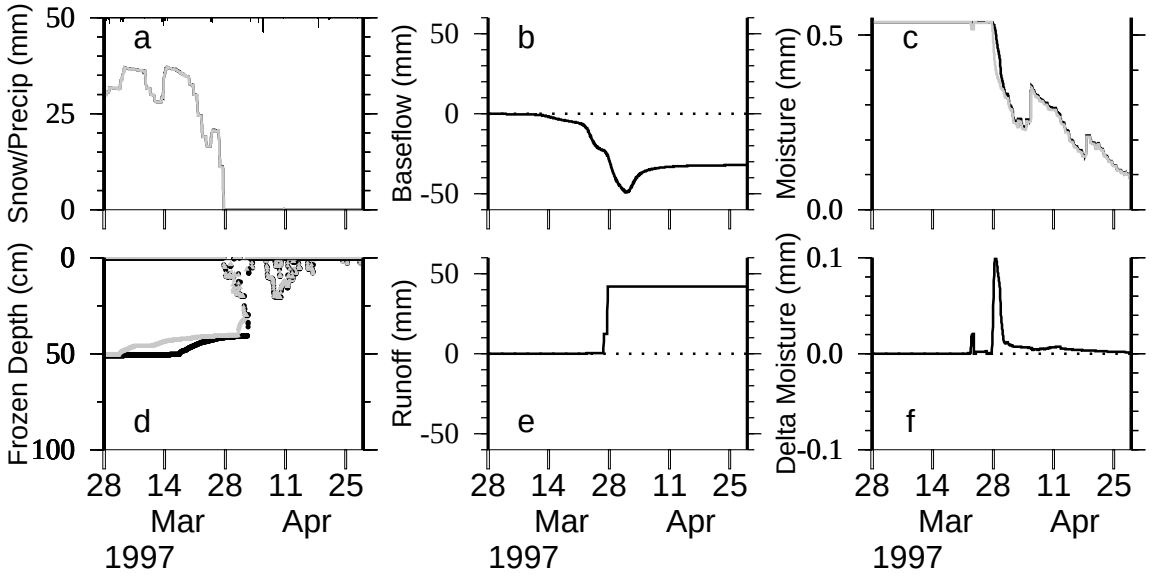

Figure 4.20: Comparison of simulations with spatially unvarying frost (black) and spatially distributed frost (grey) for the winter of 1996-1997.

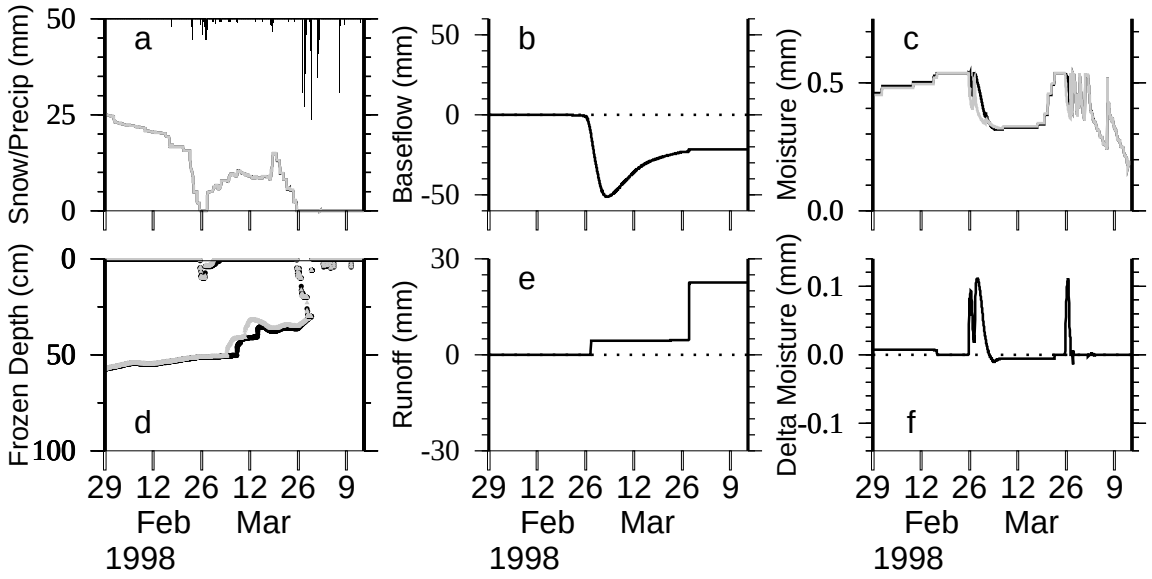

Figure 4.21: Comparison of simulations with spatially unvarying frost (black) and spatially distributed frost (grey) for the winter of 1997-1998.

The snowpack in the winter of 1997-1998 is thinner than in the previous winter and the top soil layer only saturates during the time of peak melt rate, yet it has a difference of almost 30 mm in cumulative runoff (Figure 4.21e). This is caused not by snowmelt but by heavy rains at the end of March and beginning for April (Figure 4.21a). Melt from the snowpack only causes about 5 mm more runoff than for the spatially uniform model; the largest change in the cumulative baseflow occurs only after the rain event has started.

4.3.3 Catchment Scale Tests

The spatial frost algorithm was applied to the St. Croix River to test its effect at a large scale. Figure 4.22 compares VIC model simulated flow with spatially distributed frost and with spatially unvarying frost. Baseflow during winter is slightly higher with the spatially distributed algorithm but the largest differences occur during the spring peak flow event. The spatially distributed frost model predicts higher peaks in the springs of 1973 and 1974, as the spring melt event is dominated by its quicker baseflow response. In the spring of 1975, the unvarying spatial model peaks higher in a runoff-dominated event.

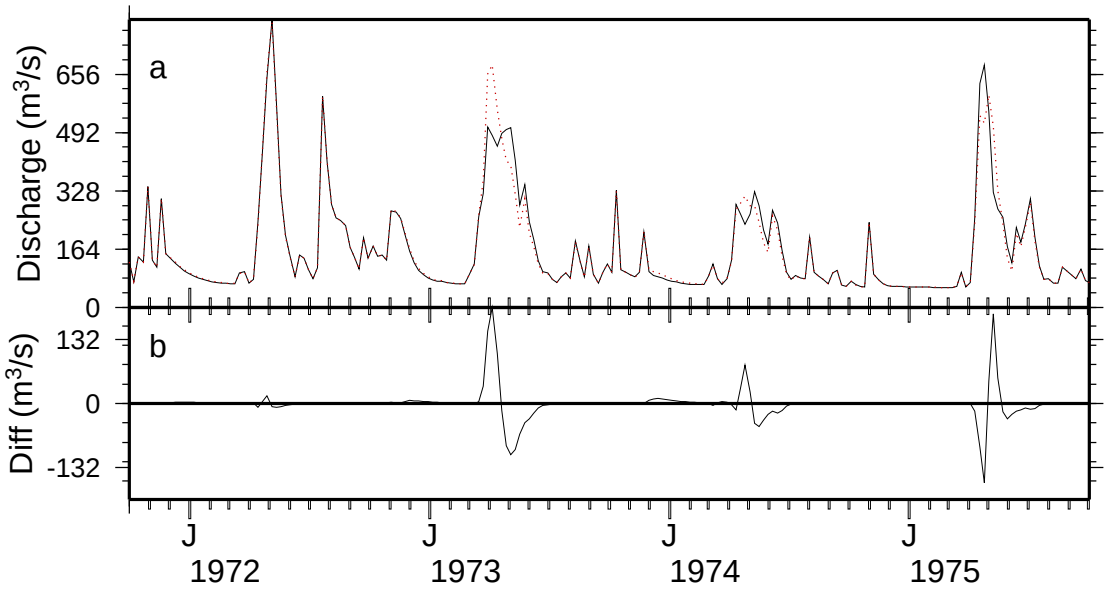

Figure 4.22: Comparison of VIC model simulations for the St. Croix River: (a) spatially unvarying frost (solid) and spatially distributed frost (dotted), (b) differences (with distribution minus without distribution).

Figure 4.23 compares simulated flows using the spatially distributed frost algorithm with those using both the spatially distributed snow and frost algorithms. As was seen in Figure 4.14 the spatial snow algorithm has very little effect on the basin discharge and in this case is clearly dominated by the effects of the spatial frost algorithm.

Finally, Figure 4.24 compares the VIC model simulated discharge for the St. Croix River using both the spatial snow and frost algorithms with observed discharge. It shows that the spatial frost model improves the representation of the peak flow event in 1973 relative to the model without spatial distributions (Figure 4.13), while decreasing the peak in 1975 makes the prediction of peak flow in that year worse.

4.4 Discussion

The addition of the spatial snow algorithm changes the timing of the melt season, especially for thin snowpacks. Once snow-free areas begin to emerge, the addition of advected sensible

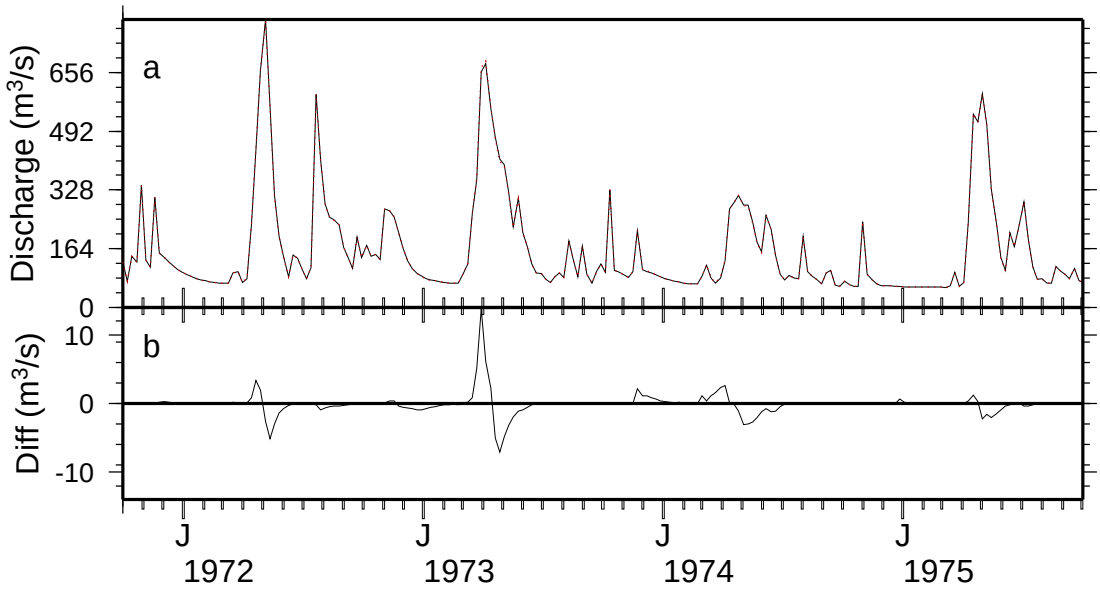

Figure 4.23: Comparison of VIC model simulations for the St. Croix River: (a) spatially distributed frost (solid) and spatially distributed frost and snow (dotted), (b) differences (with snow distribution minus without snow distribution).

heat to the energy balance of the snow pack increases the rate of melt. Due to the limitations of the uniform distribution used to define the distribution of snow, thicker snowpacks that melt quickly show little or no impact from the algorithm, as bare soil appears only late in the melt process.

When the spatial snow algorithm is applied to a large watershed, its effects on simulated discharge are muted and second order in magnitude when compared to the effects of the spatial frost distribution. The spatial snow algorithm does, however, increase sensible heat fluxes during melt throughout the St. Croix River basin, indicating that it enhances the exchange of heat fluxes between the ground surface and atmosphere.

Representation of spatial variation in soil frost increases infiltration and baseflow through the winter and especially during the melt season. The influence of the algorithm is strongest when soils are saturated prior to melt or the influx of melting snow or precipitation is high. The inclusion of both spatial distribution algorithms enhance the VIC model's ability to represent both moisture and heat fluxes in cold regions.

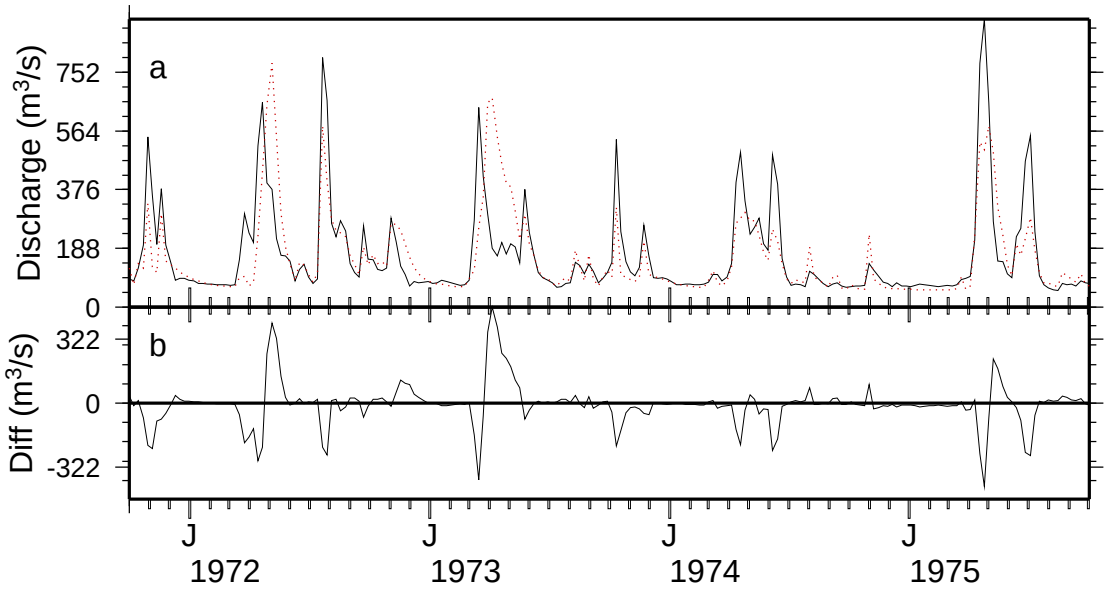

Figure 4.24: Observed (solid) versus simulated (dotted) discharge for the St. Croix River at St. Croix Falls, Wisc. for water years 1971 to 1974: (a) weekly discharge rates and (b) weekly differences (simulated minus observed). Simulated discharge was created using the standard full energy balance VIC model with frozen soil.

Chapter 5

CATCHMENT SCALE ANALYSIS

Field observations and laboratory tests have shown that when soil freezes it reduces the rate of infiltration and increases runoff generation [*Kane and Chacho*, 1990; *Storey*, 1955; *Williams and Smith*, 1989; *Gray and Prowse*, 1993]. Studies of small catchments have shown an increase in both peak flow and total runoff when snow melts and rain falls over frozen soil [*Shanley and Chalmers*, 1999; *Bathurst and Cooley*, 1996]. However, as the scale of the region increases the signal of the frozen soil-induced runoff is complicated by other factors including: ponding, spatial variability of frost, and channel networks. Ponding reduces catchment response through surface storage of melt water. Spatial variability in soil frost may decrease the regional response to the presence of frozen soil by increasing the catchment average infiltration rate. Once melt water reaches the channel, the local scale signal is progressively reduced due to the timing shifts related to channel network geometry [*Dunne and Leopold*, 1978; *Garbrecht*, 1991].

Appendix B (reproduced from *Cherkauer and Lettenmaier* [1999]) demonstrates that spring runoff response is increased due to the presence of frozen soil at both point and catchment scales. *Cherkauer and Lettenmaier* [1999] used the variable infiltration capacity (VIC) macro-scale hydrologic model described by *Liang et al.* [1994], which was modified to represent the effects of frozen soil. In Chapter 3, the spatial distribution of snow and soil frost were shown to be important to regional spring response to frozen soil, suggesting that the point model described in Appendix B needed to be modified to include a representation of these spatial processes. Chapter 4 discussed how the inclusion of spatially variable snow and soil frost into the VIC model, changed the catchment response to spring melt. This Chapter will explore the broader impact of frozen soil by addressing the questions:

- Are there catchment characteristics that help determine the significance of the effect of frozen soil?

- How significant is frozen soil as a predictor of catchment-scale hydrologic response to spring melt?

The ability to identify catchments that are likely to experience frozen soil events (*i.e.* an increase in the peak flow or total flow volume in response to the presence of frozen soil) is important both for practical purposes (*e.g.* flood prediction) and, in the context of land-atmosphere prediction, to help determine where the computation expended in a detailed frozen soil algorithm is warranted. This Chapter discusses a set of statistical tests that were used to: identify catchment characteristics that are important for describing spring hydrological response, and to assess the magnitude of the effect of frozen soil on basin response.

Statistical regressions were formulated for a set of catchments within the upper Mississippi River watershed. The design of these tests will be discussed in Section 5.1. Where possible the predictor and response variables discussed in 5.1 will be derived from observational data. These include daily discharge observations from the U. S. Geological Survey (USGS), daily meteorological forcing data (*e.g.* precipitation and air temperature) from the National Climatic Data Center (NCDC) and maps of spatial characteristics (*e.g.* vegetation cover type and soil type). Observations of catchment hydrologic conditions (*e.g.* soil moisture content and snow water equivalent), which are not often observed, were predicted using the VIC model (see Appendix A for discussion of simulations used in this Chapter). The derivation of the predictor and response variables is covered in detail in Section 5.2. Analysis of the statistical tests will be discussed in Section 5.3.

5.1 Approach

To address the issue of frozen soil significance to spring hydrologic response, a set of gauged catchments distributed over the upper Mississippi River basin was identified (see Figure 5.1). For each of these catchments the first complete melt of the snowpack was identified from VIC model simulations for all years between 1950 and 1998. The period of time between the start of melt and the end of the runoff response to the melt event was then extracted for each year. Multiple linear regression models were then derived to describe the

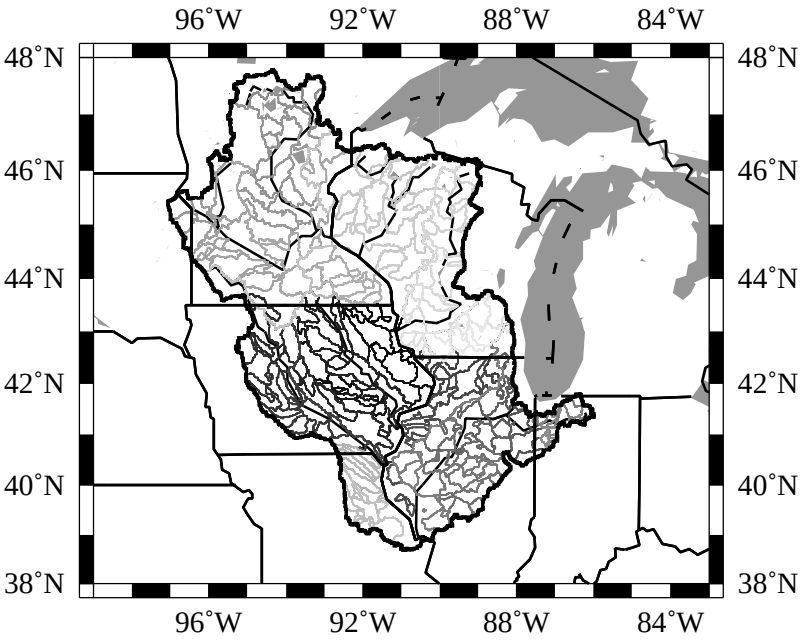

Figure 5.1: Delineation boundaries for all gauged catchments in the upper Mississippi River basin.

observed discharge response to each melt period, using selected catchment characteristics derived from the same time period. Where possible, predictor variables were based on observational data. However, some important predictors (such as soil moisture and snow water equivalent) were not available for substantial parts of the watershed and/or portions of the period of record were not available. These variables were estimated using the VIC hydrologic model described in Chapter 4 using the forcing data and calibration described in Appendix A. The resulting regression models were then used to assess the magnitude of catchment response to frozen soil.

A linear regression model, with n terms, takes the form:

$$R = \alpha_1\beta_1 + \alpha_2\beta_2 + ... + \alpha_n\beta_n + \alpha_0 \tag{5.1}$$

where R is the response variable, α_0 is the intercept, α_i is the ith coefficient and β_i is the ith predictor variable. As predictor variables are added to the model the correlation between predicted and observed response variables increases. However, this does not imply that all

of the added terms are statistically significant contributers to the final regression model.

There are several procedural approaches to determine which predictor variables are significant to the final model. A forward selection process starts with a simple linear regression ($R = \alpha_1\beta_1 + \alpha_0$). All of the available predictors are tried and the one with the highest correlation coefficient between the predicted and observed response variables is returned. All of the remaining predictors in a three parameter regression model ($R = \alpha_1\beta_1 + \alpha_2\beta_2 + \alpha_0$) are then tested and the predictor that yields the greatest increase in the correlation coefficient is kept. The process is repeated until the newest predictor fails to make a statistically significant increase in the correlation coefficient. A stepwise regression builds the regression in the same way as the forward process; however, after adding each new predictor it checks to assure that all of the predictors in the regression model are still significant. Thus a stepwise regression should yield a final regression model where all of the terms are statistically significant, but not necessarily independent.

Two types of predictor variables were identified that might influence spring discharge: intercatchment and interannual variables. Intercatchment predictor variables are physical characteristics that are assumed to be constant with time but vary among catchments. They are listed in Table 5.1 and include such things as soil properties and vegetation cover types. Gauged area was selected to represent the effects of increased drainage area and channel

Table 5.1: Definition of intercatchment regression predictor variables. These are based on spatial maps of characteristics in the upper Mississippi River basin and are assumed to be constant from 1950 to 1998.

Variable Name	Definition[1]
Gauged Area	Catchment drainage area.
Overstory	Fraction of catchment that is covered by trees.
Percent Silt	Average catchment soil percentage of silt.
Mean Annual Precip	Average annual catchment precipitation.
Mean Annual Temp	Average annual catchment air temperature.
Catchment Slope	Average slope in catchment based on a 30 arc-second DEM.

[1] Data sources are described in Section 5.2.2.

networks. Overstory represents the degree of forestation of a catchment, which significantly changes the accumulation and ablation of snow, and the formation of soil frost. Percent silt represents the impact of soil properties on the retention of soil moisture and the formation of ice. Catchment slope represents the ability of runoff to reach the stream channel. Mean annual precipitation and air temperature were selected to represent the long term effects of regional climate.

Interannual predictor variables are characteristics that change annually for each catchment. These include soil moisture content, snow cover and precipitation. A complete list of interannual predictor variables can be found in Table 5.2. Total Moist, Ice Content and

Table 5.2: Definition of interannual regression predictor variables. These variables are computed separately for all catchments and years of observations.

Variable Name	Definition
Total Moist[1]	Simulated total soil moisture (ice plus liquid) in the top 10 cm soil layer, on the day before melt starts (mm).[3]
Ice Content[1]	Simulated ice content of the top 10 cm soil layer on the day before melt starts (mm).[3]
Snow Swq[1]	Simulated snow water equivalent on the day before melt starts (mm).
Snow Density[1]	Simulated snow pack density on the day before melt starts (kg/m^3).
Frost Depth[1]	Simulated depth of frost on the day before snow melt starts (cm).
Peak Melt Rate[1]	Simulated maximum rate of melt during the melt period normalized by gauged area (mm/day).
Cum Precip[2]	Cumulative observed precipitation from the day before the start of melt until the end of the peak flow response (mm).

[1] uses average daily values obtained from 3 hour VIC model simulations (see Appendix A).

[2] uses average daily observed precipitation corrected for wind-induced gauge undercatch using the method described in Appendix A.

[3] The 10 cm thickness was used because it is the thickness of the top soil layer for all VIC model simulations used in this chapter. Thicknesses of the second and third layers were adjusted during calibration and are, therefore, not consistent across the basin.

Frost Depth represent the state of the soil prior to the start of melt, including the presence of frozen soil. Snow water equivalent (swq), Snow Depth and Peak Melt Rate represent the state of the snow pack, both as a source of melt water and as an insulator during the formation of frozen soil. Cum Precip represents another source of water during spring melt. Descriptions of how both the interannual and intercatchment predictor variables were derived, follow in Sections 5.2.2 and 5.2.3.

Regressions were used to test the influence of the predictor variables on two response variables: the runoff ratio and peak flow rate. The runoff ratio is the fraction of precipitation and snow melt that is observed in the stream channel as runoff. It is computed annually for each catchment, as described in Table 5.3, using simulated snow water equivalent, wind induced undercatch corrected precipitation (see Appendix A), and daily observations of streamflow from the U. S. Geological Survey (USGS). Peak flow response uses only the daily observations of streamflow and is also defined in Table 5.3. A detailed discussion of how the response variables were computed follows in Section 5.2.3.

Table 5.3: Definition of catchment response variables. Both are based on USGS observed daily discharge records.

Variable Name	Definition
Runoff Ratio	Cumulative discharge from the day before the start of snow melt until the end of the peak flow response divided by the cumulative precipitation and snow melt during the same time period.
Peak Flow Rate	Peak flow rate in response to the peak melt event (mm/day).

Once the predictor and response variables were computed the statistical analysis proceeded as follows:

1. The full data set (containing variable sets for all catchments and all years) was split into two independent data sets of equal size, based on the median of the soil ice content in the top 10 cm. Years for each catchment, with simulated ice contents greater than the median ice content, were put into the first set, those with simulated ice contents

less than or equal to the median went into the second set. With a higher average ice content, the first set should be more influenced by frozen soil than the second set.

2. Stepwise regressions were computed on the first data set, in which frozen soil is more likely to have an influence, using all of the predictor variables for both response variables. This results in regression models with only the statistically significant predictor variables retained.

3. Regression models resulting from the previous step were then applied to the second data set. The change in the regression model correlation coefficients between data sets should provide some indication of the impact of frozen soil (*i.e.* high ice content).

4. The regression models for both response variables were also applied to two resamplings of the complete data set: the first was filtered to isolate all years for each catchment, the second was filtered to isolate all catchments for each year. This allowed for the identification of catchments and years for which the regression models performed especially poorly or especially well.

5. A preliminary investigation was conducted to identify possible reasons for the range of performance seen in the regression models when applied to individual catchments and years.

5.2 Identification of the Predictor Variables

5.2.1 Catchment Selection

Catchments were identified by screening U. S. Geological Survey (USGS) records for record length, quality and completeness. There are 337 gauging stations in the upper Mississippi basin monitored by the USGS that have recorded daily discharge for at least 10 years between 1950 and 1998, with less than 10 percent of the record length missing. The catchments range in size from a few tens of square kilometers to 444,183 km^2 for the entire upper Mississippi River at Alton, Ill.

Catchments were delineated in Arc/Info from a 30 arc-second digital elevation model (DEM). First, the location of the major rivers was "burned" into the DEM by removing 100 m of elevation from each dem grid cell containing a stream channel as defined in an Arc/Info coverage [*Scientific Assessment and Strategy Team*, 1995b]. Next sinks, locations on the DEM that are lower than their surroundings, were filled. Finally, each catchment was delineated separately. A common issue when delineating watersheds digitally is that the station latitude and longitude provided by the USGS often do not coincide with the stream channel defined by the DEM. This results in delineated catchment areas which are significantly different than the reported gauge area. When delineating a small number of catchments, the gauge position is often adjusted manually by inspecting the DEM for a better location. Due to the large number of catchments used for this project, an automated process was needed. First, the accumulation grid, which indicates the number of grid cells that drain to each cell, was multiplied by the average size of a 30 arc-second cell, to create a grid of drainage areas at each point. The latitude and longitude for each station was used to locate the initial gauge position. The region surrounding the initial gauge position was then searched for a cell with the approximate drainage area closest to the USGS published area.

Figure 5.1 shows all of the delineated watersheds for the upper Mississippi River basin. Of the 337 original catchments, 325 were successfully delineated, meaning that there is a finite delineated area. A histogram of the percent differences between the published and delineated areas for all of the catchments is shown in Figure 5.2a. The majority of the catchments are within $\pm 10\%$ of the gauged area. There is a tendency to overestimate the delineated catchment area (negative percent difference) but on the whole the automated procedure performed well. Analysis of the distribution of delineation errors by catchment size shows that percent catchment area overestimation is greatest for the smallest catchments (see Figure 5.2b). The standard deviation of catchment delineation error increases for the largest and smallest catchments but is fairly uniform for the intermediate sizes. Overestimation of area for the catchments is related to two factors: the stream network used to burn the major rivers into the DEM did not include the smallest catchments and the grid cell resolution of the DEM is 0.6 km^2 so it loses much of the detail required to

delineate the smallest catchments accurately. To minimize the effects of delineation errors, only catchments with areas within ±5% of the USGS published areas were used for the study. This left 209 catchments with the correct record length and acceptable delineated area.

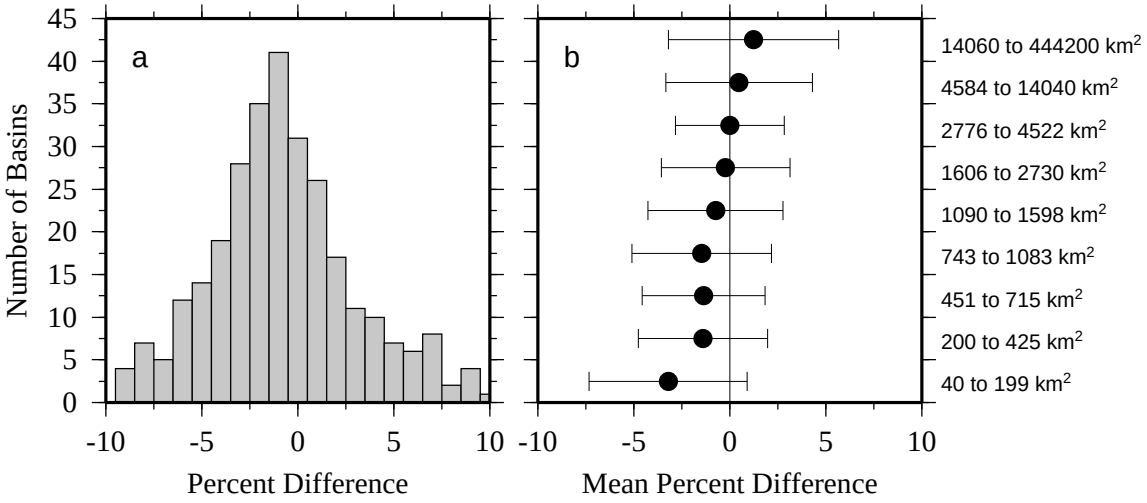

Figure 5.2: Percent difference between the gauged and delineated catchment area for all delineated catchments: (a) histogram distribution of all catchments and (b) mean (dot) and standard deviation (line) of percent differences by gauged catchment size.

5.2.2 Catchment Properties

Following delineation of the sub-catchments, average catchment characteristics were extracted and analyzed. Soil characteristics were obtained from the conterminous U. S. multilayer soil characteristics data set (CONUS-soil) [*Miller and White*, 1998]. Of particular interest are the respective distributions of the percent sand, silt and clay (see Figure 5.3). The northern portions of the upper Mississippi River basin were covered by the last continental glacier, which deposited large amounts of sand and gravel. The southern portion of the basin is dominated by finer grain materials supplied by glacial melt waters and the Great Plains to the west. Deposits of sand (*i.e.* low silt content) can still be seen in the northern portion of the basin in Figure 5.3. Higher silt contents are found to the south

and east. The average silt content in the delineated catchments falls between 10 and 70%, with the majority of catchments in the range of 40 to 60%. Clay is fairly evenly distributed around the basin and never exceeds 40% of the total soil mixture. Therefore, the percent sand map is nearly the complement of the map of percent silt and only percent silt is used in the analysis.

Vegetation cover was taken from the 1 km resolution vegetation maps produced by the University of Maryland [*Hansen et al.*, 2000]. Vegetation was classified into 14 categories, including evergreen needleleaf, deciduous broadleaf, grasslands, and croplands. Except for the northeast part of the catchment, the primary land use type is agriculture. Figure 5.4a shows the distribution of overstory vegetation (evergreen and deciduous trees) in the upper Mississippi River basin. Trees are quite clearly concentrated in the northeastern parts of the basin, with only a few patches of significant overstory coverage outside of that region. This is reflected in the distribution of overstory in the delineated catchments (see Figure 5.4b). The majority of catchments have less than 20% overstory coverage, while there is a secondary concentration of catchments with greater than 90% forestation.

Mean annual precipitation was calculated from gridded daily National Climatic Data Center (NCDC) station observations, corrected for wind induced precipitation undercatch by the method outlined in Appendix A. Precipitation increases toward the southeastern portion of the catchment (see Figure 5.5), ranging from 550 to over 1200 mm per year. The influence of lake effect precipitation from Lake Superior and Lake Michigan is evident along the eastern edges of the basin. The majority of the delineated catchments receive between 800 and 1000 mm of precipitation annually.

Daily maximum and minimum temperatures were also obtained from the daily NCDC station data. These were gridded to one-eighth degree resolution across the upper Mississippi River basin. The gradient of average annual air temperature increases from north to south, with temperatures increasing from just above 0°C near the Canadian border to nearly 12°C just above the confluence with the Missouri River (see Figure 5.6a). Delineated catchment average temperatures range from 4°C to 12°C (see Figure 5.6b).

Slopes were computed in Arc/Info from the same 30 arc-second DEM used for basin delineation. The DEM was reprojected into UTM coordinates so that the grid cell area was

constant throughout the basin. Arc/Info fits a plane to the 3x3 cell neighborhood around each grid cell (*i.e.* the cell of interest plus the 8 cells surrounding it). The direction the plane faces is then the aspect of the current cell, and the slope is found by computing the average maximum slope [*Burrough*, 1986]. The cell slopes (in geographic projection) are displayed in Figure 5.7a. Slopes are greatest along river channels. The majority of the upper Mississippi River watershed has average slopes of less than 1 degree. In the north-central region of the basin, where the Mississippi River becomes the boundary between Wisconsin and Minnesota, slopes are larger because the river flows between high bluffs. Average slopes for the delineated basins are shown in 5.7b. All of the basins have average slopes between 0 and 2 degrees. The majority of the catchments fall just below 1 degree. Thus the region as a whole is relatively flat.

Finally, the distribution of reservoirs and controlled lakes within the upper Mississippi may be another important criteria for assessing the impact of frozen soil on spring runoff as observed at the catchment mouths. Figure 5.8a shows the placement of reservoirs in and around the upper Mississippi River basin. This data set was obtained from the *Scientific Assessment and Strategy Team* [1995a]. It provides the location of reservoirs and controlled natural lakes completed by January 1, 1988, with normal holding capacities of at least 6.2 million cubic meters and maximum holding capacities of at least 30.8 million cubic meters. Figure 5.8b, shows the distribution of dams within the delineated catchments. The histogram has been truncated to show only catchments with fewer than 15 reservoirs. There are 27 catchments not shown on the histogram, including the entire upper Mississippi River basin which contains 369 reservoirs. For this analysis, catchments with reservoirs were removed leaving 112 catchments.

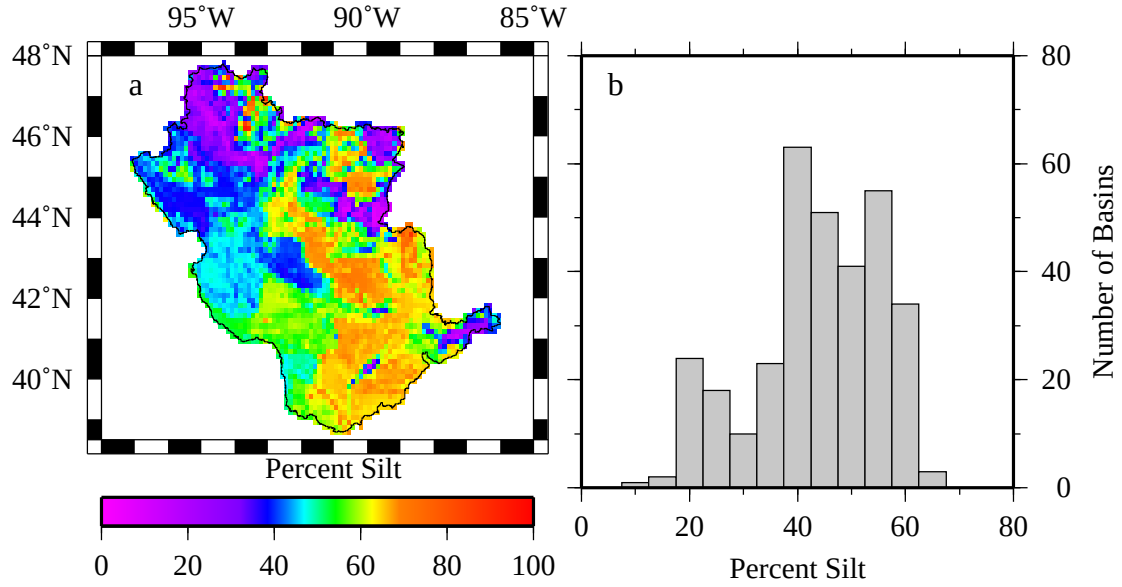

Figure 5.3: Distribution of grid cell average percent silt: (a) across the upper Mississippi River basin and (b) for all delineated catchments.

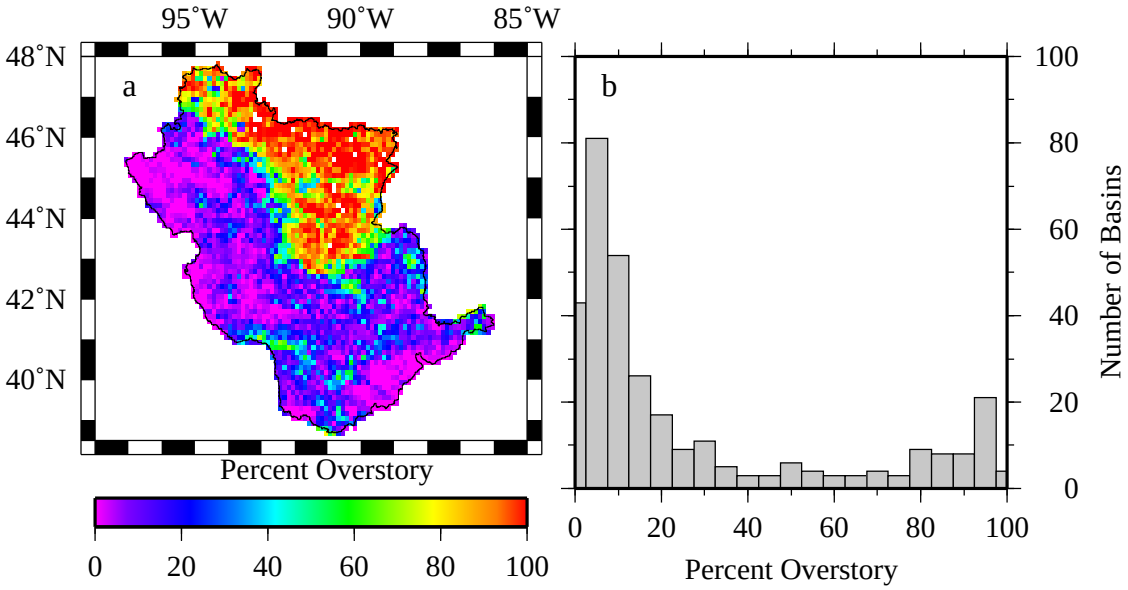

Figure 5.4: Distribution of overstory by percent of grid cell covered: (a) across the upper Mississippi River basin and (b) for all delineated catchments.

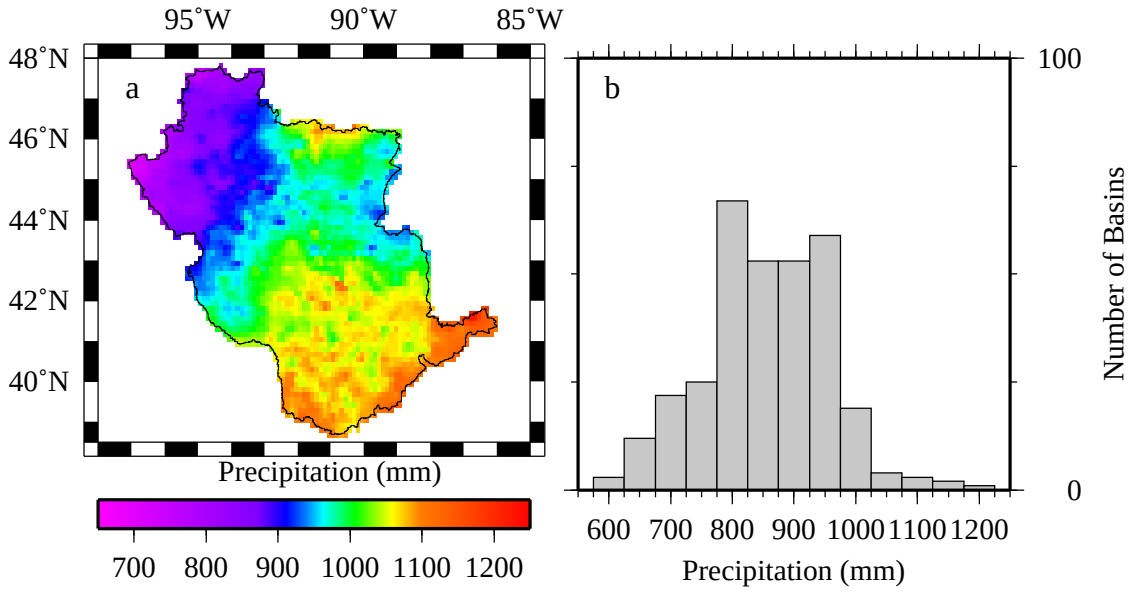

Figure 5.5: Distribution of mean annual corrected precipitation: (a) across the upper Mississippi River basin and (b) for all delineated catchments.

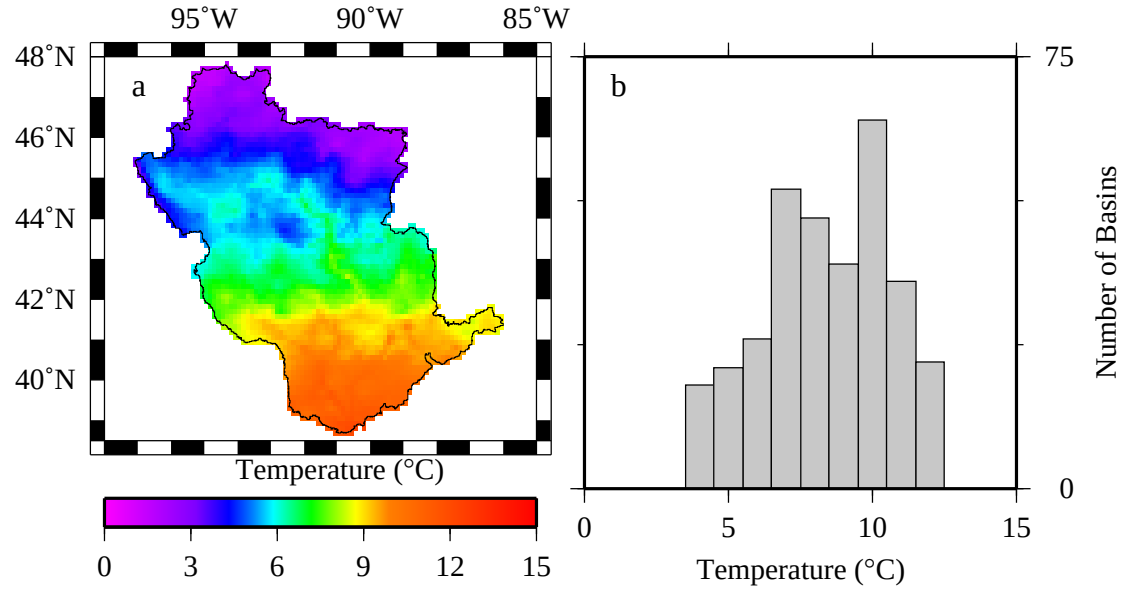

Figure 5.6: Distribution of mean annual air temperature: (a) across the upper Mississippi River basin and (b) for all delineated catchments.

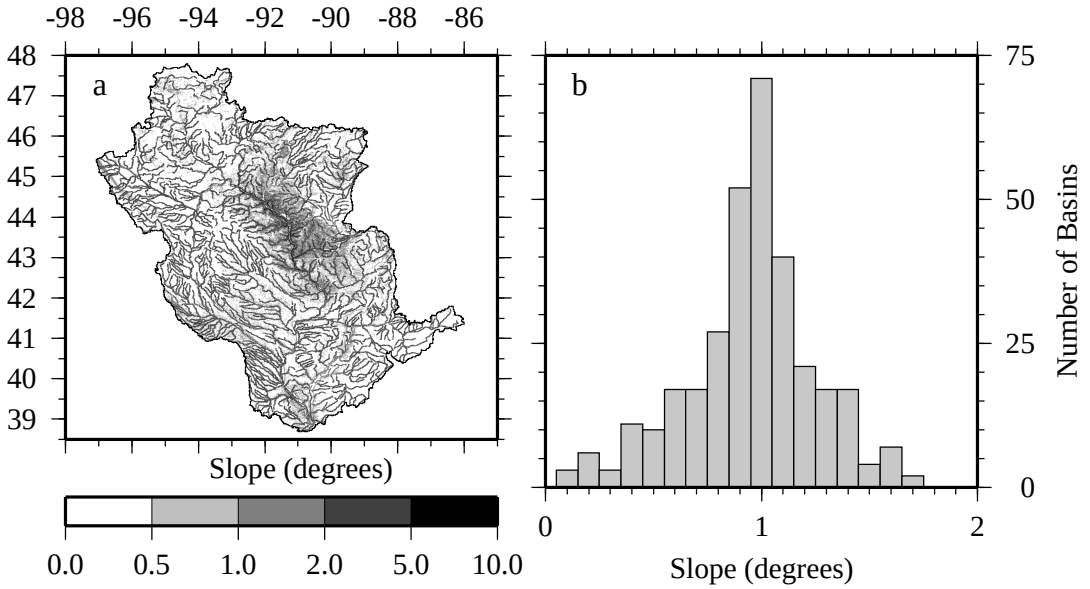

Figure 5.7: Land surface slope in degrees based on a 30 arc-second DEM: (a) across the upper Mississippi River basin and (b) averages for all delineated catchments.

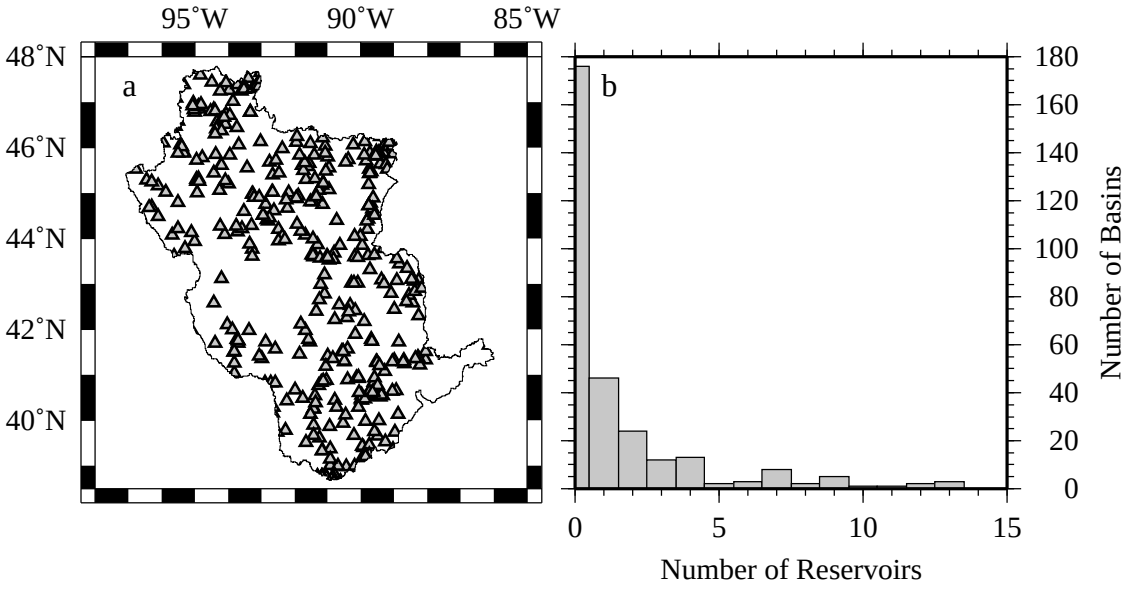

Figure 5.8: Location of reservoirs within the upper Mississippi River basin, and their distribution among the delineated catchments.

5.2.3 Analysis of Discharge Records

The interannual predictor variables in Table 5.2 and both response variables require the identification of four specific days in the simulated and observed records:

1. the day of maximum snow melt,
2. the day before melt begins,
3. the day of maximum peak flow response following melt and
4. the day that marks the end of the peak response.

Each of these dates are unique for every catchment and for every year, and are estimated using observed discharge, precipitation and simulated snow records. Due to the number of catchments and number of years used in this study, an automated system was developed to extract the time period of interest for annual snow melt response, as follows:

- Daily discharge records for all of the stations were extracted from CD-ROMs of USGS daily streamflow records and missing days were filled with zeros to yield files with no gaps from 1950 to 1998.
- Delineated catchment boundaries were projected to the VIC model grid (see Figure 5.1) and the fractional area of each delineated catchment falling within each eighth degree cell was determined.
- An average time series of simulated snow water equivalent, frost depth and frozen and liquid soil moisture was produced for each delineated catchment.
- The daily catchment average files were searched to identify the last day of snow cover for each year. The last day of snow cover is defined to be the first day after January 15th that there is no snow on the ground in the model simulation.
- Once the last day of snow cover was determined, the search backs up over the record to identify the day of peak melt rate preceding the end of snow cover.

- Daily flows were extracted for sixty days after the day of peak melt for each year with complete discharge records (see Figure 5.9).

The magnitude of each catchment's peak flow event, during the melt period defined above, is controlled by snow melt and precipitation. Timing of the event is affected not only by the day of maximum melt but also by any significant precipitation that occurs around the same time. The average number of days between the day of maximum melt and the peak flow response can be used to filter larger peak flow responses that occur later in the 60 day period and are not caused by the melt event. Complexities in the daily hydrograph can also make it difficult to automate the determination of the end of the peak flow event. Therefore, the length of peak flow response for each catchment was determined as follows:

- Flows for each year were transformed to a scale of zero to one based on the maximum and minimum flows during the sixty day period following the maximum melt rate (see Figure 5.9). This minimizes the effect of years when a major precipitation event before or after the day of maximum snow melt masked the timing of response.

- Transformed flows were averaged, over all years of observation, into a single hydrograph.

- The average hydrograph for each catchment was then searched to find the day of maximum peak flow, this determines the average number of days between peak melt and peak flow rates.

- The end of the peak flow event was found using three, five and seven day slopes, computed from the average hydrograph starting after the day of maximum flow. The day that the last of these slopes becomes positive, indicates that the hydrograph had started to rise, and was taken to be the end of the peak flow event (see Figure 5.9b).

Figure 5.9 shows a sample case for the Elk River near Big Lake, Minn., a catchment of 1,448 km^2 that has a well-behaved average response. It can be seen from the normalized values for individual years that there is considerable variability in snow cover and discharge.

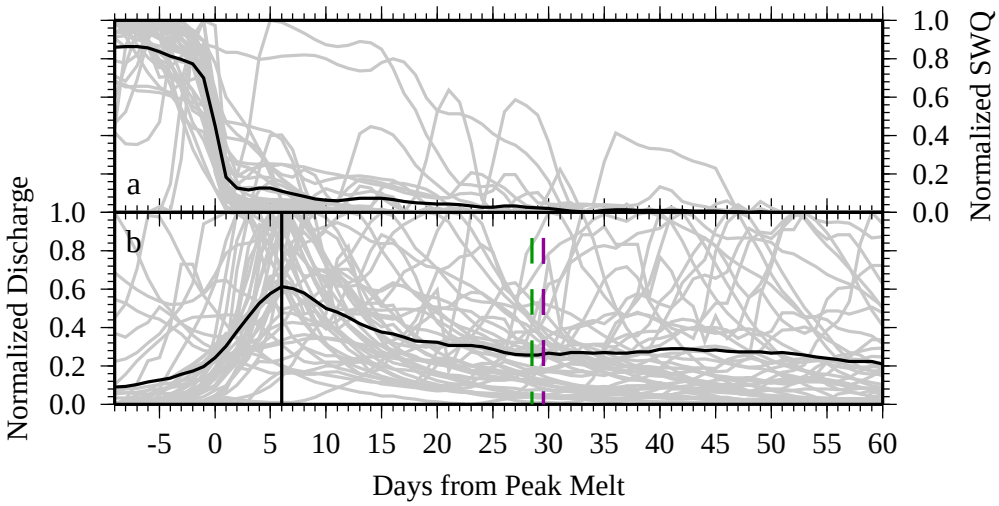

Figure 5.9: Sample peak flow response analysis for the Elk River near Big Lake, Minn.: (a) normalized snow water equivalent for all years of observation (gray) and average for all years (black): day 0 corresponds to the day of peak melt prior to the last day of snow cover; and (b) normalized daily discharge records (gray) and average for all years (black). Peak discharge is identified by a solid vertical line in (b) and the end of peak flow response as determined by three, five and seven day slope checks are shown with vertical dashed lines.

For some catchments the variability overwhelmed the annual signal and the automated search function was unable to locate the day of peak flow or the end of the peak flow response. Because average response time should increase with catchment size and the failed identifications were not size dependent, the discharge response statistics were separated into catchment size categories and averaged for each class (see Table 5.4).

Table 5.4: Number of days from the simulated occurrence of the maximum melt rate to the observed peak discharge response and the end of the peak response.

Catchment Size (km^2)			Number of Catchments	Peak Flow Day[1]	Peak End Day[1]
0	to	200	55	1.29 (3.44)	11.25 (4.02)
200	to	500	42	2.17 (5.31)	14.69 (7.39)
500	to	1000	49	1.84 (1.85)	15.02 (5.44)
1000	to	2000	56	5.50 (11.55)	18.67 (9.08)
2000	to	4000	42	6.93 (13.13)	23.27 (12.16)
4000	to	15000	46	4.98 (4.84)	23.78 (9.22)
15000	to	450000	23	6.17 (2.19)	28.74 (7.11)

[1] Mean values with standard deviations in parenthesis.

The number of days between peak flow and the end of the peak flow event increases with increasing catchment drainage area, however, the same is not true for the average number of days from peak melt to peak flow (see Table 5.4). For smaller catchments, the occurrence of peak flow is strongly influenced by precipitation during the melt period. Several days of precipitation tend to broaden the peak response, a day of intense precipitation can shift the peak response. For larger catchments, the timing of peak melt across the catchment and the shape and storage potential of the stream channel network control the delay between catchment average peak melt and the peak flow response. For this exploratory study of the catchment response to frozen soil, it was assumed that the characteristics in Table 5.4 were adequate to capture most of the peak flow response to spring melt.

Once the average values listed in Table 5.4 were obtained, all of the available records were reprocessed, as follows, to obtain values for the predictor variables in Table 5.2 and the response variables in Table 5.3. The day of peak melt was found using the method described above, then the day of maximum flow was found by searching the daily discharge record after maximum melt for three times the average number of days for that catchment size (see Table 5.4). Flow and precipitation records were truncated at the average number of days after peak flow listed in Table 5.4. The day before the start of melt was found by stepping back through the simulated melt record from the day of peak flow until a day was encountered with no melt. This day was used to start the flow and precipitation records for the calculation of cumulative values. Values for snow depth, snow water equivalent, frost depth, ice content and total soil moisture are also extracted from the catchment average value file for the same day. Tables of these values, computed independently for each catchment and for each year of discharge, were used for the statistical tests in the next section.

5.3 Statistical Analysis

This section presents the results of the statistical analyses described in Section 5.1. The full data set (derived in the previous section) contains data from 112 catchments that passed all of the selection criteria described in Section 5.2. Counting all years of usable predictor/response sets there are a total of 2,425 observation sets. These were split into two independent data sets based on the median ice content for all observation sets (25.5 mm). The first data set (high ice content) contains 1,212 observations with ice contents greater than the median, the second (low ice content) contains 1,213 observation sets with ice contents less than or equal to the median. The rationale for splitting the data is that runoff response for soils with higher ice contents is more likely to be influenced by the presence of frozen soil, than for soils with lower ice content.

Fitting multiple regression models to the high ice content data set using all of the predictor variables (see Tables 5.1 and 5.2) and without testing for predictor significance, yields maximum coefficient of determination (r^2) of 0.10 and 0.25 for the runoff ratio and peak flow responses, respectively. However, an analysis of the residuals for both regression

models shows that they both have strong trends in their residuals (heteroscedasticity) (see Figures 5.10a and 5.10c). This violates the assumption of linear regression theory that variance is constant around the regression line, and indicates that both response variables will need to be transformed before regressions can be performed. Taking the natural log of both response variables and refitting a regression model yields a more uniform distribution of the residuals (homoscedasticity) for both response variables (see Figures 5.10b and 5.10d). The r^2 values using all of the predictor variables were essentially unchanged using this procedure (0.09 and 0.30 for the runoff ratio response and peak flow response variables, respectively). Nonetheless, all of the following regression analyses are conducted on the natural logarithms of the response variables.

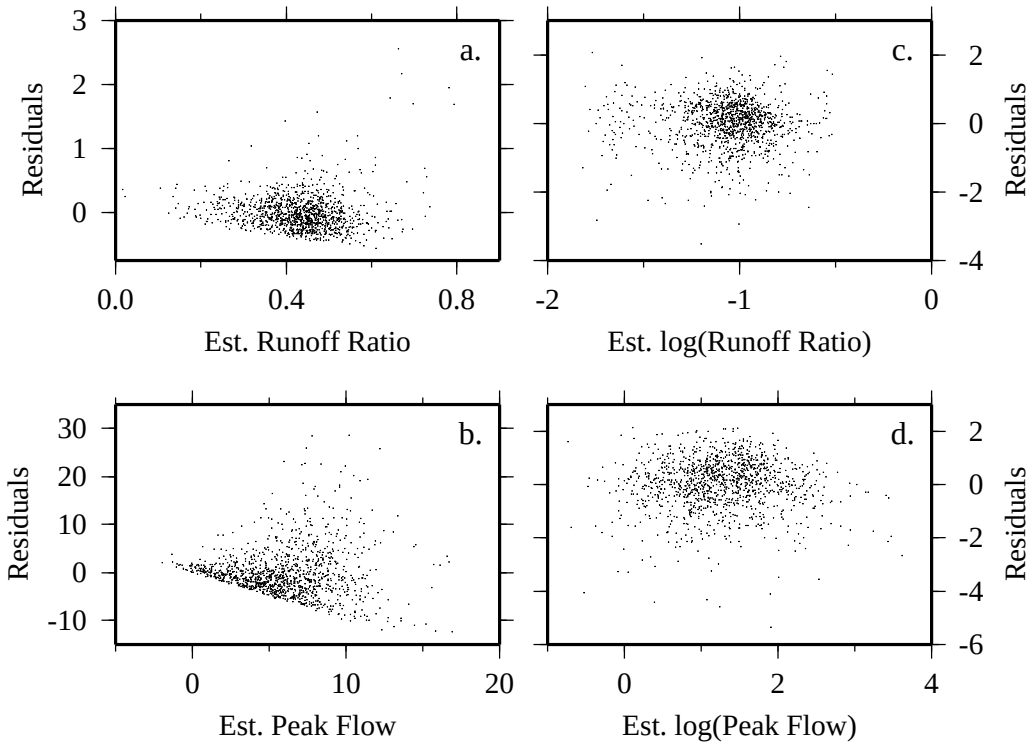

Figure 5.10: Analysis of residuals for a multiple regression using all predictor variables for: (a) runoff ratio response, (b) the log of runoff ratio response, (c) peak flow response and (d) the log of peak flow response.

To determine which of the predictor variables are statistically significant, stepwise re-

gressions were run for both response variables. Terms were included in the final regression model only if they reduced the Akaike Information Criterion of the model [*Sakamoto et al.*, 1987]. The first regression showed that Snow Swq, which was a significant predictor for peak flow response, is strongly correlated with both peak melt rate (correlation = -0.57) and snow density (-0.53). Strongly correlated predictor variables may indicate that the model is over parameterized, and that the regression model can do as well without one of the variables. Since Snow Swq had the lowest t value of the three coefficients, it was removed from the list of available predictor variables and the regressions were rerun. This reduced the r^2 value for peak flow response from 0.30 to 0.28.

Table 5.5 lists the predictor variables that were determined to be statistically significant in describing the response variables. Also listed are their coefficients, standard errors, t and p values. The most significant predictor for runoff ratio response is mean annual precipitation, while for peak flow response it is the peak melt rate. The least significant predictors are ice content for runoff ratio and gauged area for peak flow.

The runoff ratio response models can also be written as:

$$\begin{aligned} ROR(c,t) = {} & 0.00223 * MAP(c) + 5.52e^{-5} * AREA(c) + 0.00462 * PMR(c,t) \\ & + 0.220 * OVER(c) + 0.00633 * ICE(c,t) - 0.00117 * DENS(c,t) \\ & - 0.00204 * PREC(c,t) - 3.41 \end{aligned} \tag{5.2}$$

and the peak flow response model as:

$$\begin{aligned} PFR(c,t) = {} & 0.0278 * PMR(c,t) + 0.772 * OVER(c) + 0.0178 * SILT(c) \\ & + 0.00402 * PREC(c,t) + 0.00187 * MAP(c) + 0.00929 * ICE(c,t) \\ & - 3.54e^{-5} * AREA(c) - 0.00235 * DENS(c,t) - 2.36 \end{aligned} \tag{5.3}$$

where ROR and PFR are the logs of the runoff ratio and peak flow responses for year t and catchment c. The predictor variables (MAP, $AREA$, PMR, etc.) are defined in Table 5.5.

Tables 5.6 and 5.7 show the correlation matrices for the runoff ratio and peak flow response regression models, respectively. The highest correlation for the runoff ratio response model is -0.47 between the peak melt rate and snow density. Predictor correlation for the

Table 5.5: Multiple stepwise regression model coefficients, standard errors and t-values for runoff ratio and peak flow response to high ice content data set.

log Runoff Ratio Response[1]

Term	Variable	Value	Std. Error	t value	p value
Mean Annual Precip	$MAP(c)$	2.23e-03	2.58e-04	8.7	< 0.001
Gauged Area	$AREA(c)$	5.52e-05	1.46e-05	3.8	< 0.001
Peak Melt Rate	$PMR(c,t)$	4.62e-03	1.24e-03	3.7	< 0.001
Overstory	$OVER(c)$	2.20e-01	6.66e-02	3.3	0.001
Ice Content	$ICE(c,t)$	6.33e-03	3.41e-03	1.9	0.064
Snow Density	$DENS(c,t)$	-1.17e-03	4.21e-04	-2.8	0.006
Cum Precip	$PREC(c,t)$	-2.04e-03	5.48e-04	-3.7	< 0.001
(Intercept)		-3.41e+00	3.15e-01	-10.8	< 0.001

[1] Multiple correlation coefficient = 0.30.

log Peak Flow Response[2]

Term	Variable	Value	Std. Error	t value	p value
Peak Melt Rate	$PMR(c,t)$	2.78e-02	1.81e-03	15.4	< 0.001
Overstory	$OVER(c)$	7.72e-01	9.86e-02	7.8	< 0.001
Percent Silt	$SILT(c)$	1.78e-02	3.00e-03	5.9	< 0.001
Cum Precip	$PREC(c,t)$	4.02e-03	8.03e-04	5.0	< 0.001
Mean Annual Precip	$MAP(c)$	1.87e-03	3.86e-04	4.8	< 0.001
Ice Content	$ICE(c,t)$	9.29e-03	5.01e-03	1.9	0.064
Gauged Area	$AREA(c)$	-3.54e-05	2.22e-05	-1.6	0.111
Snow Density	$DENS(c,t)$	-2.35e-03	6.18e-04	-3.8	< 0.001
(Intercept)		-2.36e+00	4.64e-01	-5.1	< 0.001

[2] Multiple correlation coefficient = 0.53.

peak flow response model is also highest between the peak melt rate and snow density, with a value of -0.47. While still somewhat correlated, removal of peak melt rate from the runoff ratio model and snow density from the peak flow response model causes other predictor correlations to reach a similar magnitude so it was decided to leave the models as shown in Table 5.5.

Table 5.6: Correlation between predictor variables for the initial runoff ratio response multiple linear regression model.

	Runoff Ratio Response					
	Gauged Area	Overstory	Mean Annual Precip	Ice Content	Snow Density	Peak Melt Rate
Overstory	0.01					
Mean Annual Precip	0.02	0.09				
Ice Content	0.09	-0.04	0.01			
Snow Density	-0.04	-0.28	0.16	-0.06		
Peak Melt Rate	0.13	0.24	-0.08	0.01	-0.47	
Cum Precip	-0.13	-0.09	-0.05	0.05	0.08	-0.24

Fitted values for both regression models (see Table 5.5 and Equations 5.2 and 5.3 are plotted against the response variables for both the high and low ice content data sets in Figure 5.11. As was indicated by the correlation coefficients there is still considerable variability in the response variables that is not accounted for by the regression models. More of the variance is described for peak flow response (see Figures 5.11b and 5.11d) and can be seen as a closer fit with the 1:1 line.

The runoff ratio response model shows that the four most significant predictor variables are mean annual precipitation, gauged area, peak melt rate and cumulative precipitation (see Table 5.5). The first three are all positively related to runoff ratio response, that is, as they increase, so does the runoff ratio. Cumulative precipitation is negatively related, so as

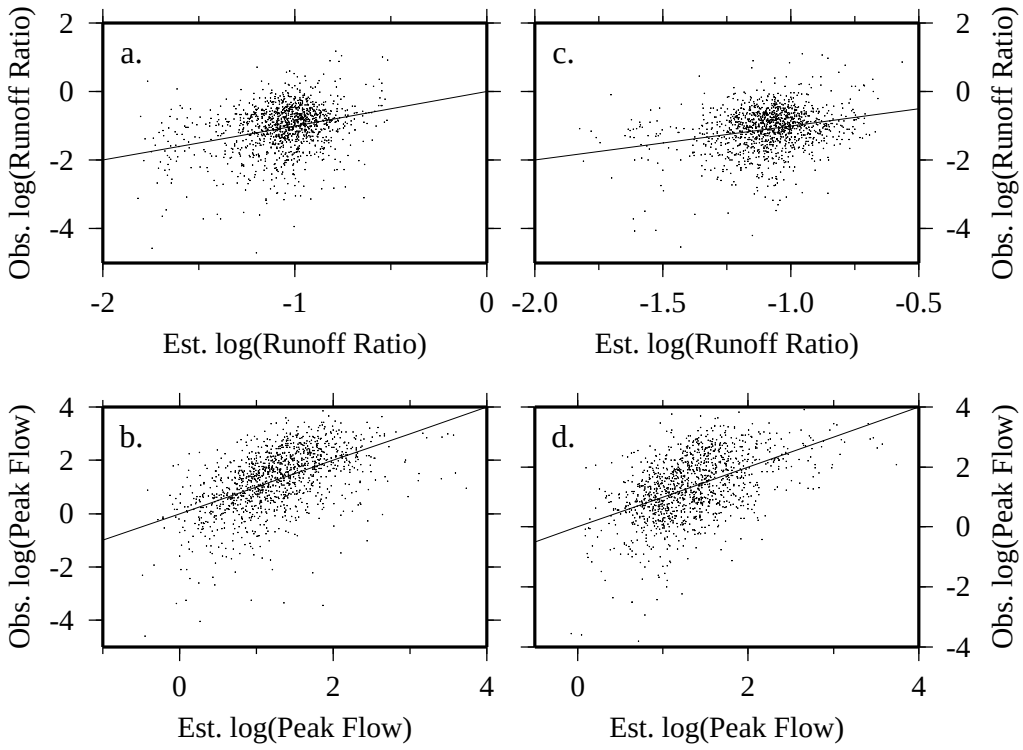

Figure 5.11: Scatter plots of regression model and observed response variables for: (a) Runoff ratio response for high ice content data set, (b) Peak flow response for high ice content, (c) runoff ratio response for low ice content data set and (d) peak flow response for low ice content data set. The 1:1 line is drawn.

Table 5.7: Correlation between predictor variables for the initial peak flow response multiple linear regression model.

	Peak Flow Response						
	Gauged Area	Overstory	Percent Silt	Mean Annual Precip	Ice Content	Snow Density	Peak Melt Rate
Overstory	0.04						
Percent Silt	0.26	0.14					
Mean Annual Precip	-0.04	0.05	-0.21				
Ice Content	0.07	-0.05	-0.09	0.03			
Snow Density	-0.04	-0.28	-0.03	0.17	-0.05		
Peak Melt Rate	0.14	0.24	0.02	-0.09	0.01	-0.47	
Cum Precip	-0.13	-0.09	-0.03	-0.05	0.05	0.08	-0.24

it increases, the runoff ratio decreases. Increasing mean annual precipitation, suggests that mean annual soil moistures will be higher, implying that there is more moisture available to form ice during the winter. Peak melt rate and cumulative precipitation are sources of water during the melt period, but they are related to runoff ratio with opposing signs. Higher peak melt rates are more likely to overwhelm the infiltration capacity of the soil, increasing the amount of runoff generated. Since convective storms are uncommon during the melt season, higher cumulative precipitation implies more days of rain. When spread out over many days, more of the precipitation can infiltrate even when the infiltration rate is reduced due to frozen soil.

Other significant predictors, which may impact the development of and response to frozen soil include the overstory fraction and snow density. Overstory shelters the ground surface, reducing the penetration of frozen soil [*Stadler et al.*, 1996; *Shanley and Chalmers*, 1999] and the accumulation of snow through interception [*Hedstrom and Pomeroy*, 1998; *Storck and Lettenmaier*, 1999]. Snow under the canopy will melt at a slower rate (producing a more continuous source of melt water) than if it was fully exposed to solar radiation and

wind, which means that even with shallower soil frost the soil will be wetter during peak melt, causing higher runoff ratios.

Lower snow densities provide increased insulation to the ground surface. If snow accumulates prior to the development of frozen soil, then the soil would remain relatively warm. If, however, the soil freezes before much snow has accumulated, the lower snow density will serve to insulate the soil during warm mid-winter days.

Peak flow response is clearly most sensitive to the peak melt rate (see Table 5.5). A higher peak melt rate indicates that more snow melt is available to reach the channel in a single day, potentially yielding a higher discharge response peak, depending on the catchment infiltration rate. Overstory fraction, percent silt and cumulative precipitation are also highly significant and positively related to peak flow response. Cumulative precipitation, while not a rate, does indicate a source of moisture. If heavy precipitation falls on the same day as a strong peak melt event, the maximum peak flow response should be larger.

As previously noted, snow melt is slower in forested regions, so despite potentially smaller accumulations, more snow will be present until later in the melt season when the likelihood of higher peak melt rates is increased. Silt is a finer grained material than sand, so it typically has a lower hydraulic conductivity and soil moisture will remain unfrozen to lower temperatures [*Bouyoucos*, 1920]. As mentioned in Section 5.2.2 percent sand is inversely correlated with percent silt, therefore it can be inferred that the positive relationship between percent silt and peak flow response is related to changes in hydraulic conductivity and ice content. From the correlation matrices in Tables 5.6 and 5.7, it can be seen that percent silt tends to be negatively correlated with total soil moisture but positively correlated with increased ice fraction. This indicates that in regions with higher percent silt, peak flow responds more to ice in the soil than to saturation level. Silt fractions tend to be highest in the south where snow melt occurs earliest, and where it is less likely for there to be multiple melt cycles to fill up soil moisture storage before the peak melt event.

The multiple linear regression models described in Table 5.5 were next applied to the low ice content data set. This resulted in multiple regression r^2 values of 0.07 for the runoff ratio response model and 0.25 for the peak flow response model. This is only slightly lower than the values for the high ice content data set. While it was expected that the correlation

coefficients for the regression models based on the high ice content data set would decrease when applied to the low ice content data set (due to the reduced importance of frozen soil), a decrease of such a small magnitude is unlikely to be statistically significant. The high ice content data have an average ice content of 37 mm, while the low ice content data set average is 17 mm (average maximum moisture content is 50 mm for both). This indicates that for the low ice content data set, 34% (17 mm/50 mm * 100%) of the pore space in the top 10 cm of soil, is still filled with ice. So it is quite likely that frozen soil is a significant predictor of spring runoff response for most of the basins for most years.

Figure 5.12a shows the number of years for which each catchment had simulated ice content greater than 25.5 mm (the median value used to separate the data set in the high and low ice content sets). Figure 5.12b displays the same information after it is normalized by the total number of years of observations available for the catchment, and multiplied by 100%. Therefore, a low number of years in Figure 5.12a may appear as a high percentage in 5.12b, if the total number of observations for the catchment is low. Catchments in the southern portion of the basin, tend to contribute fewest years of observations to the high ice content data set. However, most of the catchments in the watershed contribute more than 40% of their observed years to the high ice content data set. This indicates that except for some of the catchments along the southwestern edge of the watershed, and a few in the eastern most part of the watershed, frozen soil is a significant predictor of spring runoff response.

To get an understanding of the magnitude of the change in spring runoff response to frozen soil, the regression models for runoff ratio and peak flow response (see Equations 5.2 and 5.3) were applied to the full data set with the observed ice contents and with ice contents set to 0. The annual average change in predicted catchment responses due to ice for both models is plotted in Figure 5.13. The annual average increase in runoff ratio response due to ice content ranges from 5 to 25%, while for peak flow response it ranges from 8 to 30%. The difference in magnitude is caused by the difference in the ICE coefficients in equations 5.2 and 5.3, but should be a reflection of their relative importance to the response processes. However, the regression models only account for an average of 9% and 27% of the observed variability in the runoff ratio and peak flow responses, respectively. Therefore, the

values shown in Figures 5.13a and 5.13b are best used to analyze which catchments respond most strongly to the presence of frozen soil. Most of the catchments identified in Figure 5.12 as having fewer springs with high ice contents also have lower percent changes due to the presence of soil ice. However, there is once again no clearly defined set of catchments, and therefore region within the upper Mississippi River basin, that can be fully excluded from the study of frozen soil.

Figure 5.13c shows the distribution of annual average ice contents among the catchments. It is very similar to the distribution of changes in the runoff ratio (see Figure 5.13a), while peak flow response shows a bit more variation. This difference is largely due to increased range in significance of the peak flow response predictors (see the t values in Table 5.5), which implies that peak flow response is much more strongly influenced by the peak melt rate than the runoff ratio is by the mean annual precipitation.

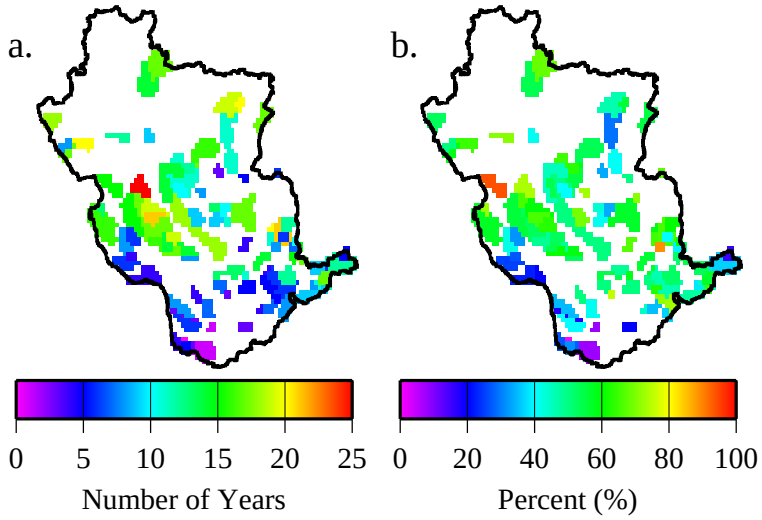

Figure 5.12: Annual ice content distribution by catchment: (a) number of years with greater than median total ice content, and (b) percentage of observed years with greater than median total ice content.

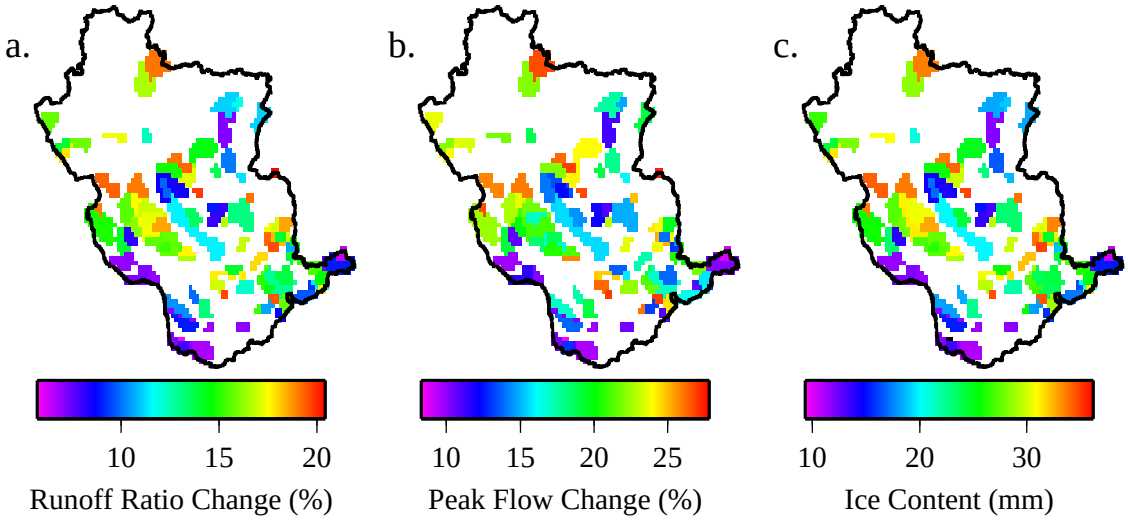

Figure 5.13: Change in predicted response due to the ice content: (a) percent change in runoff ratio response (with ice - without ice / with ice * 100%), (b) percent change in peak flow response, and (c) annual average catchment ice content (mm). Reported values are averaged over available years between 1950 and 1997.

In order to identify the effects of intercatchment and interannual properties the full data set was first split by catchment, with the regression models applied to all years for each catchment; and then split by year, with the regression models applied to all catchments for each year. The distribution of r^2 values by catchment for the multi-year analysis are shown in Figure 5.14. For runoff ratio response, 63 of 95 catchments have r^2 values of less than 0.1, with an average r^2 value of 0.11. Peak flow response r^2 values are fairly uniform below 0.50 and 4 catchments have r^2 values greater than 0.60. The average r^2 value for peak flow response for all catchments is 0.28. This indicates that peak flow response is more strongly influenced by individual catchment characteristics than is the runoff ratio response.

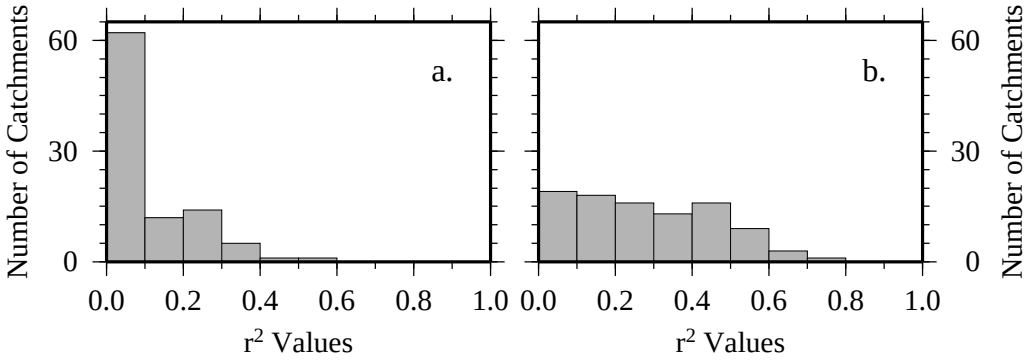

Figure 5.14: Interannual coefficients of variation for all catchments and both response variables: (a) runoff ratio response, (b) peak flow response.

Figure 5.15 shows the distribution of r^2 values by year for the multi-catchment analysis. The annual r^2 values for peak flow response tend to be higher on average than those for runoff ratio response. Distributions of r^2 values are very similar between Figures 5.15 and 5.15. However, there is less variability in the peak flow response distribution by year than by catchment (Figure 5.14), while there is more variance for runoff ratio response by year than by catchment. This suggests that runoff ratio response may be influenced more strongly by interannual conditions, while peak flow response responds more to intercatchment conditions. Years and catchments with especially high r^2 values will need to be investigated to determine if there are specific characteristics that can be used to identify them.

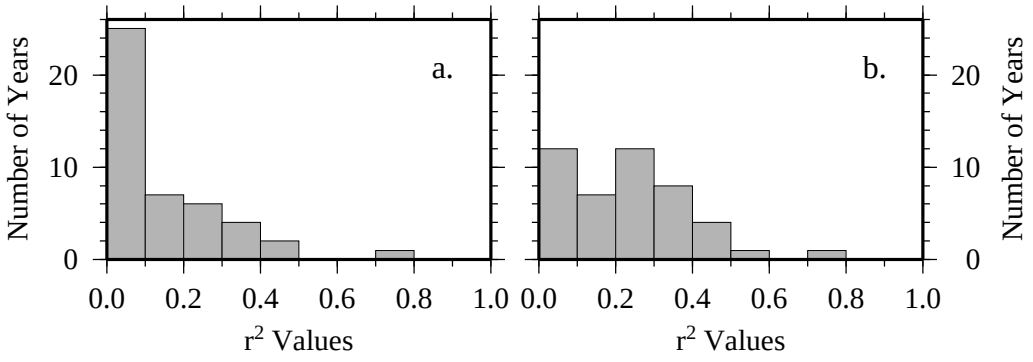

Figure 5.15: Intercatchment coefficients of variation for all years and both response variables: (a) runoff ratio response, (b) peak flow response.

To better identify which, if any of the predictor variables influence the distributions of correlation coefficients seen in Figures 5.14 and 5.15, correlations between each predictor variable (see Tables 5.1 and 5.2) and the resulting correlation coefficient (see Figures 5.14 and 5.15) were computed and are themselves listed in Table 5.8. Table 5.8 indicates that individual catchment r^2 values are somewhat correlated with gauged area (0.23). This suggests that runoff ratio response models may describe more of the observed variance when based on data sets sub-divided by gauged area, rather than the overall model from Table 5.5. Peak flow response by catchment is somewhat correlated with overstory fraction (-0.32), percent silt (-0.26) and catchment slope (-0.25). Annual correlations are much lower, with a maximum of -0.09 (ice content and snow swq) for the runoff ratio response and -0.14 (cumulative precipitation) for the peak flow response. Correlations with ice fraction and total soil moisture are low in all courses, indicating that they are not good on their own.

5.4 Discussion

Large regions of the northern hemisphere experience cold season hydrological processes, including snow accumulation and ablation, and the development of frozen soil. The upper Mississippi River basin, with annual air temperatures ranging from a few degrees Celsius in the north to over 10°C in the south, experiences a range of winter conditions. A statistical

Table 5.8: Correlation of predictor variables with the multiple regression correlation coefficients obtained by applying the regression model to individual catchments and years.

	Catchment		Annual	
	Runoff Ratio	Peak Flow	Runoff Ratio	Peak Flow
Gauged Area	0.23	0.11	0.01	-0.00
Overstory	0.15	-0.32	0.00	0.00
Percent Silt	0.07	-0.26	-0.03	0.00
Mean Annual Precip	0.02	0.13	-0.01	-0.01
Mean Annual Temp	-0.09	0.21	-0.01	-0.03
Catchment Slope	0.16	-0.25	-0.02	0.01
Total Moist	-0.05	0.02	-0.07	-0.12
Ice Content	0.02	0.00	-0.09	-0.12
Snow Swq	0.03	-0.11	-0.09	-0.07
Snow Density	0.02	-0.08	-0.04	-0.05
Frost Depth	0.00	-0.02	-0.07	-0.13
Peak Melt Rate	0.01	0.08	-0.06	-0.00
Cum Precip	0.03	0.04	0.01	-0.14

study was conducted to assess the importance of the role played by frozen soil in controlling the peak flow and runoff ratio responses of catchments within the upper Mississippi River basin. The springtime peak flow response is an indicator of the impact of cold season processes on regional flooding maximums, while the runoff ratio response is an indicator of the effect of snow and frozen soil on average streamflow during the melt season.

Regression analysis of the data set showed that ice content was significant for both response variables. With a p value of 0.06, it is not the most important of the significant predictors, but an increase in the ice content does tend to produce increases in both response variables. Both regression models found that mean annual precipitation, gauged area, peak melt rate, overstory fraction, snow density and cumulative precipitation were also statistically significant. Peak flow response also made use of the catchment silt content.

Differences in the significance of these parameters helps in interpreting the response variables. Mean annual precipitation is the most significant predictor of runoff ratio response. An increase in mean annual precipitation implies an increase in mean annual soil moisture. Since mean annual temperature is highly correlated with mean annual precipitation (see Figures 5.6 and 5.5), the gradient of mean annual precipitation does not imply an increase in mean annual snow accumulation. The peak flow response is clearly dominated by the peak melt rate, indicating that if the rate of water input to the system is high enough, it overwhelms the infiltration rate (*i.e.* Hortonian overland flow) and the current soil conditions will have little impact on the response.

Splitting the data set into two halves based on the median observed ice content for all all years and all catchments, does not produce a visible spatial pattern to the location of high ice contents. This implies that frozen soil is important for determining the spring runoff response for the entire upper Mississippi River basin. A map of average annual ice contents, indicates that frozen soil may be less important in some of the catchments in the southwest and far eastern regions of the basin, but the overall difference is small.

Maps of the change in predicted response due to the absence of ice in the soil, showed that 5 to 25% of predicted runoff ratio response and 8 to 30% of peak flow response is controlled by the ice content. The majority of the catchment responses change by 13.5 to 16.5% for runoff ratio and 18 to 22.5% for peak flow. Since the regression correlation

coefficients are on the order of 0.30 for runoff ratio response and 0.53 for peak flow response, the magnitude of the actual response cannot be determined, however, the spring response of most of the catchments in the upper Mississippi River basin is increased by the presence of frozen soil.

Multiple correlation coefficients varied substantially between catchments and between years, when applied to the full data set resampled to isolate all years for each catchment and all catchments for each year. Analysis of how the correlations were impacted by both interannual (see Table 5.2) and intercatchment (see Table 5.1) predictors showed that intercatchment predictors, especially gauged area for runoff ratio response and overstory fraction for peak flow response, could have a substantial impact on the performance of the regression model. Interannual predictors showed less of an impact, indicating that there may be significant intercatchment predictors not included in this study.

Chapter 6

DISCUSSION

This dissertation was intended to address the two science questions introduced in Chapter 1:

1. How does the spatial distribution of snow and frozen soil influence the hydrologic response of a watershed?

2. How does the hydrologic response to frozen soil change with basin size, climate, vegetation, and other watershed properties?

This chapter summarizes the research described in the previous chapters in the context of these science questions. It then makes recommendations for further research to address issues raised but not addressed in the previous chapters.

6.1 Spatial Distribution Analysis

Field observations at the Rosemount experiment station (see Chapter 3) clearly show that spatial variability of both snow and frozen soil are important to the hydrologic response of the basin during spring melt. Snow is redistributed throughout the winter by wind and preferential melt. During spring melt, areas with deeper snowpacks continue to melt hours or days after the rest of the region is snow free. This impacts both the water and energy cycles (see Chapter 4).

Due to the relative flatness of the Vermillion River watershed, the impact of frozen soil on spring hydrologic response is complex. Ice in the soil reduces infiltration locally, but the spatial variability of ice content and soil properties dictate that relatively small areas of high infiltration can also occur. Melt water flowing across the ground surface can infiltrate in these areas, reducing the impact of frozen soil on streamflow. Frozen soil in low regions

causes melt water to pond at the surface rather than infiltrating. Large low regions cause localized flooding and if melt water fills the available storage it will overflow, in many cases flowing over roads, and continue to flow towards the stream channels. Eventually ponded drains through the underlying frozen soil, typically through drain holes. These conditions are most likely to occur in regions with relatively low ice contents, which are expanded by the infiltration of warmer surface water.

Observations of the spatial distribution of snow and frozen soil indicate that these distributions change through the season but that much of the variability can be represented using a uniform spatial distribution. Other statistical distributions may represent the observations slightly better, but the uniform distribution captures the dominant effects of spatial variability and results in less computational burden than more complex representations. Algorithms to represent the effects of spatial variability in ice content and snow properties based on the Rosemount field observations were developed and implemented in the VIC macroscale hydrologic model. Testing was conducted at point and catchment scales (see Chapter 4).

The spatial snow algorithm described in Chapter 4 had the largest impact on thin snowpacks, which in the previous form of the snow model (see Appendix B) melted over several days. For thicker snowpacks and when melt occurred quickly, the spatial snow algorithm has limited impact. With the addition of advected sensible heat from snow free areas, snow melt of partially covering snowpacks is accelerated. This can shift the stream flow response slightly earlier and can result in slightly higher peak discharge. However, the total effect on streamflow is minor. More importantly, the spatial snow algorithm changed the dynamics of the land surface-atmosphere interaction by modifying the sensible heat exchange. Snow free regions warm up the grid cell surface temperature and increase the sensible heat flux exchange with the atmosphere as compared to the model with a uniform snow cover. This makes the transition between snow covered and snow free less abrupt and more natural, within each vegetation type.

The spatial frost algorithm increases infiltration into the soil during the winter and during melt events. In years without deep frost, the spatial algorithm produces only minimal changes in the catchment response. Under conditions of deep soil freezing, however, the

spatial algorithm modifies the basin response substantially. Increases in peak flow caused directly by frozen soil (rapid snow melt over soils with low unfrozen moisture contents) are reduced due to higher infiltration. When melt occurs slowly, soil moisture contents are increased prior to the day of peak melt, and the spatial frozen soil model may increase the initial streamflow response. Increased infiltration into the soil means that the soil will be wetter at the time of peak melt, and increased soil moisture drainage implies that baseflow will react more quickly, increasing the total discharge response.

Taken together, the spatial frost and snow algorithm development and testing suggest, with respect to the first science question, that:

- The spatial distribution of snow and frozen soil play an important role in defining the hydrologic response of a watershed.

- Advection of sensible heat from snow-free to snow-covered areas can increase the rate of melt, shortening the snow covered period by several days for thin snow.

- Snow-free surface temperatures warm up faster than snow covered areas, and by representing partial snow cover, changes in sensible heat exchange with the atmosphere are not as abrupt as when the all of the snow cover melts at the same instant. Average monthly sensible heat flux from February to May is increased on average by 10 W/m^2.

- Spatially distributed frost increases infiltration and drainage during the winter and spring, over spatially unvarying frost.

- Increased infiltration can reduce peak flow response in situations where the unfrozen soil moisture content is low. However, for prolonged melts, the increased infiltration rate will yield a more saturated soil and increased baseflow response, which can yield higher peak flows to later melt or precipitation events. For the St. Croix River, changes in peak flow rates can be on the order of 30%.

- Increased drainage through the winter causes small increases in winter baseflow, which have a very minor effect on streamflow. However, drier soils in the spring will allow

more infiltration than is predicted by the point algorithm. Just prior to the start of snow melt, soils for the Rosemount point model simulations were as much as 20% drier, than those predicted using the parameterization of ice content spatial variation.

- Though these processes appear to have minimal effect on larger catchments in the upper Mississippi River basin, they are important for local flooding and for smaller catchment response, and are likely to play larger roles in other regions of the world.

Spatially distributed snow and frozen soil play important roles in the hydrologic response of smaller catchments, specifically by changing the timing of melt and increasing the infiltration of melt water into frozen soil.

6.2 Catchment Properties Analysis

The statistical analysis of catchment properties and their impact on the catchment's response to frozen soil highlighted the complexity of the processes involved. Catchment properties were identified for over 100 gauged catchments in the upper Mississippi River basin, and variations in the streamflow response during the spring melt period was examined. None of the selected catchment characteristics were able to describe much of the observed variability in the runoff ratio and peak flow responses individually. Combined into multiple regression models, only 9% of runoff ratio variability and 28% of peak flow variability could be explained. Specific catchments and years showed much higher correlations indicating that there might be processes occurring within specific catchments or years that are not represented by the characteristics selected for the study.

Despite the limited amount of variance described by the regression models, the analysis did provide some insights into the issues suggested by the second science question:

- Ice content, which is a direct indicator of frozen soil extent, was a significant predictor for both response variables. Higher ice content prior to melt yields an increase in both the runoff ratio and peak flow responses.

- Frozen soil processes appear to influence spring runoff response throughout the upper

Mississippi River basin, with little to no apparent trend in magnitude or likelihood of a change in response.

- Basin characteristics that are significant in predicting runoff ratio and peak flow response include:
  - Mean annual precipitation - increasing mean annual precipitation implies wetter soils which can yield higher ice contents.
  - Peak melt rate - increasing the peak melt rate increases the rate with which water is added to the catchment, increasing runoff response independent of frozen soil.
  - Overstory fraction - increasing overstory fraction implies an increase in forestation, which in turn implies a decrease in snow accumulation, the retention of ground snow until later in the melt season, and a reduction in the formation of frozen soil.
  - Snow density - decreasing snow density, implies an increase in ground surface insulation, which protects frozen soil from warmer air temperatures.
- The analysis suggests that improved representation of observed variability in both runoff ratio and peak flow responses could be obtained by computing separate regressions for subsets of catchments based on various intercatchment characteristics (*i.e.* gauged area and fraction of overstory). The same does not appear to be true of interannual predictors (*i.e.* soil moisture and snow water equivalent).

This study shows that frozen soil is indeed a significant factor in controlling catchment response to spring melt, and that certain catchment properties also contribute. Due to the many interactions between the predictor variables, it is difficult to assess the magnitude of the effect.

6.3 Recommendations for Further Research

This section presents four recommendations for further research to address issues and questions suggested by the results of the research reported in this dissertation. The recom-

mendations include further field observations, expanded statistical analysis of observed and simulated runoff response, analysis of the effects of ponded water, and a reevaluation of model performance.

The field observation program in Chapter 3 identified the importance of the spatial distribution of snow and frozen soil to local spring runoff response. It also allowed the derivation of statistical distributions that could be used to represent the observed spatial variability. Due to equipment failures the field program was unable to provide verification of the applicability of the distributions estimated from field scale data to the larger catchment scale. The limited variety of vegetation cover types and topographical relief within the Rosemount site also limited the ability to test the applicability of the spatial distributions to different catchments and regions. Furthermore, field observations were limited primarily to snow depth and soil temperature, while hydrologic response is much more clearly controlled by the water balance components of snow water equivalent and soil liquid and soil moisture content (which are of course harder to measure). Another limitation of the study is that the three winters of field observations all had lower than normal snow accumulations. Larger snow accumulations occurred the winter before (1996-1997) and the winter after (2000-2001). The spring melts following both of these winters lead to flood conditions in the Red River basin (1997) and the Mississippi River basin (2001).

In order to better address these issues, and expanded field program is advisable. Large scale transects should be implemented to assess the distribution of snow and soil frost at the catchment scale. Several catchments with different properties (forested, agricultural, urban, more topographic variation) should be included to investigate how each of these impacts both the distribution of snow and frozen soil, as well as the hydrologic response to spring conditions. More observations of snow water equivalent and soil moisture contents should be included and observations should be collected for several years (although most likely coincidental, in the recent past there has been a cycle of large floods every four years (1993, 1997, 2001 within the upper Mississippi basin). Remote sensing may also prove valuable for identifying regional distributions for both snow and frozen soil, especially with an improved ground observation data set.

The statistical tests conducted in Chapter 5 found that soil ice content was a significant

predictor of spring runoff response, though the total amount of explained variance was low (30% for peak flow response and 9% for runoff ratio response). There were, however, catchments and years for which the explained variance was much higher. Further analysis of these catchments and years may yield insight into why they are more predictable and whether frozen soil plays any role in this behavior. Efforts should also be made to determine which reservoirs in the upper Mississippi River basin have a significant impact on observed discharge. By excluding only those basins, it may be possible to increase the number of catchments that can be used in the analysis, especially in the northern reaches of the watershed where frozen soil would be expect to be more important. Selecting catchment pairs to compare and contrast specific catchment characteristics may also provide valuable insight into the conditions and characteristics most important in determining a catchments spring runoff response.

Model simulations could be used to identify catchments and years with large simulated frozen soil responses, by comparing simulated runoff and baseflow between the model with and without the frozen soil algorithm. Observed records for catchments and years selected in this fashion can be analyzed to determine whether or not there is an observed response. This may also help to better understand the relative contribution of frozen soil to peak runoff response.

As observed during the field campaign described in Chapter 3, ponding of melt water is an important process controlling spring runoff in and around the Rosemount Agricultural Experiment Station. During many years, it dominates the effect of frozen soil on spring runoff response. The VIC model has recently been modified to represent the effects of lakes and wetlands on runoff and baseflow generation as well as evaporation [*Bowling et al.*, 2000]. The upper Mississippi River basin may prove a valuable place to test the new algorithms to determine how well they can represent transient storage of water over frozen soil. Field surveys and remote sensing data (*i.e.* air photos, high resolution satellite images) may be useful in identifying the storage capacity of fields in the local catchments, which could be used to parameterize the VIC model.

When the ponded water eventually finds a way through the underlying frozen soil, it will recharge the local aquifer. If changes in future climate, historical vegetation cover or

current tillage practices modify the amount of water that is recharged in this fashion, there is a question as to the impact these altered conditions would have on local groundwater recharge. The VIC model represents soils on the order of 1 to 2 m thick, but around Rosemount soils reach a depth of 25 m. Adding one or more layers to the VIC model may improve its representation of these regions, but it is quite likely that deeper aquifers play an important role locally and that only by coupling the VIC model, or other surface water model, with a ground water model will the local hydrologic cycle be accurately simulated.

Finally, the algorithms developed to represent spatially varying frost and snow (Chapter 4) have resulted in considerable computational burden when implemented within the VIC model. Some streamlining of algorithms was achieved during the course of this work which reduced run times by more than half, however the full frozen soil and snow spatial variability parameterizations still incur too much computational overhead to make their use practical for large area, multi-year simulations (e.g., the decadal simulations of the Mississippi River basin reported by Maurer et al, 2001). Furthermore, transferability of model parameters needs to be addressed in greater detail. Sensitivity of the VIC model simulations to the parameters included in the new paramterizations must also be investigated in greater detail.

BIBLIOGRAPHY

Abdulla, F. A., D. P. Lettenmaier, E. F. Wood, and J. A. Smith, Application of a macroscale hydrologic model to estimate the water balance of the Arkansas-Red River basin, *J. Geophys. Res.*, *101*, 7449–7459, 1996.

Allis, J. A., B. Harris, and A. L. Sharp, A comparison of performance of five rain-gage installations, *J. Geophys. Res.*, *68*, 4723–4729, 1963.

Avissar, R., Which type of soil-vegetation-atmosphere transfer scheme is needed for general circulation models: a proposal for a higher-order scheme, *J. Hydrol.*, *212-231*, Pages 136–154, 1998.

Baker, J. M., The efficiency of soil moisture recharge by snowmelt in the upper midwestern United States, in *Eos Trans.*, vol. 81, AGU, 2000, fall Meet. Suppl.

Bathurst, J. C., and K. R. Cooley, Use of the SHE hydrological modelling system to investigate basin response to snowmelt at Reynolds Creek, Idaho, *J. Hydrol.*, *175*, 181–211, 1996.

Benoit, G. R., and S. Mostaghimi, Modeling soil frost under conservation tillage systems, *Pap. Am. Soc. Agric. Eng.*, 1984.

Benoit, G. R., and S. Mostaghimi, Modeling soil frost depth under three tillage systems, *Trans. A. S. A. E. Am. Soc. Agric. Eng.*, *28*, 1499–1505, 1985.

Benoit, G. R., S. Mostaghimi, R. A. Young, and M. J. Lindstrom, Tillage-residue effects on snow cover, soil water, temperature and frost, *Trans. A. S. A. E.*, *29*, 473–479, 1986.

Betts, A. K., and J. H. Ball, FIFE surface climate and site-average dataset 1987-1989, *J. Atmos. Sci.*, *55*, 1091–1108, 1998.

Betts, A. K., J. H. Ball, A. C. M. Beljaars, M. J. Miller, and P. Viterbo, The land-surface-atmosphere interaction: A review based on observational and global modeling perspectives, *J. Geophys. Res.*, *101*, 7209–25, 1996.

Bouyoucos, G. J., Degree of temperature to which soils can be cooled without freezing, *J. Agric. Res.*, *20*, 267–269, 1920.

Bowling, L. C., K. A. Cherkauer, and D. P. Lettenmaier, Simulation of the effect of lakes and wetland storage on the flow of Arctic rivers, *Eos Trans.*, *81*, 2000.

Bras, R. L., *Hydrology: an introduction to hydrologic science*, Addison-Wesley, 1990.

Brennan, P., Less pollution may boost global warming, *The Orange County Register*, 2001.

Burrough, P., *Principles of Geographical Information Systems for Land Resources Assessment*, p. 50, Oxford University Press, 1986.

Cherkauer, K. A., and D. P. Lettenmaier, Hydrologic effects of frozen soils in the upper Mississippi River basin, *J. Geopys. Res.*, *104*, 19,599–19,610, 1999.

Daly, C., R. Neilson, and D. Phillips, A statistical-topographic model for mapping climatological precipitation over mountainous terrain, *J. Appl. Meteor.*, *33*, 140–158, 1994.

Dingman, S., Hydrologic effects of frozen ground - literature review and synthesis, *Special Report 218*, U.S.A.C.E Cold Regions esearch and Engineering Laboratory, 1975.

Dunne, T., and L. B. Leopold, *Water in Environmental Planning*, chap. 10, W. H. Freeman and Company, New York, 1978.

Engelmark, and Svensson, Numerical modelling of phase change in freezing and thawing unsaturated soil, *Nord. Hydrol.*, *24*, 95–110, 1993.

Flerchinger, G. N., and K. E. Saxton, Simultaneous heat and water model of a freezing snow-residue-soil system I. Theory and development, *Trans. A. S. A. E.*, *32*, 565–71, 1989a.

Flerchinger, G. N., and K. E. Saxton, Simultaneous heat and water model of a freezing snow-residue-soil system II. Field verification, *Trans. A. S. A. E.*, *32*, 573–8, 1989b.

Flerchinger, G. N., J. M. Baker, and E. J. A. Spaans, A test of the radiative energy balance of the SHAW model for snowcover, *Hydrol. Process.*, *10*, 1359–1367, 1996.

Fox, J. D., Incorporating freeze-thaw calculations into a water balance model, *Water Resour. Res*, *28*, 2229–2244, 1992.

Fuchs, M., G. S. Campbell, and R. I. Papendick, An analysis of sensible and latent heat flow in a partially frozen unsaturated soil, *Soil Sci. Soc. Am. J.*, *42*, 379–85, 1978.

Garbrecht, J., Effects of spatial accumulation of runoff on watershed response, *J. Environ. Qual.*, *120*, 31–35, 1991.

Gel'fan, A. N., Comparison of two methods of calculating soil freezing depth, *Sov. Meteorol. Hydrol.*, *2*, 78–83, 1989.

Gray, D. M., and D. H. Male (Eds.), *Handbook of snow. Principles, processes, management and use*, Pergamon, Toronto, Ont., 1981.

Gray, D. M., and T. D. Prowse, Snow and floating ice, in *Handbook of Hydrology*, edited by D. R. Maidment, p. 58, McGraw-Hill, Inc., San Francisco, 1993.

Gusev, Y. M., and O. N. Nasonova, An experience of modelling heat and water exchange at the land surface on a large river basin scale, *J. Hydrol.*, *233*, Pages 1–18, 2000.

Halldin, S., L. Gottschalk, A. A. van de Griend, S.-E. Gryning, M. Heikinheimo, U. Hgstrm, A. Jochum, and L.-C. Lundin, NOPEX - a northern hemisphere climate processes land surface experiment, *J. Hydrol.*, *212-213*, 172–187, 1998.

Hansen, M. C., R. S. Defries, J. R. G. Townshend, and R. Sohlberg, Global land cover classification at 1km spatial resolution using a classification tree approach, *Int. J. Remote Sensing*, *21*, 1331–1364, 2000.

Hanson, C. L., G. L. Johnson, and A. Rango, Comparison of precipitation catch between nine measuring systems, *J. Hydrol. Eng.*, *4*, 1999.

Hedstrom, N. R., and J. W. Pomeroy, Measurements and modelling of snow interception in the boreal forest, *Hydrol. Process.*, *12*, 1611–1625, 1998.

Hohmann, M., Soil freezing - the concept of soil water potential. state of the art, *Cold Reg. Sci. Tech.*, *25*, 101–110, 1997.

Kalnay, E., et al., The NCEP/NCAR 40-year reanalysis project, *Bull. Am. Meteorol. Soc.*, *77*, 437–471, 1996.

Kane, D. L., and E. F. Chacho, Frozen ground effects on infiltration and runoff, in *Cold Regions Hydrology and Hydraulics*, pp. 259–300, American Society of Civil Engineers, New York, 1990.

Kienholz, R., Frost depth in forest and open in Connecticut, *Journal of Forestry*, *38*, 345–350, 1940.

Koren, V., J. Schaake, K. Mitchell, Q.-Y. Duan, F. Chen, and J. M. Baker, A parameterization of snowpack and frozen ground intended for NCEP weather and climate models, *J. Geophys. Res.*, *104*, 19,569–19,586, 1999.

Koren, V. I., Modeling of processes of river runoff formation in the forest zone of the European USSR, *Meteorologiya*, *10*, 78–85, 1980.

Liang, X., D. P. Lettenmaier, E. F. Wood, and S. J. Burges, A simple hydrologically based model of land surface water and energy fluxes for general circulation models, *J. Geophys. Res.*, *99*, 14,415–28, 1994.

Liang, X., D. P. Lettenmaier, and E. F. Wood, One-dimensional statistical dynamic representation of subgrid spatial variability of precipitation in the two-layer variable infiltration capacity model, *J. Geophys. Res.*, *101*, 21,403–21,422, 1996a.

Liang, X., E. F. Wood, and D. P. Lettenmaier, Surface soil moisture parameterization of the VIC-2L model: Evaluation and modification, *Global and Planetary Change*, *13*, 195–206, 1996b.

Liang, X., E. F. Wood, and D. P. Lettenmaier, Modeling ground heat flux in land surface parameterization schemes, *J. Geophys. Res.*, *104*, 9581–9600, 1999.

Liang, X., et al., The project for intercomparison of land-surface parameterization schemes (PILPS) phase 2(c) Red-Arkansas River basin experiment: 2. Spatial and temporal analysis of energy fluxes, *Global and Planetary Change*, *19*, 137–159, 1998.

Linsley, R. K., M. A. Kohler, and J. L. H. Paulhus, *Hydrology for Engineers*, McGraw-Hill Series in Water Resources and Environmental Engineering, 3 ed., McGraw-Hill, Inc, San Francisco, 1982.

Lohmann, D., E. Raschke, B. Nijssen, and D. P. Lettenmaier, Regional scale hydrology; I, formulation of the VIC-2L model coupled to a routing model, *Hydrological Sciences Journal*, *43*, 131–141, 1998a.

Lohmann, D., E. Raschke, B. Nijssen, and D. P. Lettenmaier, Regional scale hydrology; II, application of the VIC-2L model to the weser river, germany, *Hydrological Sciences Journal*, *43*, 143–158, 1998b.

Lohmann, D., et al., The project for intercomparison of land-surface parameterization schemes (PILPS) phase 2(c) Red-Arkansas River basin experiment: 3. Spatial and temporal analysis of water fluxes, *Global and Planetary Change*, *19*, 161–179, 1998c.

Luce, C. H., and D. G. Tarboton, Scaling up snowpack accumulation and melt models, *submit. Water Resour. Res.*, -, –, 2000.

Luce, C. H., D. G. Tarboton, and K. R. Cooley, The influence of the spatial distribution of snow on basin-averaged snowmelt, *Hydrol. Process.*, *12*, 1671–1683, 1998.

Luce, C. H., D. G. Tarboton, and K. R. Cooley, Sub-grid parameterization of snow distribution for an energy and mass balance snow cover model, *Hydrol. Process.*, *13*, 1921–1933, 1999.

Lundin, L.-C., Hydraulic properties in an operational model of frozen soil, *J. Hydrol.*, *119*, 289–310, 1990.

Marsh, P., and J. W. Pomeroy, Meltwater fluxes at an Arctic forest-tundra site, *Hydrol. Process.*, *10*, 1383–1400, 1996.

Marsh, P., and M. Woo, Soil heat flux, wetting front advance and ice layer growth in cold, dry snow covers, in *Snow Property Measurements Workshop*, pp. 497–524, National Research Council of Canada, Lake Louise, Ab, Canada, 1987.

Marsh, P., J. W. Pomeroy, and N. Neumann, Sensible heat flux and local advection over a heterogeneous landscape at an Arctic tundra site during snowmelt, *Annals of Glaciology*, *25*, 132–135, 1997.

Marshall, T. J., J. W. Holmes, and C. W. Rose, *Soil Physics*, 3 ed., Cambridge University Press, New York, 1996.

Miller, D. A., and R. A. White, A conterminous United States multilayer soil characteristics dataset for regional climate and hydrology modeling, *Earth Inter.*, *2*, 1998.

Mynenui, R., R. R. Nemani, and S. W. Running, Estimation of global leaf area index and absorbed par using radiative transfer models, *IEEE Trans. Geosci. Remote Sens.*, *35*, 1380–1393, 1997.

National Snow and Ice Data Center, 1978 - 1995. Northern Hemisphere weekly snow cover and sea ice extent, NSIDC Distributed Active Archive Center, University of Colorado, 1996.

Nespor, V., *Investigation of wind-induced error of precipitation measurements using a three-dimensional numerical solution*, vol. 63 of *Zürcher Geographische Schriften*, Geographisches Institut ETH, Zürich, 1996.

Newman, G. P., and G. W. Wilson, Heat and mass transfer in unsaturated soils during freezing, *Can. Geotech. J.*, *34*, 63–70, 1997.

Nijssen, B., D. P. Lettenmaier, X. Liang, S. W. Wetzel, and E. F. Wood, Streamflow simulation for continental-scale river basins, *Water Resour. Res.*, *33*, 711–24, 1997.

Nijssen, B., R. Schnur, and D. P. Lettenmaier, Global restrospective estimation of soil moisture using the VIC land surface model, 1980-1993, *in review J. Clim.*, 2000.

Pierce, R. S., H. W. Lull, and H. C. Storey, Influence of land use on time soil freezing and thawing in the Northeast, *Forest Science*, *4*, 246–263, 1958.

Pomeroy, J. W., P. Marsh, and D. M. Gray, Application of a distributed blowing snow model to the Arctic, *Hydrol. Process.*, *11*, 1451–1464, 1997.

Sakamoto, Y., M. Ishiguro, and G. Kitagawa, *Akaike Information Criterion Statistics*, Kluwer Academic Publishers, 1987.

Sand, K., and D. L. Kane, Effects of seasonally frozen ground in snowmelt modeling, in *Cold Regions Hydrology*, edited by D. L. Kane, pp. 321–327, American Water Resources Association, Bethesda, MD, 1986.

Schnur, R., and D. P. Lettenmaier, A global gridded data set of soil moisture, in *13th Conference on Hydrology*, AMS, Long Beach, CA, 1997.

Scientific Assessment and Strategy Team, RESERVOIR Arc/Info coverage, http://edcwww.cr.usgs.gov/sast-home.html, 1995a.

Scientific Assessment and Strategy Team, RIV2M Arc/Info coverage, http://edcwww.cr.usgs.gov/sast-home.html, 1995b.

Seyfried, M. S., and B. P. Wilcox, Scale and the nature of spatial variability: field examples having implications for hydrologic modeling., *Water Resour. Res.*, *31*, 173–184, 1995.

Shanley, J. B., and A. Chalmers, The effect of frozen soil on snowmelt runoff at Sleepers River, Vermont, *Hydrol. Process.*, *13*, 1843–1857, 1999.

Shook, K., and D. M. Gray, Synthesizing shallow seasonal snow covers, *Water Resour. Res.*, *33*, 419–420, 1997.

Shook, K., D. M. Gray, and J. W. Pomeroy, Temporal variation in snowcover area during melt in prairie and alpine environments, *Nord. Hydrol.*, *24*, 183–198, 1993.

Shoop, S. A., and S. R. Bigl, Moisture migration during freeze and thaw of unsaturated soils: Modeling and large scale experiments, *Cold Regions Sci. Tech.*, *25*, 33–45, 1997.

Stadler, D., H. Wunderli, A. Auckenthaler, H. Fluhler, and M. Brundl, Measurement of frost-induced snowmelt runoff in a forest soil, *Hydrol. Process.*, *10*, 1293–1304, 1996.

Stadler, D., H. Fluhler, and P. E. Jansson, Modelling vertical and lateral water flow in frozen and sloped forest soil plots, *Cold Regions Science and Technology*, *26*, 181–194, 1997.

Stahli, M., P. E. Jansson, and L. C. Lundin, Preferential water flow in a frozen soil - a two-domain model approach, *Hydrol. Process.*, *10*, 1305–1316, 1996.

Stewart, R. E., et al., The Mackenzie GEWEX study: The water and energy cycles of a major North American river basin, *Bull. Amer. Meteor. Soc.*, *79*, 2665–2684, 1998.

Storck, P., and D. P. Lettenmaier, Predicting the effect of a forest canopy on ground snow accumulation and ablation in maritime climates, in *67th Western Snow Conference*, edited by C. Troendle, Colorado State University, 1999.

Storey, H. C., Frozen soil and spring and winter floods, in *Yearbook of Agriculture 1955*, pp. 179–184, The United States Department of Agriculture, 1955.

Tarnawski, V. R., and B. Wagner, On the prediction of hydraulic conductivity of frozen soils, *Can. Geotech. J.*, *33*, 176–180, 1996.

Warnick, C. C., Experiments with windshields for precipitation gages, *Trans. Am. Geophysical Union*, *34*, 379–388, 1953.

Wheeler, L., Expert says warming is not the culprit in higher hurricane activity, *Gannett News Service*, 2001.

Williams, C. J., U. S. rebuked over Bush global-warming position, *Los Angeles Times*, 2001.

Williams, P. J., and M. W. Smith, *The Frozen Earth: Fundamentals of Geocryology*, Cambridge University Press, Cambridge, NY, 1989.

Wood, E. F., et al., The project for intercomparison of land-surface parameterization schemes (PILPS) phase 2(c) Red-Arkansas River basin experiment: 1. Experiment description and summary intercomparisons, *Global and Planetary Change*, *19*, 115–135, 1998.

Yang, D., B. E. Goodison, S. Ishida, and C. S. Benson, Adjustment of daily precipitation data at 10 climate stations in Alaska: Application of World Meteorological Organization intercomparison results, *Water Resour. Res.*, *34*, 241–256, 1998a.

Yang, D., B. E. Goodison, J. R. Metcalfe, V. S. Golubev, R. Bates, T. Pangburn, and C. L. Hanson, Accuracy of NWS 8" standard nonrecording precipitation gauge: Results and application of WMO intercomparison, *J. Atmos. Oceanic Tech.*, *15*, 54–68, 1998b.

Yang, D., et al., Accuracy of Tretyakov precipitation gauge: result of WMO intercomparison, *Hydrol. Process.*, *9*, 877–895, 1995.

Zhao, L., and D. M. Gray, A parametric expression for estimating infiltration into frozen soils, *Hydrol. Process.*, *11*, 1761–1775, 1997.

Zhao, L. T., D. M. Gray, and D. H. Male, Numerical analysis of simultaneous heat and mass transfer during infiltration into frozen ground, *J. Hydrol.*, *200*, 345–363, 1997.

Appendix A

CORRECTION OF METEOROLOGICAL FORCING DATA

Macroscale hydrologic models rely on meteorological forcings derived from observations. Over most of the United States, daily precipitation, and maximum and minimum air temperature are provided by the NOAA cooperative observer network. Data are archived by the National Climatic Data Center (NCDC). These data have been used in many previous applications to drive the variable infiltration capacity (VIC) macroscale hydrologic model (see Chapter 4) [*Abdulla et al.*, 1996; *Nijssen et al.*, 1997; *Cherkauer and Lettenmaier*, 1999]. While air temperature, aside from the possible effects of station relocation, is fairly easy to measure, precipitation, especially in the form of snow, poses many difficulties. Gauge undercatch due to wind is the most serious error associated with the measurement of precipitation, especially snow [*Linsley et al.*, 1982, Chap. 3]. Aerodynamic effects cause precipitation (both rain and snow) to be transported away from the mouth of the gauge [*Nespor*, 1996]. Because snowflakes are lighter than raindrops, gauge undercatch errors are greatest with snowfall [*Warnick*, 1953; *Allis et al.*, 1963; *Yang et al.*, 1998a, b; *Hanson et al.*, 1999]. Undercatch is even more of a problem when the gauge is not sheltered from the wind, so many attempts have been made to design shields that can be erected around the gauge. Comparisons of these shielded gauges indicate that even the best shields do not prevent all losses to the wind [*Warnick*, 1953; *Allis et al.*, 1963; *Yang et al.*, 1998a, b; *Hanson et al.*, 1999]. Various empirically derived equations [*Yang et al.*, 1998a, b; *Linsley et al.*, 1982, Chap. 3] have been developed to account for the undercatch losses.

Undercatch increases with wind speed [*Yang et al.*, 1995, 1998b], implying that the accuracy of the correction factor changes with the proximity of the wind speed observations to the mouth of the gauge. Wind speed is observed at only a few of the cooperative observer stations, making direct correction of the precipitation, with adjacent wind speeds, impossible at most stations. This chapter explores two methods for precipitation correction within the

upper Mississippi River basin and assesses the importance of gauge undercatch correction in the basin.

A.1 Correction of Precipitation and Wind Speed

Figure A.1 compares uncorrected and corrected precipitation at the University of Minnesota's Rosemount Agricultural Experiment Station. Both precipitation and wind speed

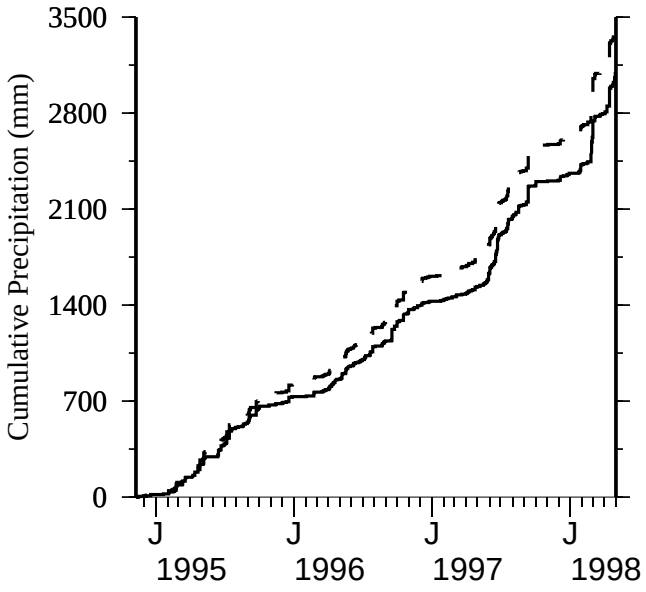

Figure A.1: Cumulative observed (solid) and corrected (dashed) precipitation at the Rosemount experiment site for December 1994 through May 1998.

observations are available for Rosemount on an hourly basis. Correction of precipitation was made using the correction equations for the unshielded National Weather Service (NWS) 8-inch standard rain gauge derived by *Yang et al.* [1998b] as a result of the World Meteorological Organization's (WMO) precipitation gauge intercomparison project, as follows:
Snow:

$$R_{unshielded} = exp(4.606 - 0.157Ws^{1.28}) \tag{A.1}$$

Mixed Precipitation:

$$R_{unshielded} = 100.77 - 8.34Ws \tag{A.2}$$

Rain:

$$R_{unshielded} = exp(4.605 - 0.062Ws^{0.58}) \tag{A.3}$$

where R is the precipitation correction factor (percent), Ws is the wind speed in m/s. Over the course of three and a half years, correction of wind-induced undercatch at Rosemount adds nearly 338 mm of precipitation, increasing the total precipitation by 10.9%. Rain gauge precipitation observations are also affected by errors caused by wetting and evaporation [*Yang et al.*, 1998b]. In most cases these errors are significantly smaller than those caused by wind-induced undercatch and are highly dependent on gauge sampling frequency and other gauge specific criteria. Due to the lack of detailed information to quantify this process these errors are ignored in this analysis.

The problem with correcting precipitation on a larger scale is the sparseness of wind observations. Figure A.2 shows the location of NCDC stations that report both daily precipitation and wind speed. The density of precipitation stations is quite high, especially in the southern part of the basin. Only about 30 of those stations also report daily wind speed. This means that a direct application of Equations A.1, A.2 and A.3, which requires observations of wind speed and precipitation in close proximity, is impossible for the majority of precipitation stations.

Some recent VIC model applications have made use of NCEP/NCAR reanalysis near-surface wind speeds [*Kalnay et al.*, 1996]. This provides gridded daily winds at a reference height of 10 m and a resolution of 2.5° by 2.5°. Reanalysis wind fields are available from January 1, 1948 through the present. Since the reanalysis wind data are available for the entire upper Mississippi River basin, the feasibility of using it to correct station precipitation observations for wind induced gauge undercatch is investigated.

For VIC model applications, the reanalysis wind data are interpolated to the one-eighth degree model grid. Grid cells that also contained a wind reporting observer station were

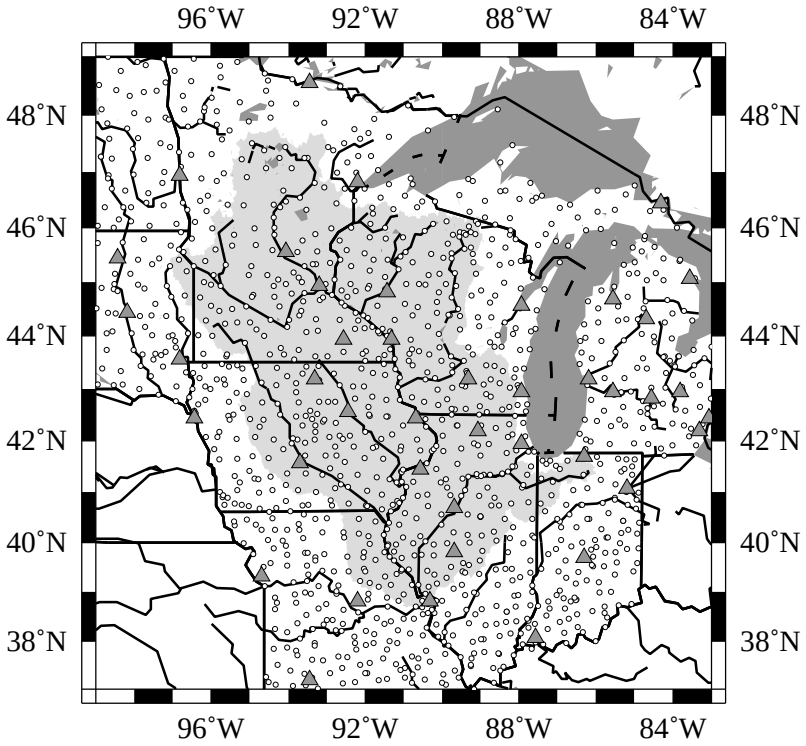

Figure A.2: Location of NCDC stations that report daily wind speed (triangles) and precipitation (circles) in and around the upper Mississippi River basin.

used to assess the accuracy of the reanalysis winds. Scatter plots for three of those comparisons are shown in Figure A.3a. Reanalysis winds underestimate almost all observed wind speeds and the underestimation is most pronounced for the highest observed wind speeds. Another issue is the scatter shown in the plot; reanalysis winds can vary by almost 5 m/s for any observed wind speed. Since the precipitation correction equations are strongly wind dependent, the variance in reanalysis winds is likely to cause errors in the corrected precipitation field even if the bias is corrected. To test this theory the wind speed bias was corrected.

Most observer stations did not begin to report wind speed until 1984, thus the station data could not be used to adjust wind speeds on a daily basis. Instead mean monthly adjustment factors were computed as follows:

- Daily observed wind was raised from its 2 m measurement height to the 10 m height of the reanalysis wind field using a logarithmic profile and assuming ground cover was grass (0.75 m tall).

- Daily reanalysis wind speeds were divided by daily station wind speeds to determine the adjustment factor.

- Monthly average adjustment factors were computed and averaged over all years of observations.

- Monthly adjustment factors were interpolated over the model domain to determine the correction needed for each grid cell.

The resulting monthly bias adjustment factors for the reanalysis wind are shown in Figure A.4. Adjustment factors for all months are greater than 40% year round, with the highest factors in the summer. The northeastern region of the basin, which is the most heavily forested, has the lowest correction factors for wind speed. Ignoring the effects of forestation, the rest of the basin shows no clear trend in the correction factor.

The effect of the correction factor on gridded annual average wind speed can be seen in Figure A.5. Unadjusted wind speeds are in the range of 3 to 4 m/s and fairly uniform

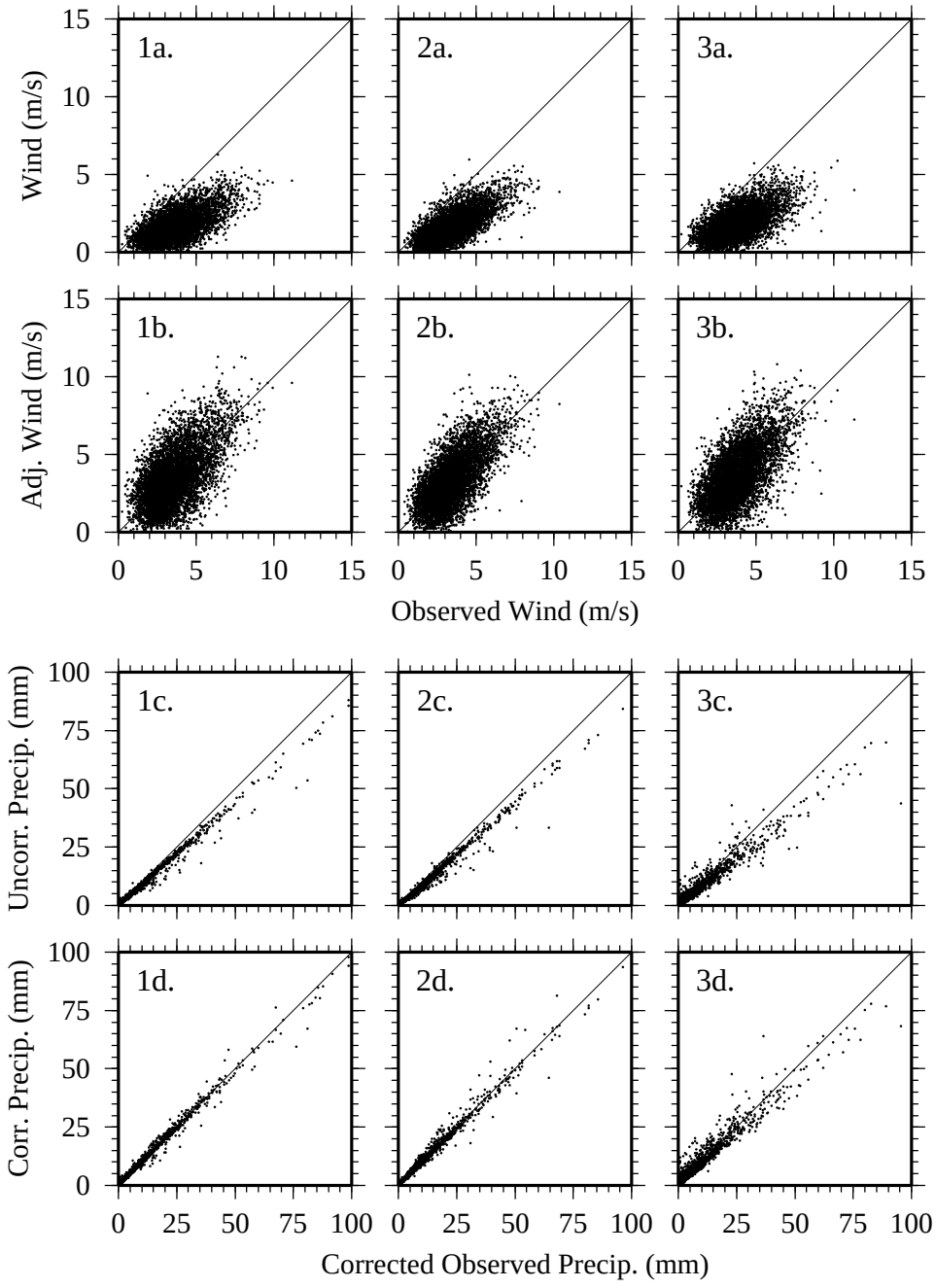

Figure A.3: Station data compared with VIC gridded forcing data: columns are (1) Station located at 39° 51' N, 89° 41' W, (2) station located at 41° 42' N, 86° 20' W and (3) station located at 44° 53' N, 93° 14' N. (a) plots for each station show station versus reanalysis wind at 1 m gauge height, (b) station versus adjusted reanalysis wind at 1 m gauge height, (c) station corrected versus uncorrected gridded precipitation and (d) station corrected versus corrected gridded precipitation.

across the basin. The adjustment of wind speed increases most basin-average winds by 3 to 3.5 m/s with no clear trend. Resulting wind speeds across the basin are mostly between 6 and 7 m/s.

Adjusted reanalysis wind speeds are plotted against station wind speeds in Figure A.3b. The resulting wind speeds compare more favorably with the station observations but the scatter has been increased. Table A.1 lists monthly cumulative observed and gridded precipitation. Also listed are station precipitation corrected for gauge undercatch using station wind and gridded precipitation corrected using the adjusted reanalysis winds. Both cases make use of equations A.1, A.2 and A.3. Differences between the station precipitation and gridded precipitation are due to the location of the station within the grid cell and the adjustment of monthly mean gridded precipitation so that it agrees with monthly average precipitation field from the PRISM (Parameter-elevation Regressions on Independent Slopes Model) monthly precipitation dataset [*Daly et al.*, 1994]. During the summer months, reanalysis wind corrected precipitation is 2 to 3% lower than corrected station precipitation, which is similar to the difference in uncorrected amounts. In the winter months when the correction factor is highest, the reanalysis winds overcorrect precipitation by 20 to 25%.

Comparing gridded precipitation with corrected station precipitation at the same three stations used for the reanalysis wind speed comparisons, shows that the uncorrected gridded precipitation is low (see Figure A.3c). The underestimation increases for larger precipitation events. There is some scatter in the comparisons but it is quite clear that the gridded precipitation is missing a sizeable portion of the annual precipitation. In the summer, wind induced undercatch errors are on the order of 8 to 10% (see Table A.1) for the middle station in Figure A.3. Winter corrections range from 25 to 60% of the observed precipitation. Precipitation in the upper Mississippi tends to be lower in the winter, but an overestimation of 20 mm on top of a correction of 50 mm is still a significant amount of water.

Table A.1: Average monthly cumulative precipitation (undercatch corrected and uncorrected) for the observer station at 41° 42' N, 86° 20' W, and the grid cell containing it.

	Uncorrected		Undercatch Corrected		
Month	Station Precip. (mm)	Gridded Precip. (mm)	Station Precip.[1] (mm)	Gridded Precip.[2] (mm)	Gridded Precip.[3] (mm)
January	58.03	54.24	92.31	112.36	87.66
February	54.27	50.55	82.01	102.81	78.71
March	55.08	52.09	69.26	71.89	65.49
April	85.19	83.10	97.14	95.35	94.57
May	83.67	85.98	92.51	95.81	95.28
June	102.62	98.15	112.33	108.60	106.85
July	101.89	99.35	111.37	108.89	108.14
August	100.51	98.15	108.90	106.77	105.86
September	93.86	94.59	102.88	104.15	103.92
October	98.28	96.63	109.03	108.54	107.11
November	92.10	90.79	109.18	113.96	107.85
December	71.05	68.32	96.60	118.31	94.09

[1] Station precipitation corrected using station wind.

[2] Gridded precipitation corrected using monthly adjusted reanalysis wind.

[3] Gridded precipitation corrected using monthly correction factors derived from average station corrections.

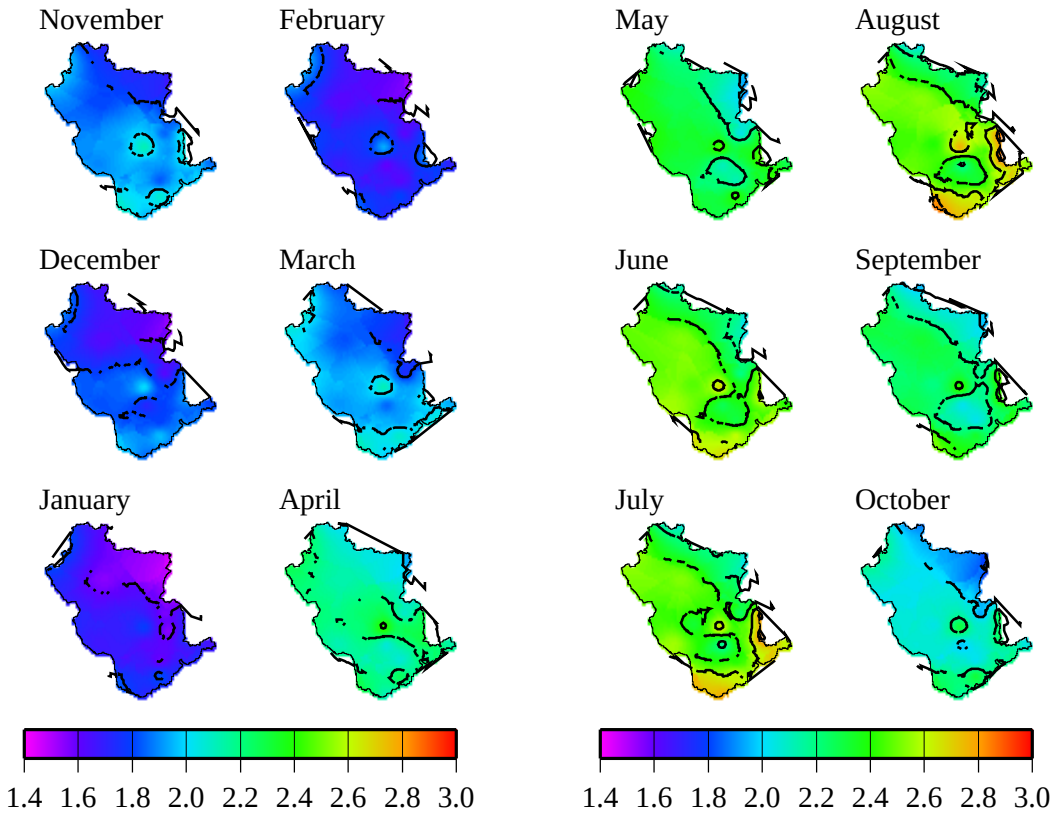

Figure A.4: Monthly reanalysis 10 m wind speed adjustment factors for the upper Mississippi River basin. Daily reanalysis wind speeds are multiplied by the adjustment factors to reduce their bias with observed wind speeds.

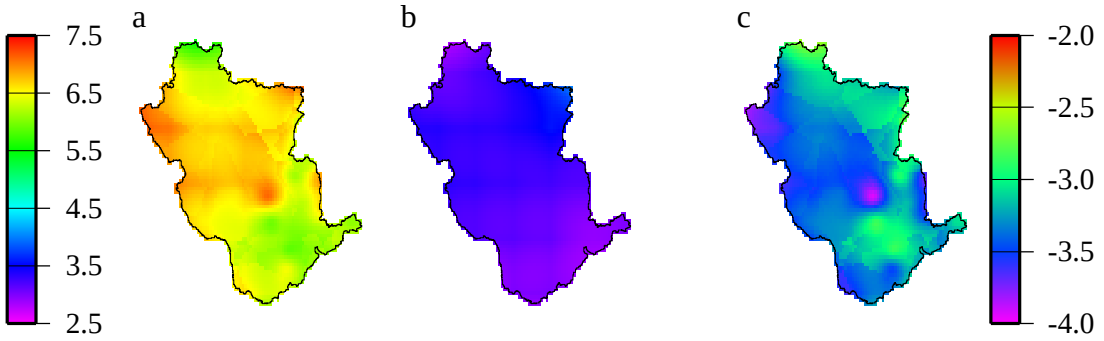

Figure A.5: Changes in annual average wind speed with monthly adjustment factors: (a) adjusted gridded wind speed (m/s), (b) unadjusted gridded wind speed (m/s) and (c) wind speed difference (unadjusted minus adjusted wind speed) (m/s).

The preliminary analysis with wind bias correction indicates that precipitation correction works best when wind speed and precipitation are measured close to one another. Gridding average monthly correction factors calculated for individual stations, might therefore yield better average monthly precipitation than using the reanalysis wind speeds. Monthly average correction factors for wind induced undercatch were computed using a method similar to that for reducing the bias in reanalysis winds:

- Daily corrected precipitation was computed for all observer stations reporting both precipitation and wind speed. Correction factors were obtained from equations A.1, A.2 and A.3. If maximum daily temperature is less than 0°C precipitation is assumed to fall as snow, if minimum daily temperature is greater than 0°C precipitation falls as rain, and for remaining cases precipitation is mixed.

- For months with complete records of precipitation and wind speeds, monthly cumulative corrected precipitation was divided by cumulative observed precipitation to obtain a monthly correction factor.

- Monthly correction factors were averaged for each station and the values were interpolated linearly across the model domain.

- Gridded precipitation was multiplied by the monthly correction factors to obtain daily corrected precipitation values.

The resulting gridded monthly correction factors are shown in Figure A.6. Four stations in the northern part of the basin were removed from the final gridded product. They reported significantly smaller correction factors than all of the neighboring stations. There is no reason to suspect that all four stations would have reporting errors; however, they are all located along the main channel of the Mississippi and Chippewa Rivers. It is possible that all four stations are located very near the rivers and are therefore surrounded by high bluffs. If the stations are protected by the bluffs, they may not be representative of wind speeds across the larger scale of the basin.

Precipitation correction factors are highest in the months of November through April when snow is a major part of the precipitation mix. The correction factor is also highest to the north of the basin where air temperatures are colder and the snow accumulation season is longer. From June through September, the gauge undercatch error is no more than 12% over the entire basin. As snow begins to fall in October, the correction increases to almost 20% in the northern reaches of the basin. By November, the correction factor doubles the observed precipitation. The highest correction factors during the winter are in the north central part of the basin where the snow accumulation is increased significantly by the presence of Lake Superior just to the north. Differences seen in the correction factor fields for March are probably driven by early spring snowfalls. Since average air temperature in the southern part of the basin is typically above freezing, the annual average correction factor is more strongly driven by the annual temperature gradient than by the annual precipitation gradient.

Figure A.7 shows how the monthly correction factors affect annual average precipitation across the basin. Precipitation increases across the basin in a southeasterly direction. The exception to this is the northeast shoulder of the basin that receives some lake-effect snow in the winter. Correction of monthly averages accentuates the lake effect region, but leaves the general trend in precipitation relatively untouched. The difference between the corrected and uncorrected precipitation fields shows an inverted trend, with the northern reaches showing the largest increase in annual average precipitation.

Figure A.3d shows that gridded precipitation corrected using monthly correction factors is very similar to station corrected precipitation for stations 1 and 2. The bias has been reduced for station 3, but not completely removed. Scatter is increased but the representation of larger precipitation events is significantly improved. From Table A.1 it can be seen that gridded precipitation, corrected for wind induced undercatch using monthly correction factors, compares favorably with station corrected precipitation. The percent difference between gridded and station precipitation is similar for both the corrected and uncorrected precipitation sets, indicating that the monthly correction factor preserves the change ratio (correction factor), as should be expected from this method.

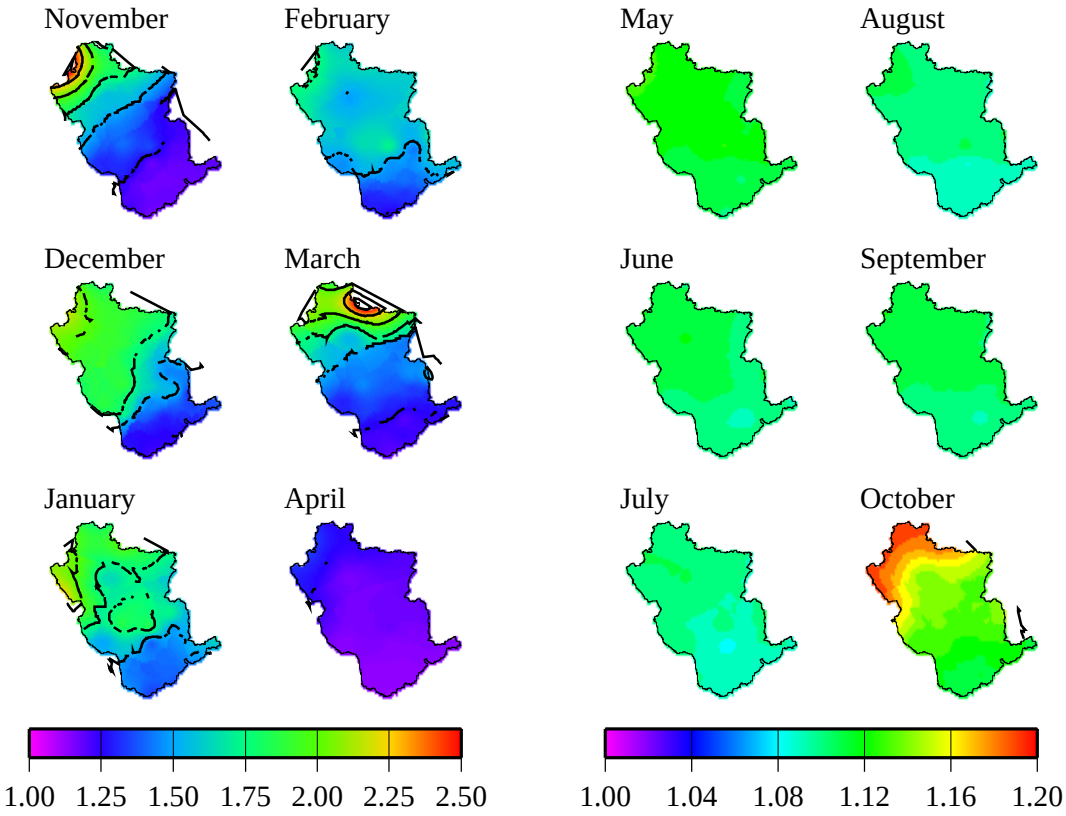

Figure A.6: Monthly precipitation correction factors for upper Mississippi River basin. Daily gridded precipitation is multiplied by the monthly correction factor to correct for wind induced undercatch.

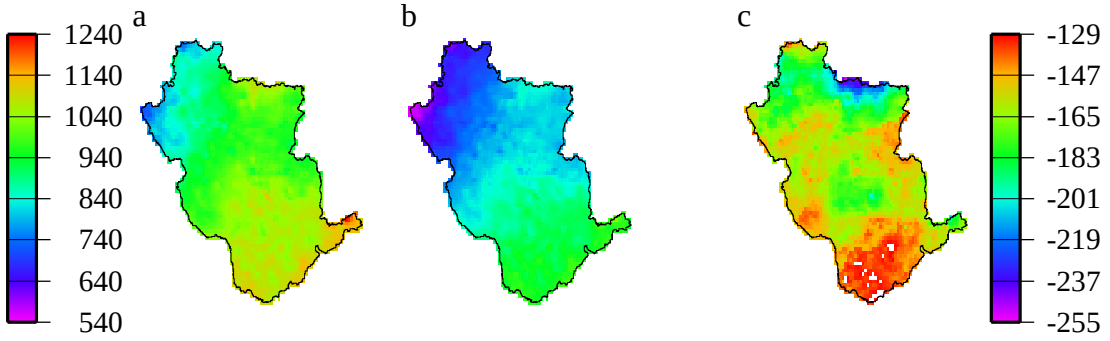

Figure A.7: Changes in annual average precipitation with monthly correction factors: (a) corrected gridded precipitation (mm), (b) uncorrected gridded precipitation (mm) and (c) precipitation difference (uncorrected minus corrected precipitation) (mm).

As an independent test of the precipitation correction, snow depth at all of the wind reporting stations was compared with simulated snow depths from the VIC model. The VIC model was run in three hour water balance mode for all grid cells that contain a station reporting snow depth. For all years where stations observed a complete snow season, seasonal statistics were computed for both the station data and the VIC model simulated snow. Figures A.8 and A.9 compare station and simulated snow statistics without and with precipitation correction respectively. There is very little change in the number of snow

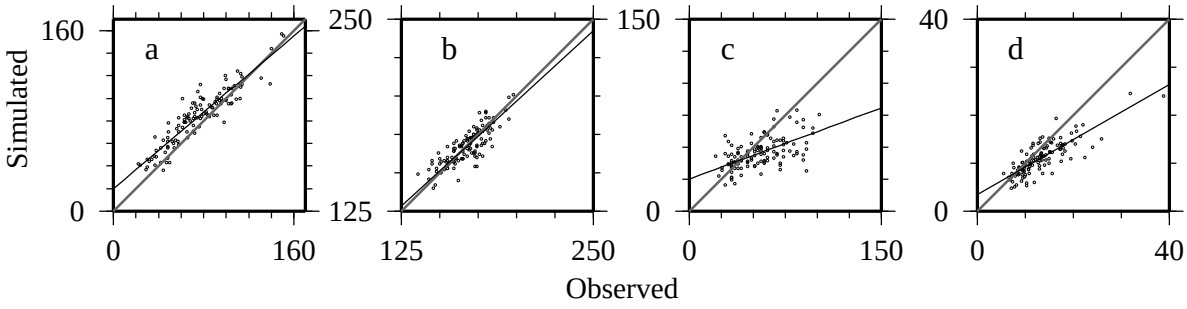

Figure A.8: Comparison of average annual snow statistics with station observations of snow depth and simulated snow depths using uncorrected precipitation: (a) number of snow covered days (*julian day*), (b) last day of snow cover (*julian day*), (c) maximum snow depth (*cm*) and (d) mean snow depth (*cm*).

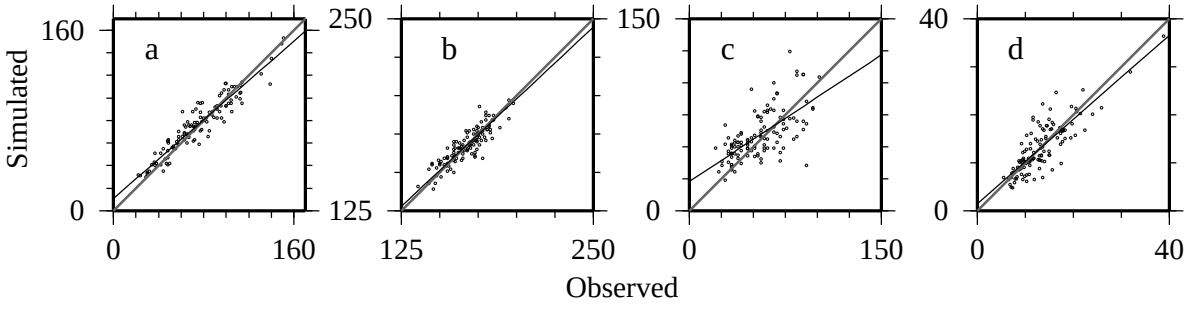

Figure A.9: Comparison of average annual snow statistics between station observations of snow depth and simulated snow depths using corrected precipitation.

covered days or in the last day of snow cover between the model simulations.

Snow depth and density are not generally required for the VIC model, though observations of snow depth are far more common than for snow water equivalence. A snowpack compaction routine was added to the VIC model both to improve the simulation of heat fluxes through the pack and to allow for more direct comparisons with observed snow depths. The method accounts for compression of the pack from new snow and for densification as the pack ages [*Bras*, 1990, Chap. 6]. Both maximum snow depth (Figure A.8c) and mean seasonal snow depth (Figure A.8d) are biased low with deeper snowpacks when simulated without corrected precipitation. Correction of precipitation improves the representation of deeper snowpacks, although it increases the variability. Without observations of snow water equivalent, it is difficult to separate errors due to the correction of precipitation from those caused by the compaction routine; however, snow depth comparisons do provide a general assessment of model performance.

A.2 Spatial Model Tests

To demonstrate the impact of corrected precipitation on spatial watershed simulations, the VIC model was applied to the upper Mississippi River basin (above its confluence with the Missouri River, drainage area of 444,000 km^2) (see Figure A.10). As seen in Figure A.7 annual precipitation increases gradually across the basin to the southeast. Annual average air temperature increases on a more southerly gradient. The Wisconsin, Chippewa and St. Croix Rivers as well as the Mississippi above Anoka, Minn. are highly forested (see Figure A.10), while the other sub-basins are primarily agricultural. Tests were made comparing two simulations, with and without corrected precipitation. Comparisons were also made with gridded observations of snow depth and extent.

A.2.1 Parameter Estimation

When possible, model parameters were estimated from available soil measurements, previous model simulations or literature values [*Cherkauer and Lettenmaier*, 1999]. Six parameters were adjusted during calibration: b_i the infiltration parameter, D_s and W_s which control the shape of the baseflow curve, D_m the maximum baseflow rate, and the depths of the second

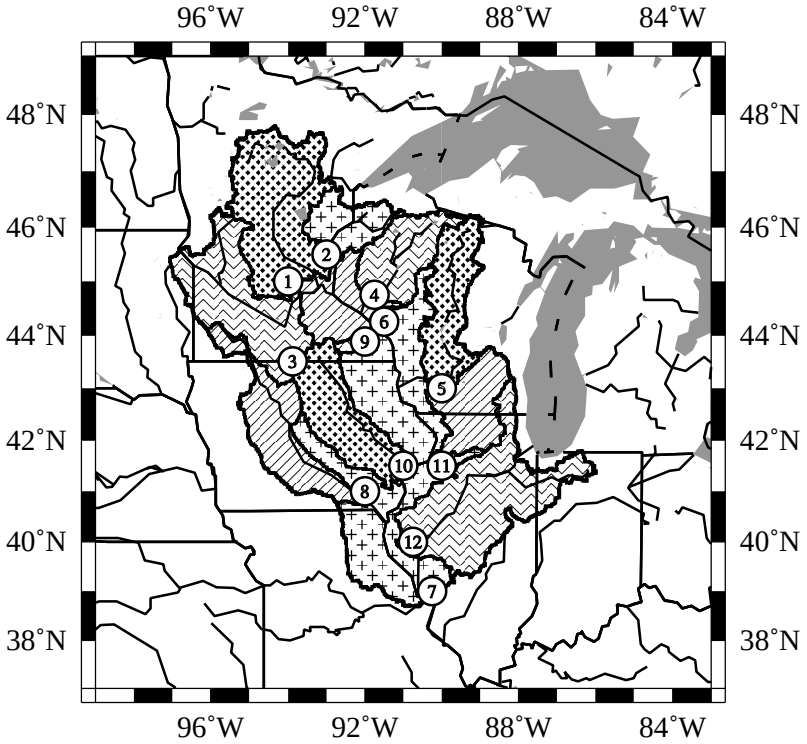

Figure A.10: Delineated watersheds for the upper Mississippi River basin and the sub-basins.

and third soil layers (the top layer was held constant at 10 cm) [*Cherkauer and Lettenmaier*, 1999]. None of these parameters are used directly by the freezing soil algorithm, but they affect the soil moisture content, which is an important factor in determining infiltration into frozen soil [*Zhao and Gray*, 1997; *Zhao et al.*, 1997].

Vegetation cover classes were obtained from a dataset of partial land cover types based on the University of Maryland (UMD) 1 km resolution classification [*Hansen et al.*, 2000], which includes 13 cover types. Monthly leaf-area indexes (LAI) were extracted from the global quarter degree LAI dataset produced by *Mynenui et al.* [1997] and processed using the method of *Nijssen et al.* [2000]. Vegetation parameters other than fractional coverage and LAI were taken from those used by *Cherkauer and Lettenmaier* [1999].

A.2.2 Discharge Comparisons

A direct comparison of the effect of correcting precipitation on discharge hydrographs was made in the St. Croix River basin. Figure A.11 compares observed weekly discharge with simulated weekly flows using the corrected precipitation data set. This shows that with corrected precipitation the model underpredicts about half the peaks while reproducing the observed baseflow quite well. In order to compare simulations forced with and without corrected precipitation, the VIC model was rerun in the St. Croix River with the same parameters, using the uncorrected forcing data. Weekly discharge for both simulations are shown in A.12. Without the corrected precipitation the model underestimates the spring melt peaks. Since the winter accumulation period is when the precipitation undercatch error is highest, its biggest effect is on the size of the snowpack. By increasing the storage in the snowpack, the VIC model is better able to predict spring events. Changing the model calibration for the uncorrected precipitation forcing data will yield a better simulation but it will be difficult to match the observed annual volume of discharge.

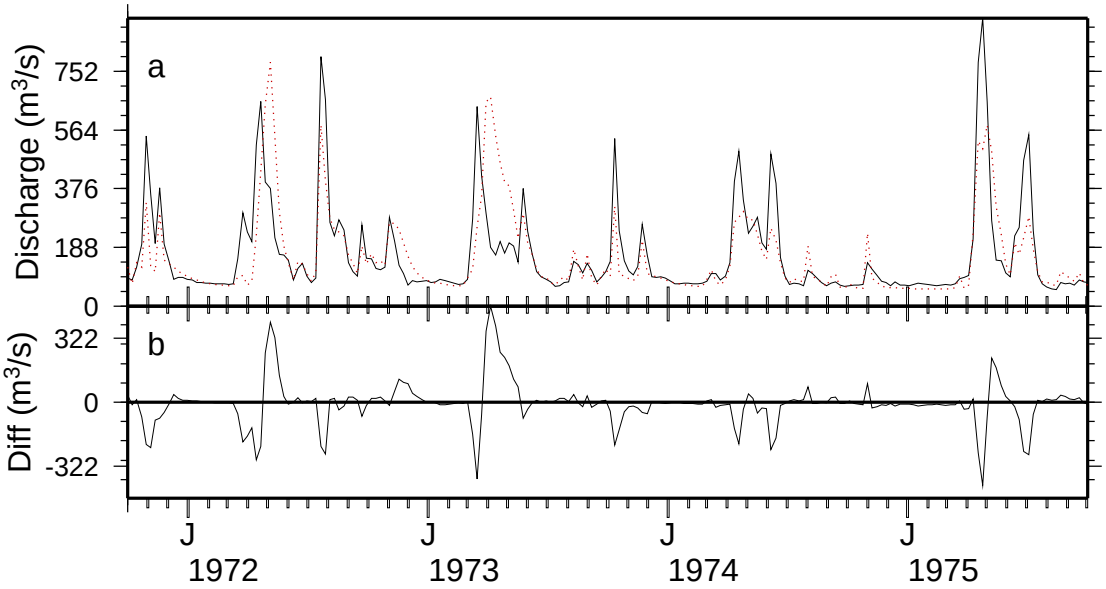

Figure A.11: Observed (solid) versus simulated with corrected precipitation (dotted) weekly discharge in the St. Croix River basin for water years 1971-1974

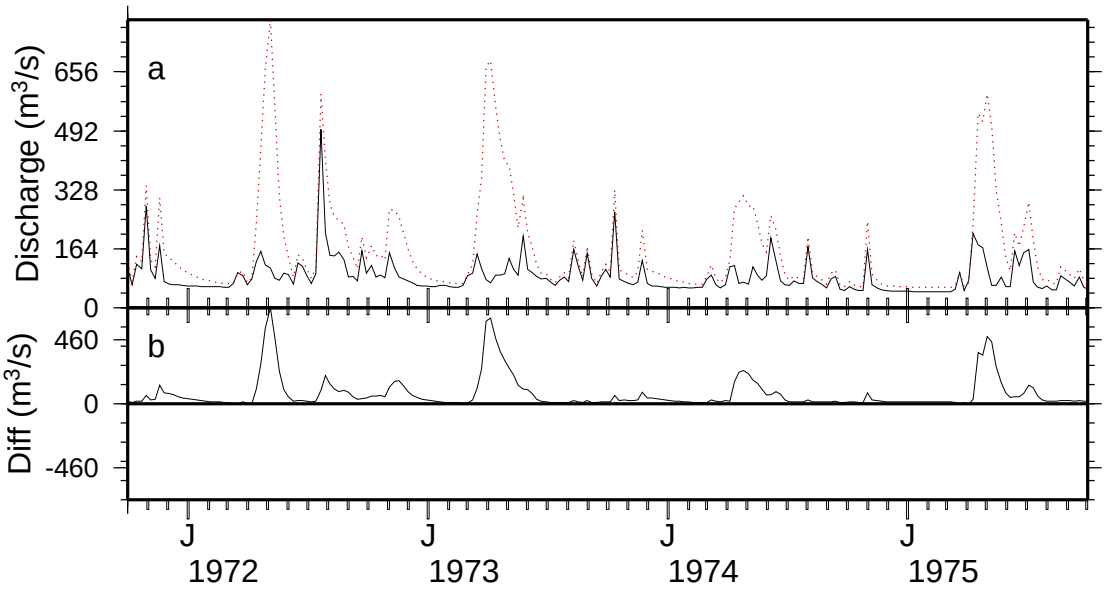

Figure A.12: Simulated weekly discharge in the St. Croix River basin with (dotted) and without (solid) corrected precipitation.

A.2.3 Spatial Snow Comparisons

The biggest impact of correcting precipitation is on snow accumulation. This can be seen spatially by comparing maps of the annual average last day of snow in the St. Croix River basin (see Figure A.13). Between 1971 and 1975 snow remains in the northern part of the basin almost two weeks longer when forced with corrected precipitation. In the southern part of the basin snow melt is only a few days later. The northern part of this basin is influenced by lake effect snow from Lake Superior. This was a region with especially high corrections so a larger effect on the date of snow melt is expected. Since the only wind reporting station in the area is outside the modeled basin no direct station comparisons could be made.

Figure A.14 compares simulated snow depths on February 18, 1972. Snow depths from the model forced with corrected precipitation are higher across the entire basin. Even the southern part of the basin where the last day of snow cover varies by no more than a week experiences increased snow depths of 10 to 30 cm. This indicates that the corrected precipitation increases storage of water in the snowpack but has less of an effect on the timing of melt processes. This is the same conclusion reached by comparing the changes to point station simulations in Figures A.8 and A.9.

The average last day of snow cover over the entire upper Mississippi River basin for the winters from 1975-1995 is shown in Figure A.15. Simulated snow cover in Figure A.15c was obtained by forcing the model with corrected precipitation. Observed data came from two sources. Figure A.15a shows the annual average last day of snow extracted from weekly snow extent maps obtained from the EOSDIS NSIDC Distributed Active Archive Center (NSIDC DAAC), University of Colorado at Boulder [*National Snow and Ice Data Center*, 1996]. These maps are derived from visible satellite observations, usually AVHRR or GOES, and gridded to a resolution of 25 km. The second observed data set was obtained by gridding all observations of daily snow depth in the NCDC database.

In the southern and western regions the simulated last day of snow compares favorably with observations. Simulated snow lasts on the order of 10 days longer in the northeastern reaches of the basin than either of the observed data sets indicate. This region is the most

heavily forested part of the basin, which complicates satellite snow extent estimation. Also, some differences may be attributed to the locations of the observation stations, which are typically located in clearings where snow tends to ablate more rapidly. The model simulates average snow depth for each grid cell, including areas protected by an overstory.

Basin average annual snow depth from 1975 to 1995 is mapped in Figure A.16. Simulations estimate deeper snow packs on average than the observations indicate. NSIDC snow extent maps do not provide depth information so they are not included in the comparison. Differences in the annual average depth are highest in the north where accumulation is greatest. In the south, simulated and observed depth differences are typically about 5 cm. Patterns of snow depth are similar, with mean annual depth increasing in a northerly direction. Because the patterns are similar and the model overpredicts almost uniformly, the most likely source of error is the compaction routine. Differences may also be caused by issues of timing, both at the beginning and end of the snow season. Average depths will be higher if the period of record is shorter.

Mid-winter and spring snow pack simulation is most important for proper simulation of the spring melt event. To determine how well the model simulates the snowpack at these times, monthly snow depths for January through April, 1975-1995, are plotted in Figure A.17. Once again the snow depths are overestimated by the model simulation but the largest differences are in mid-winter. This implies that most of the difference is in the compaction routine. As snow melts in March and April, simulated depth remains high but the difference rapidly falls to about 10 cm. By April there is still snow in the simulation set, though it is primarily in the forested regions of the basin. Since most observations are taken in clearings, it is not unreasonable for the model to retain snow under the canopy after the observation stations report that all snow has melted.

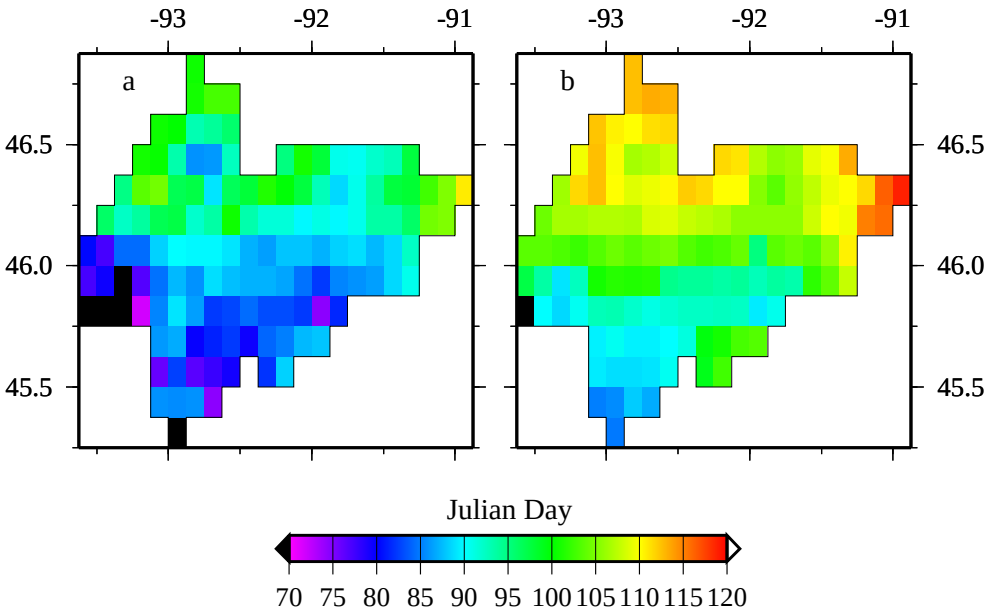

Figure A.13: Annual average last day of snow cover in the St. Croix River basin for 1971 to 1975: (a) without corrected precipitation and (b) with corrected precipitation.

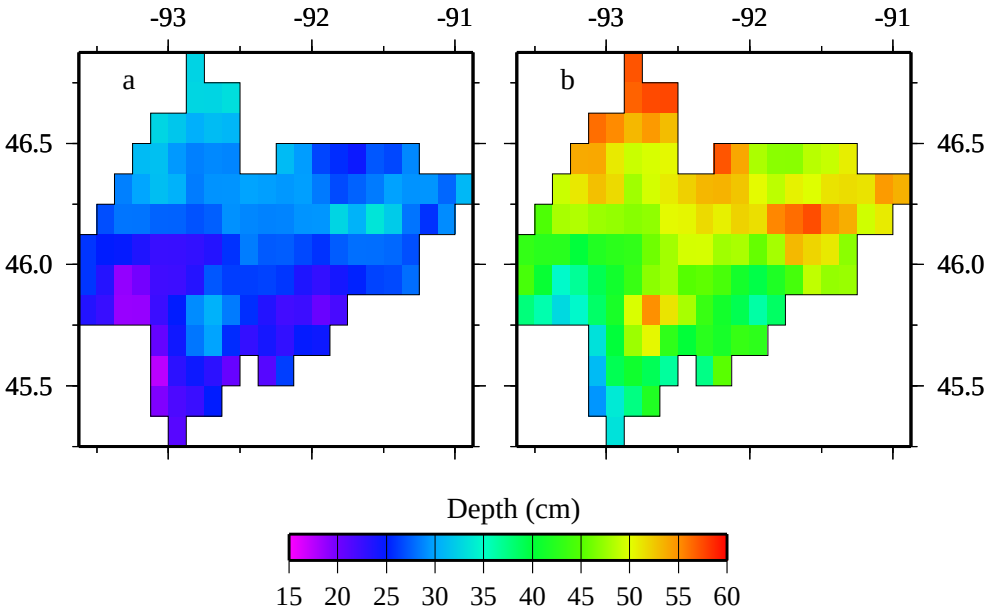

Figure A.14: Simulated snow depth on February 18, 1972: (a) without corrected precipitation and (b) with corrected precipitation.

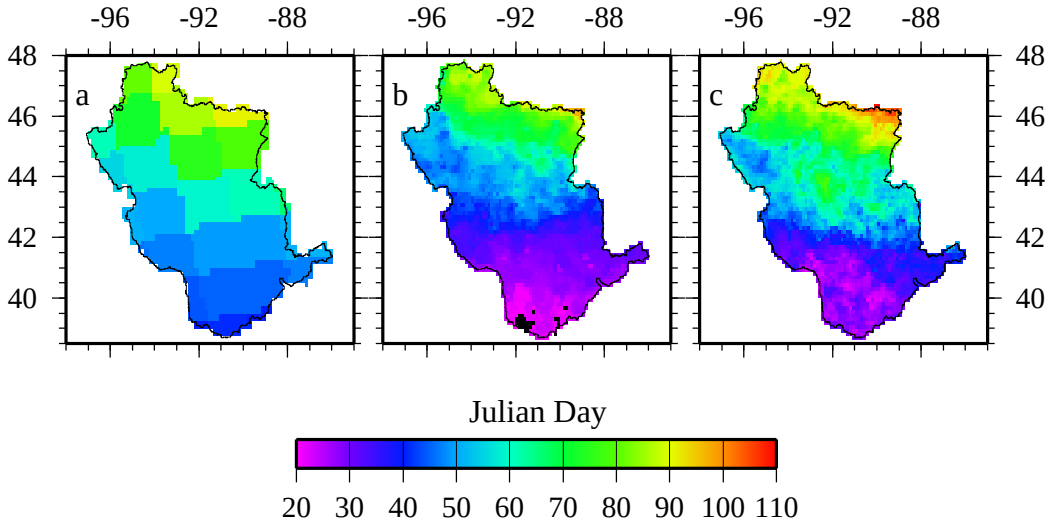

Figure A.15: Annual average last day of snow cover in the upper Mississippi River basin, 1975-1995: (a) NSIDC weekly snow extent maps, (b) gridded daily observed snow depth and (c) daily simulated snow depth using corrected precipitation.

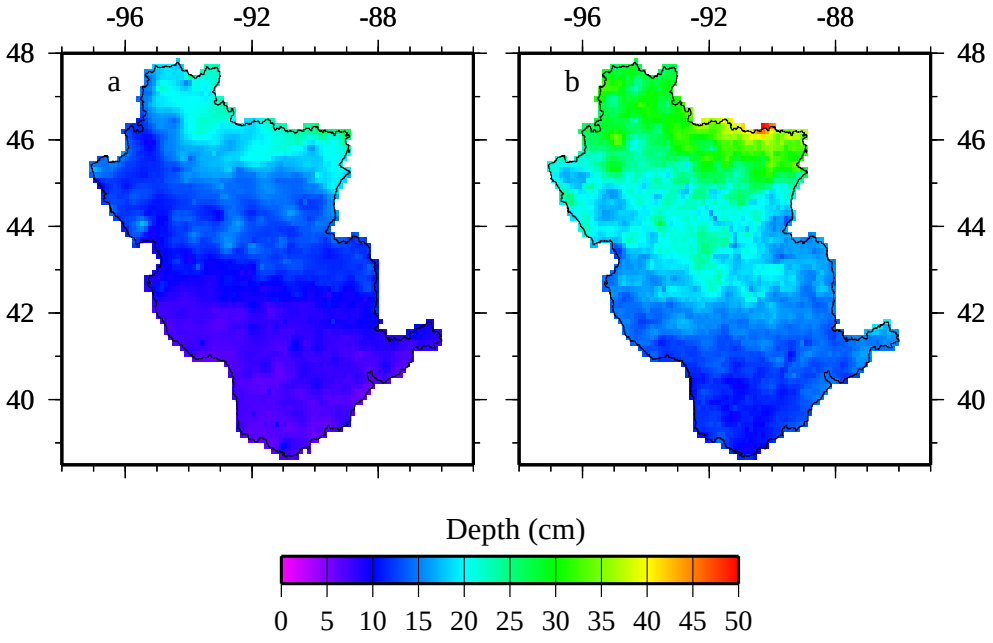

Figure A.16: Average annual snow depth from 1975 to 1995: (a) gridded station snow depths and (b) simulation snow depths using corrected precipitation.

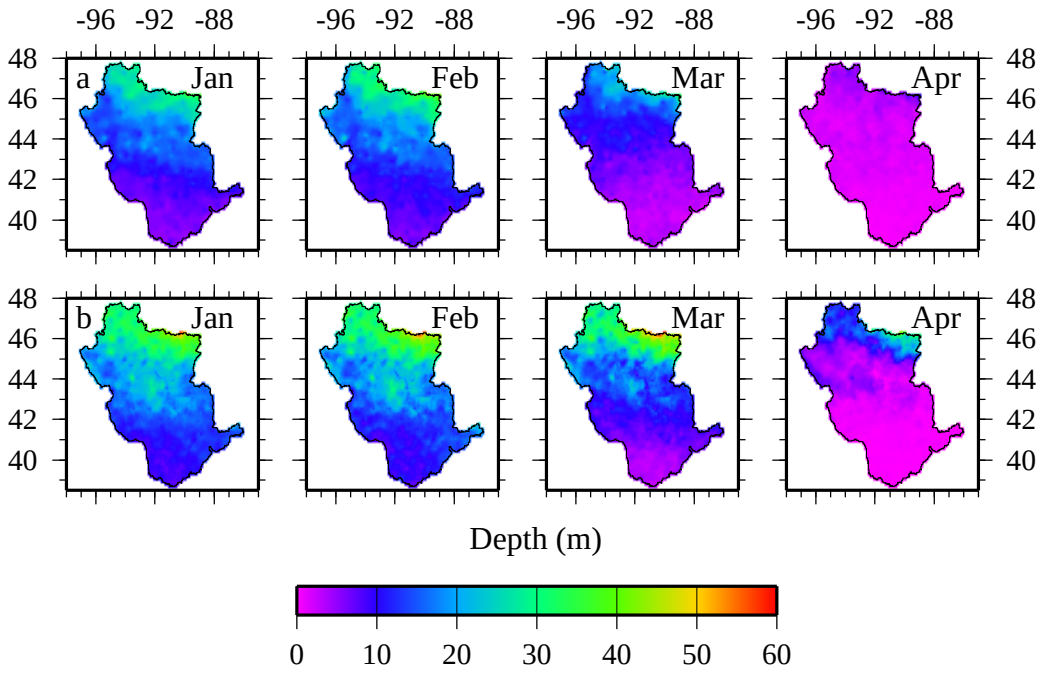

Figure A.17: Average annual monthly snow depths for the months of January through April, 1975-1995: row (a) gridded station observation snow depth and row (b) simulated snow depths using corrected precipitation.

A.2.4 Frost Extent Comparisons

As with snow cover, maps of the last day of frozen soil were made for the St. Croix River basin. Comparing simulated soil thaw dates with and without corrected precipitation (see Figure A.18) yields results similar to those of the last day of snow cover (see Figure A.13). In both cases the soil remains frozen for about a week after the last of the snow cover. This agrees with observations at the Rosemount Experiment Station (see Chapter 3) implying that on average the VIC model correctly simulates the interaction between snow and soil frost.

Without satellite or in situ observations of frost no direct comparisons of model predictions with observations can be made. Instead Figure A.19 shows the annual average last day of soil frost and snow for 1975 to 1995. Soils appear to thaw on the order of 20 days after snow melt in the north and 10 days after snow melt in the south. The day of last snow cover shows more of an effect from lake effect snow in the north east. Soil frost follows the temperature gradient through the southern half of the basin but in the north the last day of soil frost seems more random. In the southern regions of the basin, snow cover tends to be thin (see Figure A.17) and therefore provides very little insulation so soil freezing is driven primarily by air temperature. Where snow accumulation is deeper, the timing of snow pack development is more important. For example, if air temperatures fall below freezing for several weeks before significant accumulations of snow, soils will freeze deeply. If the snow arrives about the same time as the cold temperatures then there will be little formation of frozen soil. Averaging the effects annually will derive fewer spatial trends as the driving forces are more random.

A.3 Discussion

Hydrologic models are highly dependent on meteorological forcings to make accurate predictions of streamflow, snow cover, soil moisture and other hydrologic variables. In the United States, daily precipitation and air temperature data are readily available. Precipitation is a difficult quantity to measure, especially in colder regions where snowfall makes up a large portion of annual precipitation. By correcting for wind driven gauge undercatch, a large

part of the error in the precipitation measurement can be corrected. By using observations of precipitation and wind speed within the upper Mississippi basin, monthly correction factors for precipitation were derived. Annual changes in precipitation ranged from 129 mm in the south to 255 mm in the north.

Applying the corrected precipitation fields to the upper Mississippi River basin improved the representation of the average snowpack. Without the additional precipitation from the correction process there is simply not enough precipitation to simulate many of the watersheds in northern Wisconsin and Minnesota. The correction factors may introduce increased variability in the precipitation record, but without better observations of both precipitation and wind speed it is unlikely that the precipitation data set can be further improved.

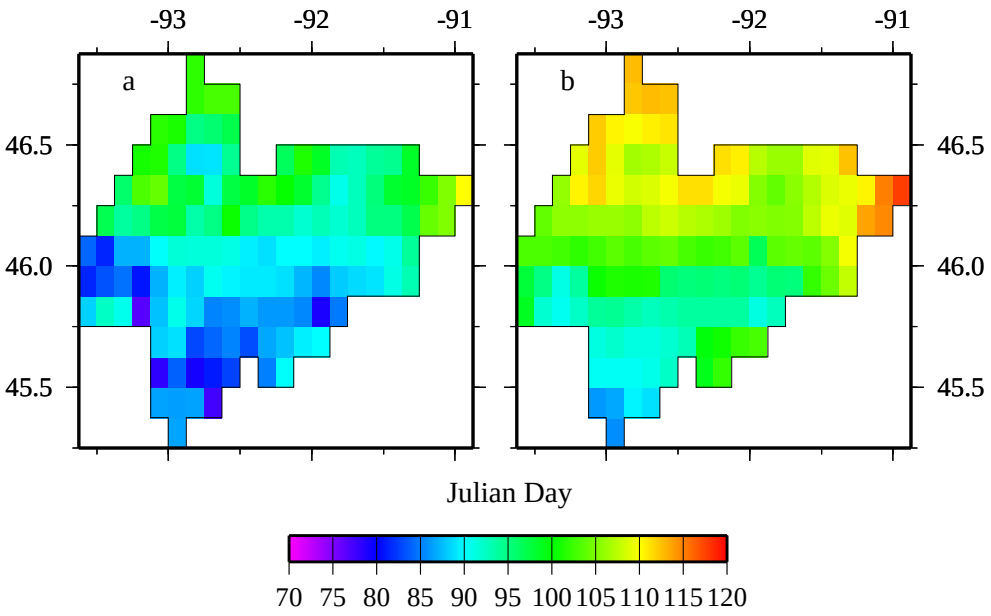

Figure A.18: Annual average last day of frozen soil in the St. Croix River basin for 1971 to 1975: (a) without corrected precipitation and (b) with corrected precipitation.

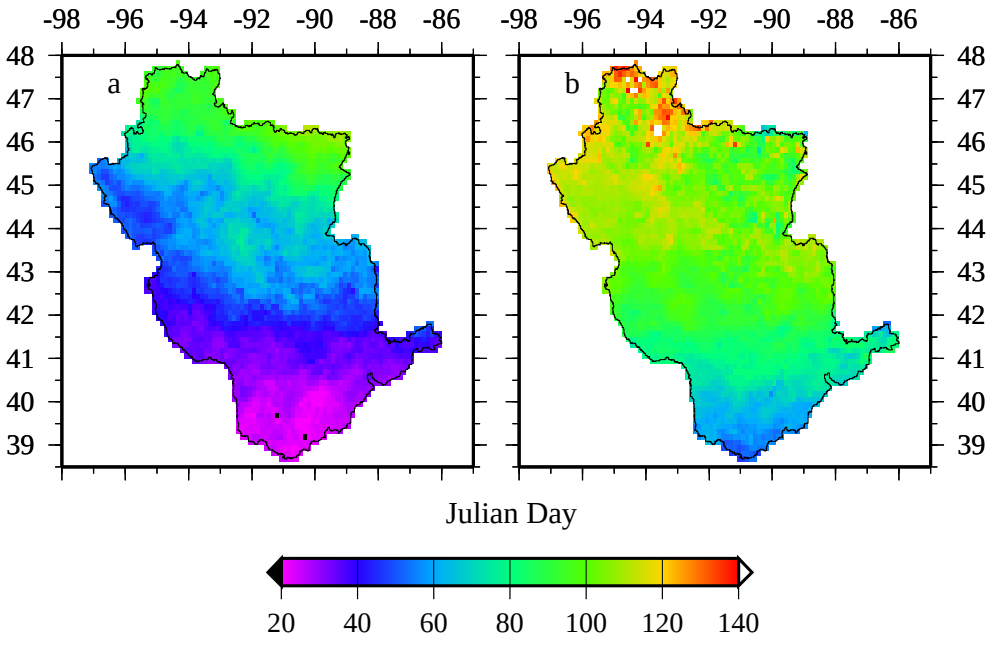

Figure A.19: Last day of frozen soils in the upper Mississippi River basin: (a) 1971 and (b) annual average from 1950 to 1999.

Appendix B

HYDROLOGIC EFFECTS OF FROZEN SOILS IN THE UPPER MISSISSIPPI RIVER BASIN

Attached as an appendix is a copy of the recently published paper by *Cherkauer and Letternmaier* [1999] describing the development of the new snow and frozen soil algorithms for the variable infiltration capacity (VIC) hydrologic model. These algorithms were developed in order to improve the VIC model's ability to simulate cold regions processes so that it could be used to study the impact of snow and frozen soil on the winter hydrology of watersheds.

Though this paper was published in the Journal of Geophysical Research in August of 1999, te copy on the following pages was actually produced using AGU++ LaTeX preprint format. This was done so that the original figure files could be used, yield higher quality initial output.

Hydrologic effects of frozen soils in the upper Mississippi River basin

Keith A. Cherkauer and Dennis P. Lettenmaier

Department of Civil and Environmental Engineering, University of Washington, Seattle

Abstract. The variable infiltration capacity (VIC) macroscale hydrologic model was modified to improve its performance in cold regions by adding frozen soil and energy balance snow accumulation and ablation algorithms. Frozen soil penetration was determined by solving thermal fluxes through the soil column. Infiltration and runoff response parameterizations were modified to reflect the simulated ice content of the soil. The revised model was tested using point data from the University of Minnesota Rosemount Agricultural Experiment Station and subsequently applied to two subcatchments in the upper Mississippi River basin. The point tests showed that the model was able to reproduce observations of the snowpack, soil liquid water content, and freezing and thawing front depths. Comparisons of simulated discharge from the two subbasins showed that the frozen soil algorithm reduced infiltration during winter and spring thaws and increased rapid runoff response. However, the magnitude of the increased runoff response is relatively modest, at the scale of the two upper Mississippi subbasins tested.

1. Introduction

Frozen soil plays an important role in the hydrology of cold regions, both through direct effects on infiltration and indirect effects on heat transfer to and from overlying snowpacks. Until recently, macroscale hydrologic models, for example, those applicable to large continental river basins and global land-atmosphere simulations, have largely ignored these effects. As the resolution of coupled land-atmosphere models improves and the focus shifts to regional questions, the deficiencies of models that have been developed and tested primarily in temperate latitudes become important. For instance, *Betts et al.* [1996] have shown that considerable improvement in forecasts of Northern Hemisphere weather was achieved by better representation of the effects of soil temperature on latent and sensible heat flux in the boreal forest. Their work implies a need to improve the representation of frozen soil physics in macroscale hydrologic models.

The depth of seasonal frost penetration is driven by the diurnal cycle of the soil surface temperature. If the net daily heat flux out of the ground is positive, the freezing front advances; if it is negative, the freezing front retreats, and a thawing front may form at the surface and advance into the soil. This diurnal cycle, which may only penetrate the top few centimeters of exposed soil, can drive the seasonal freezing front as deep as 2-3 m [*Williams and Smith*, 1989]. The presence of a snowpack insulates the soil surface and dampens daily fluxes, thus decreasing the seasonal penetration of frost. An early snow that remains throughout the winter will result in shallower freezing depths than a late snow that falls after many weeks of cold weather.

Soil ice content directly controls infiltration. Ice forms in the spaces between soil particles, as far as possible from their surfaces. At low ice contents, liquid water will continue to flow unhindered, but as the ice content increases, the open channels narrow, and liquid water movement is restricted. The total soil water potential, or the maximum amount of water that can remain unfrozen in the soil, is primarily a function of the specific surface area and temperature of the soil. Soils with finer particles have larger specific surface areas and retain more liquid water to lower temperatures. *Fuchs et al.* [1978] showed that the relationship between the freezing point depression in a soil and the soil water potential could be represented as

$$\phi = \pi + \psi = \pi + \frac{L_f T}{g\,(T + 273.16)}, T < 0°C \qquad (1)$$

where ϕ is the total soil water potential (m), π is the soil osmotic potential (m), ψ is the soil matric potential (m), L_f is the latent heat of fusion (J kg^{-1}), g is the acceleration of gravity (m s^{-1}), and T is the soil temperature (°C). Since macroscale models typically do not simulate soil solutes, the osmotic potential term π is ignored. Therefore the ice content is the soil moisture in excess of the matric potential.

Aside from its effects on infiltration, ice also changes the dynamics of soil thermal fluxes through the dependence of soil thermal properties (thermal conductivity and volumetric heat capacity) on soil water and ice content. The thermal conductivity of water is 0.57 W m^{-1} K -1, while that of ice is 2.2 W m^{-1} K^{-1}. A frozen soil with high ice content will have a higher thermal conductivity than a soil with an equivalent content of liquid water. Furthermore, the volumetric heat capacity of water is 4.2 MJ m^{-3} K^{-1}, versus 1.9 MJ m^{-3} K^{-1} for ice, so increasing the ice content of the soil decreases its thermal storage capacity.

The thermal and hydraulic characteristics of frozen soils have been modeled using various methods. *Fox* [1992] employed a variation of the Stefan equation, a widely used empirical relationship for estimating frost depth, to compute the penetration of the freezing and thawing fronts in a hydrologic model. *Koren* [1980] and *Koren et al.* [1999] used a gamma distribution to represent the fraction of impermeable area within a model grid cell. *Gel'fan* [1989] derived an analytical solution to the combined moisture and heat transfer equations which predicts the freezing front depth as a function of soil thermal properties and thermal fluxes through the snowpack. *Flerchinger and Saxton* [1989a, b] developed a detailed physically based column model for computing soil heat and water fluxes simultaneously.

Ideally, simulation of frozen soil effects in a macroscale hydrologic model would preserve the important physical processes in a computationally efficient framework. The surface energy balance, especially soil thermal fluxes, is difficult to represent accurately with simplified equations. Ice in the soil precludes the use of most numerical approximations and forces a more complete solution of both the soil moisture and the thermal fluxes. This paper investigates the development of a frozen soil algorithm motivated by the dual considerations of computational efficiency and physical realism. The resulting algorithm was added to the variable infiltration capacity (VIC) macroscale hydrologic model and demonstrated through applications to a well-measured point location and large-scale basins.

2. Model Development

The VIC model is a macroscale hydrologic model that solves a full energy and water balance on a grid mesh basis. It is designed to represent surface energy and hydrological fluxes and states, for example, soil moisture, snow accumulation and ablation, evapotranspiration, and latent heat fluxes, at scales from large continental river basins to the entire globe. The VIC model has been run at a number of resolutions and on a variety of basins with very different climates, including the Columbia and Delaware Rivers [*Nijssen et al.*, 1997], the Arkansas and Red Rivers [*Abdulla et al.*, 1996], and the Weser River, Germany [*Lohmann et al.*, 1998a, b]. It has also been used to simulate global soil moisture and runoff [*Schnur and Lettenmaier*, 1997]. Previous versions of the model have largely ignored or had difficulty with important cold region processes. This paper focuses on the upper Mississippi basin where winter air temperatures often fall well below 0°C, therefore making the proper representation of cold season processes critical.

Liang et al. [1994] describes in detail the formulation of the VIC model with two soil layers; therefore only a summary of the model will be presented here. A third layer was added following the work of *Liang et al.* [1996] who determined that a thin top layer (5-15 cm) significantly improved evapotranspiration predictions in arid climates. The VIC model uses a mosaic-type surface cover representation, which allows N vegetation types within each grid cell as shown in Figure 1. The user

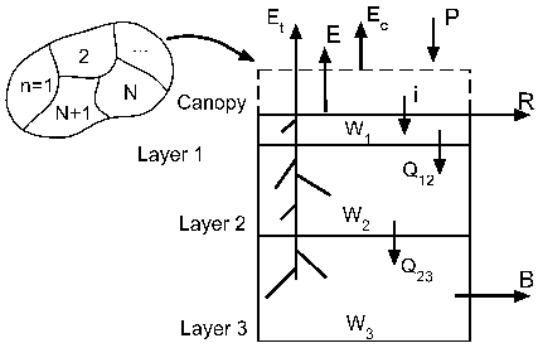

Figure 1. Schematic of the variable infiltration capacity (VIC) macroscale hydrologic model water balance for one grid cell with three soil layers.

can change the number of soil layers, though all previ-

ous applications have used either two or three layers. Vegetation can intercept precipitation, or precipitation can reach the ground surface as throughfall. Water can also reach the soil surface as snowmelt.

The amount of infiltration i is controlled by a variable infiltration curve, which is based on the available moisture content of the top two layers $W_1 + W_2$. Water that cannot infiltrate is removed from the cell as runoff R. Infiltrating water first fills the thin top layer, set to 10 cm for the simulations in this paper, then the excess infiltration is added to the second layer. Water can leave the top two layers only through evapotranspiration E_t, or by gravity drainage to the next lower layer, Q_{12} and Q_{23}. The bottom layer loses water through both evapotranspiration and baseflow B. Baseflow is generated using a nonlinear empirical relationship based on the soil moisture of the bottom layer, W_3.

The basic equation for the surface energy balance over bare soil is [*Liang et al.*, 1994]

$$R_n = H + \rho_w L_e E + G + \Delta H_s \quad (2)$$

where R_n is the net radiation (W m^{-}2), H is the sensible heat flux (W m^{-2}), ρ_w is the density of liquid water (kg m^{-3}), L_e is the latent heat of vaporization (J kg^{-1}), E is evaporation (mm), $rho_w L_e E$ is the latent heat flux (W m $-$2), G is the ground heat flux (W m^{-2}), and ΔH_s is the change in energy storage in a layer of air just above the surface (W m^{-2}). This equation is modified to solve for the surface energy balance above the canopy, if present, by multiplying the ground heat flux by an attenuation factor τ, which accounts for the reduction of incoming radiation by vegetation [*Liang et al.*, 1999].

When the model is implemented over a grid mesh (i.e., watershed), evaporation, energy fluxes, runoff, and baseflow are predicted independently for each grid cell. Streamflow is then predicted at a specified location by routing runoff and baseflow from each grid cell using the method of *Lohmann et al.* [1998a, b]

2.1. Frozen Soils Algorithm

The motivation for development of the frozen soil algorithm is to represent the effects of seasonally frozen ground on surface hydrologic response and the surface energy balance, at a level of complexity consistent with the previously developed VIC algorithms. In this spirit, the VIC soil moisture transport scheme was retained, and the thermal and moisture fluxes are solved separately. At each time step, thermal fluxes through the soil column are solved prior to the prediction of soil layer ice content. Subsequently, moisture fluxes are computed using the updated ice contents. Finally, soil thermal properties for the next time step are estimated from the revised distribution of soil moisture and ice.

2.1.1. Thermal Flux Solution. A general equation for heat flux through the soil column can be written as

$$C_s \frac{\partial T}{\partial t} = \frac{\partial}{\partial z}\left(\kappa \frac{\partial T}{\partial z}\right) + \rho_i L_f \frac{\partial \theta_i}{\partial t} \quad (3)$$

where κ is the soil thermal conductivity (W m^{-1} K^{-1}), C_s is the soil volumetric heat capacity (J m^{-3} K^{-1}), T is the soil temperature (°C), ρ_i is the density of ice (kg m^{-3}), L_f is the latent heat of fusion (J kg^{-1}), θ_i is the ice content of the layer (m^3 m^{-3}), t is time (s), and z is the depth (m) taken as a positive length downward from the surface. The last term in equation 3 represents the change in latent heat due to freezing and so applies only when the soil is frozen.

The soil thermal flux predictions described by *Liang et al.* [1999] are based on temperatures at the surface (T_s), at the bottom of the first layer (T_1), and at the bottom of the soil column (T_b) (Figure 2). An exponential temperature profile is assumed between T_1 and T_b [*Liang et al.*, 1999], while T_s is solved explicitly as a part of the surface energy balance. Preliminary tests indicated that these three temperatures were insufficient

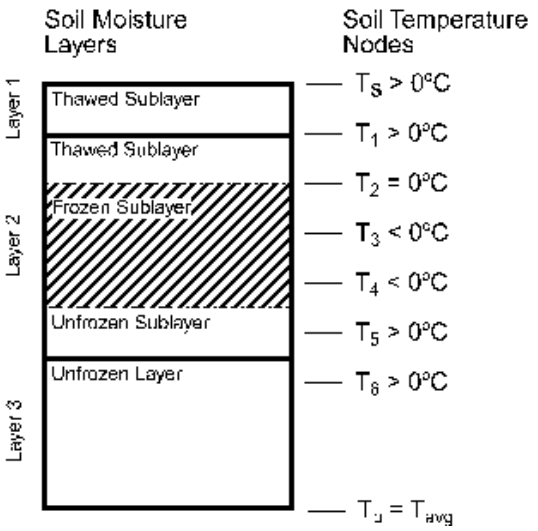

Figure 2. Schematic of the VIC frozen soil algorithm for three soil moisture layers and eight soil thermal nodes. Soil layers can be subdivided into thawed, frozen, and unfrozen sublayers on the basis of the temperatures of the soil thermal nodes.

for accurate solution of soil freeze-thaw status through the soil column. The new soil thermal flux algorithm does not use the exponential temperature profile, instead it solves soil temperatures explicitly at a user-defined number of nodes through the soil column (*e.g.*, T_2 - T_6 in Figure 2). T_s and T_1 are still defined at the top and bottom of soil layer 1, while T_b remains the temperature at the bottom of the soil column. Point model tests were run with 16 nodes to a depth of 4 m, in the first meter, thermal nodes were fixed to measurement depths. The spatial tests were conducted with seven thermal nodes. Reducing the number of nodes not only decreases the computational time but also the accuracy of the solution.

Thermal fluxes are solved numerically at an hourly time step via an explicit finite difference approximation of equation 3. Applying equation 3 to discrete soil layers results in

$$C_s \frac{\partial T}{\partial t} = C_s \frac{T_i^t - T_i^{t-1}}{dt}, \tag{4}$$

$$\frac{\partial \kappa}{\partial z}\frac{\partial T}{\partial z} = \left(\frac{\kappa_{i+1}^t - \kappa_{i-1}^t}{z_{i+1} + z_{i-1}}\right)\left(\frac{T_{i+1}^t - T_{i-1}^t}{z_{i+1} + z_{i-1}}\right), \tag{5}$$

$$\kappa \frac{\partial^2 T}{\partial z^2} = \kappa_i^t \frac{2T_{i+1}^t + 2Y_{i-1}^t - 4T_i^t - 2(\Delta z_1 - \Delta z_2) f\prime(z)}{\Delta z_1^2 + \Delta z_2^2}, \text{and} \tag{6}$$

$$\rho_i L_f \frac{\partial \theta_i}{\partial t} = \rho_i L_f \frac{(\theta_i)_i^t - (\theta_i)_i^{t-1}}{dt}. \tag{7}$$

Reassembling these terms produces an equation that can be solved numerically:

$$C_s \frac{T_i^t - T_i^{t-1}}{dt} = \left(\frac{\kappa_{i+1}^t - \kappa_{i-1}^t}{\alpha}\right)\left(\frac{T_{i+1}^t - T_{i-1}^t}{\alpha}\right) + \kappa_i^t \left[\frac{2T_{i+1}^t + 2T_{i-1}^t - 4T_i^t - 2\gamma f\prime(z)}{\beta}\right] + \rho_i L_f \frac{(\theta_i)_i^t - (\theta_i)_i^{t-1}}{dt} \tag{8}$$

where $\alpha = (\Delta z_1 + \Delta z_2)$; $\beta = (\Delta z_1^2 + \Delta z_2^2)$; and $\gamma = (\Delta z_1 - \Delta z_2)$.

Once initial and boundary conditions are set, equation 8 can be solved through the soil column at explicit depths. Initial soil profile temperatures are taken from data collected at the site or are estimated from the current air temperature. The lower boundary T_b is set to the average annual air temperature. The upper boundary, or surface temperature, is predicted as part of the surface energy balance calculation (equation 2). A root-finding numerical scheme is used to solve for the surface temperature at which the surface energy fluxes balance. As the numerical scheme tries new surface temperatures, heat fluxes through the soil column are recomputed to provide updated ground heat flux inputs. The numerical scheme stops when it has minimized the surface energy balance error to within an acceptable tolerance.

Thermal conductivity and volumetric heat capacity of the soil layers are calculated at each time step from the revised soil water and ice contents. Various methods for computing thermal conductivity have been developed, but comparisons conducted by *Farouki* [1986] indicated that the method of *Johansen* [1975] is generally the most accurate. The basic equation used is

$$\kappa = (\kappa_{sat} - \kappa_{dry})\,\kappa_e \tag{9}$$

where κ is the soil thermal conductivity (W m^{-1} K^{-1}),

$$\kappa_{sat} = \begin{cases} 0.5^n \left(7.7^q 2.0^{1-q}\right)^{(1-n)} & unfrozen \\ 2.2^n \left(7.7^q 2.0^{1-q}\right)^{(1-n)}\, 0.269^{W_u} & frozen \end{cases} \tag{10}$$

$$\kappa_{dry} = \frac{0.17\gamma_d + 64.7}{2700 - 0.947\gamma_d} \tag{11}$$

$$\kappa_e = \begin{cases} logS_r + 1.0 & unfrozen \\ S_r & frozen \end{cases} \tag{12}$$

n is the porosity, q is the quartz content, W_u is the fractional volume of unfrozen water (m^3 m^{-3}), γ_d is bulk density (kg m^{-3}), and S_r is the fractional degree of saturation.

Volumetric heat capacity C_s is computed by summing the volumetric heat capacities of the soil constituents [*Flerchinger and Saxton*, 1989a]:

$$C_s = \sum \rho_j c_j \theta_j \tag{13}$$

where ρ_j is the density (kg m^{-3}), c_j is specific heat capacity (J kg^{-1} K^{-1}), and θ_j is the volumetric fraction (m^3 m^{-3}) of the jth soil component.

2.1.2. Moisture flux solution . Incorporating the ice content of the soil layers into the model allows for simulation of the effects of frozen soil on moisture transport. Ice content is incorporated into the soil moisture transport scheme in two ways: (1) through available moisture storage and (2) through moisture available for transport. First, each of the three soil layers is subdivided into thawed, frozen, and unfrozen sublayers. The thickness of each of these sublayers is dependent on the temperature profile, as shown in Figure 2. When there are no frozen soil layers present, each layer defaults to the unfrozen sublayer type, and the model functions as if the frozen soil algorithm were not present. However, when there is a frozen layer present, it has an ice content based on the average temperature of the sublayer. *Flerchinger and Saxton* [1989a] represented the fraction of unfrozen water, from equation 1, as

$$W_i = W_i^c \left[\left(\frac{1}{g\psi_e}\right)\left(\frac{L_f T}{T + 273.16}\right)\right]^{-B_p} \tag{14}$$

where W_i is the liquid water content of layer i (mm), W_i^c is the maximum water content of layer i (mm), g is acceleration due to gravity (m s^{-2}), L_f is the latent heat of fusion (J kg^{-1}), T is the soil temperature (°C), ψ_e is the air entry potential (m), and B_p is the pore-size distribution. This equation relates the amount of unfrozen soil moisture, which can be held in the soil column to soil composition, temperature, and maximum

water content. The effects of solutes were omitted from the original equation, because the VIC model does not predict solute chemistry.

The second way in which ice content affects soil moisture transport is through its effect on infiltration and drainage. Infiltration calculations are based on the total (frozen and unfrozen) moisture content of the upper layers. Therefore a layer with a high ice content will appear nearly saturated to the runoff calculations. Soil moisture fluxes, on the other hand, are computed using the unfrozen water content. Thus a soil layer with a high ice content will appear dry, and very little moisture will be allowed to drain to the next lower layer.

2.2. Snow Model

The snow model used is similar to the two-layer model used in the distributed hydrology-soil-vegetation model (DHSVM) [*Storck and Lettenmaier*, 1999]. This model employs two snow layers of variable thickness. A thin surface layer is used to solve the surface energy balance, while the bottom or pack layer is used to simulate deeper snowpacks. The model also incorporates a snow interception algorithm that allows snow to be retained in an overstory, if present.

A representation of the heat flux through the snowpack was added to couple the snow and frozen soil algorithms. Temperatures within the snowpack are assumed to follow a linear profile, so the balance of fluxes at the surface is solved in a fashion similar to *Gel'fan* [1989], except that the soil surface temperature is allowed to change:

$$\kappa_{snow} = \frac{dT_{snow}}{dz_{snow}} = G = -\kappa \frac{dT}{dz}\Big|_{z=0} \tag{15}$$

where κ_{snow} is the thermal conductivity of snow (W m^{-1} K^{-1}), dT_{snow} is the change in temperature from the snow surface to the ground surface (°C), κ is the thermal conductivity of the soil, and dz_{snow} is the depth of the snowpack (m). The thermal conductivity of snow is approximated with [*Gel'fan*, 1989]

$$\lambda_{snow} = 0.007\rho_{snow}^2 \tag{16}$$

where ρ_{snow} is the snow density (kg m^{-3}).

Snow depth, z_{snow}, is not computed in the snow model, as described by *Storck and Lettenmaier* [1999], but is needed for the calculation of the heat flux through the pack. Depth of the snowpack is related to the snow water equivalent by the density of the pack. Since the insulating properties of the pack are highly dependent on its depth and density, the VIC model simulates the development of the snowpack by allowing it to be compressed by the weight of new falling snow [*Anderson and Crawford*, 1964]:

$$\Delta z_{snow} = \frac{P z_{snow}}{SWE}\left(\frac{z_{snow}}{10}\right)^{0.35}, \tag{17}$$

where Δz_{snow} is the change in depth (mm), P is the water equivalent of new snow (mm), z_{snow} is the depth of the present snowpack (mm), and SWE is the snow water equivalent (mm). The density of new snow is assumed to be 50 kg m^{-3}, unless the air temperature is above 0°C in which case the snow density increases as a function of temperature [*Anderson and Crawford*, 1964]. The version of the snow model used here does not simulate the densification of the snowpack with age, which may result in the overprediction of spring snowpack depths.

3. Model Testing Strategy

The model was tested in two stages: at a single well-instrumented location as a point model and over two subcatchments within the upper Mississippi River basin. Point model tests allowed for direct comparison between the model-simulated frozen soils and the actual measurements of frozen soil characteristics. The spatial tests, conducted on basins of 42,000 and 69,000 km^2, evaluated the ability of the model to simulate the runoff response of moderate-sized catchments and the sensitivity of that response to frozen soils.

3.1. Point Simulations

The University of Minnesota Rosemount Experimental Station is located approximately 30 km south of St. Paul (44° 42' N, 93° 32' W, 290 m elevation). Detailed measurements of a soil water and temperature profile, as well as extensive atmospheric forcing data, have been collected for several years in the middle of a relatively flat, cultivated 17 ha field. Data used for this test were provided by J. Baker, E. Spaans, and B. Breiter of the University of Minnesota and include daily and hourly precipitation, as well as hourly air temperature, wind speed, incoming solar, and longwave radiation. The model was tested using hourly point data (effectively representing the single point as a model grid cell) starting in December 1994 and running through spring 1996.

3.1.1. Model parameters. Soil parameters were estimated from several soil surveys conducted at the measurement site and at nearby fields. During the winter it was assumed that the field was bare, neglecting the effects of tillage and residue. However, to predict the antecedent soil moisture conditions correctly for the second winter, summer vegetation cover, corn in this case, was needed. The growth and harvest cycle was simulated by allowing the vegetation height to increase each month starting in April, until a maximum height was reached in August. Harvest (the removal of vegetation) was assumed to take place in October. The leaf area index (LAI) was also allowed to increase monthly

from April to August and then decrease slightly in the fall as the crop dried out before harvest.

Snow depth was measured in the field using a circle of snow sticks. The number of snow sticks used in the circle varied each winter, and none were located above the soil profile site. For comparison with the model, the mean depth and standard deviation for all snow sticks were computed for each day that measurements were collected.

3.1.2. Point results. Figures 3 and 4 compare simulated surface temperature, snow depth, frost depth, and soil moisture content with measurements taken at the Rosemount field site for the winters of 1994-1995 and 1995-1996. Soil moisture comparisons were made for two layers, the top 10 cm and the next 90 cm, for a total depth of 1 m. Surface temperature comparisons were made at a depth of 2.5 cm, which is the shallowest depth at which soil temperature was measured. Simulated snow is compared against the mean snow stick depths (circles). The error bars indicate snow depths of the mean plus and minus one standard deviation. Smaller error bars indicate a more uniform snow cover, so error bars typically grow wider as melt and drifting redistribute the observed snowpack.

Predicted and observed surface temperatures are for the most part in good agreement. The largest differences (midwinter in 1994-1995 and late winter 1996) were due primarily to differences between observed and simulated snow depth. These errors occur in part because the model does not simulate drifting or aging of the snowpack, both of which do influence the actual depth. When the predicted snow pack is thicker than observed, it provides the soil surface with more insulation. Therefore during early February 1995 and late January to early February 1996 the measured surface temperature dropped considerably, while the simulated temperature remained fairly constant. In both cases the simulated snowpack was deeper than the mean observed depth plus one standard deviation, placing it with the deepest of the observed snow depths. The reverse situation occurs from late February to early March 1996, when the simulated snowpack was thinner than observed, and the model surface temperature was well below the observations.

Differences in surface temperature generally correspond to differences in freezing front penetration. Colder simulated surface temperatures drove the frost depth deeper than observations early in the winter of 1995-1996. Both simulated winters missed the extension of the freezing front in January-February, because of the insulating effect of the thicker snowpack. However, by the end of winter, both simulated freezing fronts reached the observed depth, indicating that the model was able to simulate premelt conditions in the spring despite the differences observed during the winter.

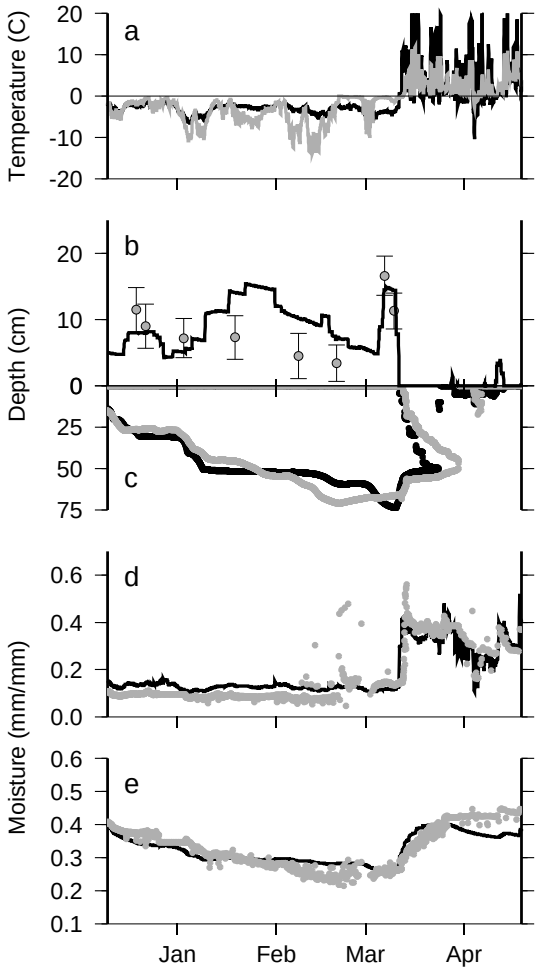

Figure 3. Point simulation (black) versus observations (gray) at the Rosemount Experiment Station during the winter of 1994-1995 for (a) soil surface temperature, (b) simulated snow depth versus mean and standard deviation of observations, (c) freezing and thawing front depths, (d) unfrozen soil moisture content for 0-10 cm depth, and (e) unfrozen soil moisture content for 10-90 cm depth.

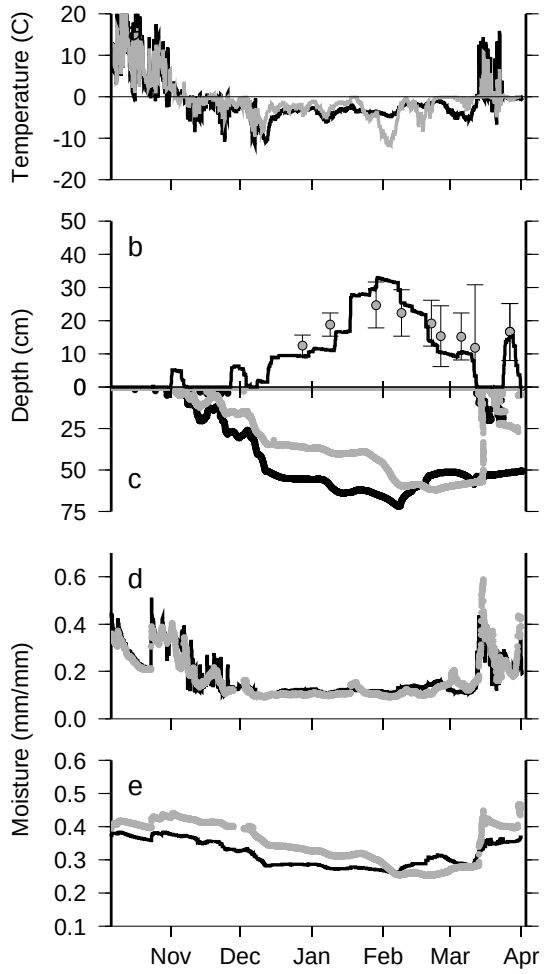

Figure 4. Point simulation (black) versus observations (gray) at the Rosemount Experiment Station for the winter of 1995-1996.

Soil moisture comparisons are for unfrozen soil moisture only, because no measurements of ice content were available. These comparisons show that the model does quite well in matching the observed soil moisture content in its top two layers. Soil moisture predictions immediately following spring thaw are also quite similar to observations, which suggests that modeled ice contents are reasonably accurate. Differences in soil moisture are most noticeable during and just after the thawing of the soil column. This is primarily due to the differences in freezing front depth and therefore the ratio of ice to liquid water.

Thawing of the soil column occurred about five days early in the model relative to the observations in the spring of 1995 (Figure 3). Spring of 1996 had a much greater difference between the observed and the predicted thaw. The observed thaw occurred in about a day, while the modeled thaw started as a partial thaw from the surface but then completely refroze before a mid-March snowfall. Observations made at Rosemount during spring melt indicate that melt occurred first from the high points in the field, with meltwater ponding in the low spots. Ponded water can remain trapped by underlying frozen soil for many days before suddenly draining through a thawed gap. Draining water rapidly thaws frozen soils surrounding the initial drainage pathway and could be the reason for the rapid thaw observed in the data record from 1996. Meltwaters may also travel horizontally within the soil to vertical cracks in the ice, causing rapid melt in the area immediately surrounding the flow. Because VIC is not designed to reproduce such small-scale phenomena, it does not simulate either the ponding of water on the field or the horizontal flow of meltwater.

3.2. Spatial Simulations

Spatial model tests were conducted on two subcatchments within the upper Mississippi River basin. The upper Mississippi, defined as the Mississippi River above its confluence with the Missouri River, has a drainage area of 444,000 km^2. The two subcatchments, the Minnesota River (42,000 km^2) and the Illinois River (69,000 km^2), are moderately sized basins located in the northwest and southeast, respectively, of the upper Mississippi basin. Basin size is an important consideration since the effects of frozen soil on streamflow are expected to decrease with increasing basin size, due to the attenuating effects of river routing [*Garbrecht*, 1991]. Figure 5 shows the derived routing network for the upper Mississippi along with the location of the two smaller catchments.

3.2.1. Model parameters. Atmospheric forcing data were taken from National Climate Data Center (NCDC) daily precipitation and hourly surface airways stations. Precipitation, air temperature, relative humidity, wind speed, pressure, and cloud cover fraction were used to force the model at an hourly time step from 1980 to 1993. Calibration runs were made using the first half of the period (1980-1986). The first year of the calibration period was used for model spin-up and was not included in the model analysis.

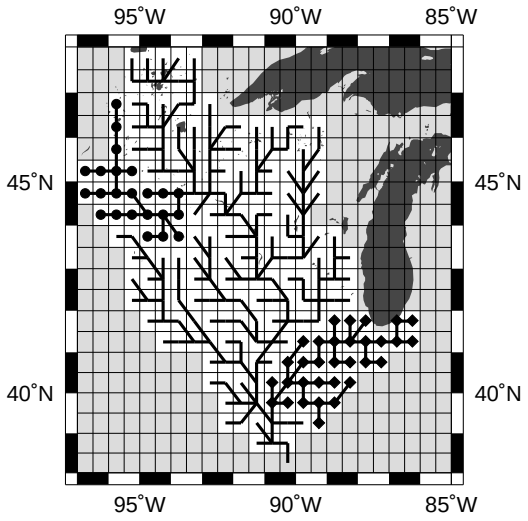

Figure 5. Routing network for the upper Mississippi River basin at 1/2° by 1/2° resolution. Subbasins shown are the Minnesota River (circles), and the Illinois River (diamonds).

Model soil parameters were extracted from the conterminous U. S. multilayer soil characteristics data set (CONUS-soil) [*Miller and White*, 1998], which is maintained by the Earth System Science Center (ESSC) at Pennsylvania State University. This database contains soil information from the State Soil Geographic (STATSGO) database, which have been filtered and checked before being assembled into a single map of parameters for the lower 48 states. Percent sand, silt, and clay, bulk density, and texture information were processed within ARC/INFO to produce 1/2° by 1/2° grids of necessary soil parameters. These parameters were output in the form of ASCII ARC/INFO grid file, and read directly into the VIC model.

Vegetation coverage classifications were obtained from a grid of BATS (Biosphere-Atmosphere Transfer Scheme) classifications for North America also obtained from the ESSC. To reduce the computation time, the 14 classes used by the BATS model were reduced to five: evergreens, deciduous trees, grasslands, agricultural fields, and bare soil.

3.2.2. Model calibration. The VIC model was calibrated by adjusting the following parameters: the thickness of the second and third layers, the value of the infiltration parameter b_i, the baseflow parameters W_s and D_s, and the aerodynamic and stomatal resistances of the vegetation coverage. These parameters affect the energy balance indirectly through changes in evaporation and do not directly impact the snow and frozen soil algorithms. Other parameters, such as hydraulic conductivity and pore-size distribution, were estimated directly from measured soil properties and were not changed during calibration.

Calibration was achieved by comparing simulated to observed daily discharge for the calibration period. Efforts were made first to match the peak flows and then to match the total flow volume for the calibration period. Model performance in the summer months is similar with and without the frozen soil model; therefore calibration focused on matching winter and spring discharge peaks. Most of the calibration was conducted without the frozen soil algorithm, since it required less simulation time; however, the frozen soil algorithm was turned on periodically to evaluate winter streamflow simulations with the current set of calibration parameters. A discussion of the sensitivity of the model to the parameters b_i, W_s, and D_s can be found in the paper by *Liang et al.* [1994]. Layer depths were adjusted primarily to provide the soil moisture storage capacity needed to maintain the proper ratio between annual runoff and evaporation. The thickness of the upper layer also impacts infiltration while that of the lower layer affects baseflow response, so some independent adjustments of the upper and lower zone moisture capacities were performed as well.

3.2.3. Spatial model results. Figures 6 and 7 compare simulated versus observed daily discharge for the calibration period of 1981-1986 from the Illinois and Minnesota Rivers. Figures 6a and 6b and 7a and 7b show model results with and without the frozen soil model activated. When run without the frozen soil algorithm, the model used the original soil thermal flux equations and did not compute ice content, or frozen layers. Both simulations used the new snow model and the same calibration parameters.

Visual inspection of the discharge plots shows that spring runoff peaks from the model with frozen soil (Figures 6a and 7a) are typically higher than those from the model without frozen soil (Figures 6b and 7b). To facilitate interpretation of the simulation errors, the percent difference between simulated flows was computed as

$$PD = \frac{\left(Q_f^i - Q_{uf}^i\right)}{Q_{uf}^t} 100\% \qquad (18)$$

where Q_f and Q_{uf} are simulated discharge, for the ith day, for the model with and without the frozen soil al-

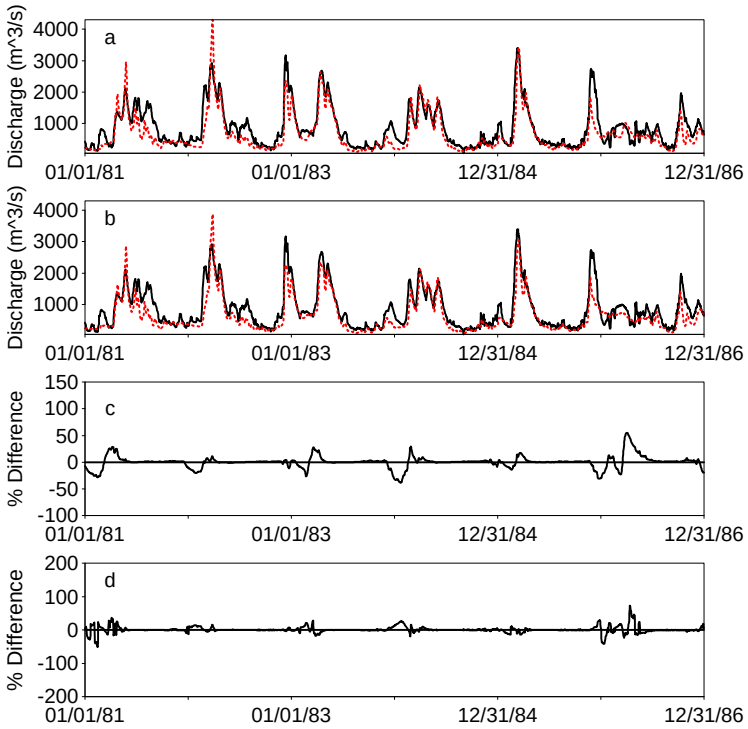

Figure 6. Comparison of simulated (dashed) and observed (solid) flow for the Illinois River during the calibration period of 1981-1986. (a) Simulated discharge with the frozen soil algorithm versus observed discharge. (b) Simulated discharge without the frozen soil algorithm versus observed discharge. (c) Percent differences between simulated discharges (frozen soil-without frozen soil). (d) Percent differences between the absolute errors (simulated - observed) of the simulations with and without frozen soil.

gorithm, respectively. Results from this computation are plotted in Figures 6c and 7c. Both plots display negative differences (lower flows with the frozen soil algorithm) through the winter followed by positive differences during the spring. When the soil freezes, a portion of the soil moisture is converted to ice. The ice is unable to drain through the soil, so it is stored through the winter. Without the frozen soil algorithm, VIC allows the unfrozen soil moisture to drain causing higher winter baseflow. The positive spring percent differences are caused by a combination of two processes: snowmelt being forced to leave the basin as runoff when it cannot infiltrate into the frozen soil and the release of stored soil moisture when the ice in the soil melts.

Average basin parameters, based on the simulations using the frozen soil algorithm, are shown in Table 1. It is apparent from the table that the Illinois River, which is farther south and has a higher mean annual air temperature, experiences fewer snow-covered days and thinner snowpacks than the Minnesota River. The Illinois also has fewer days of frozen soil and shallower maximum frost depths. This implies that the Illinois River simulation should be less sensitive to representation of frozen ground and other cold season processes than the Minnesota River simulation. This is in fact the case as shown by the comparison of Figures 6c and 7c.

Simulations for the postcalibration period 1987-1993 are shown in Figures 8 and 9. As in the calibration period, the frozen soil algorithm produces less winter baseflow and higher spring peak flows. The effect of the frozen soil algorithm in the Minnesota basin is also

10

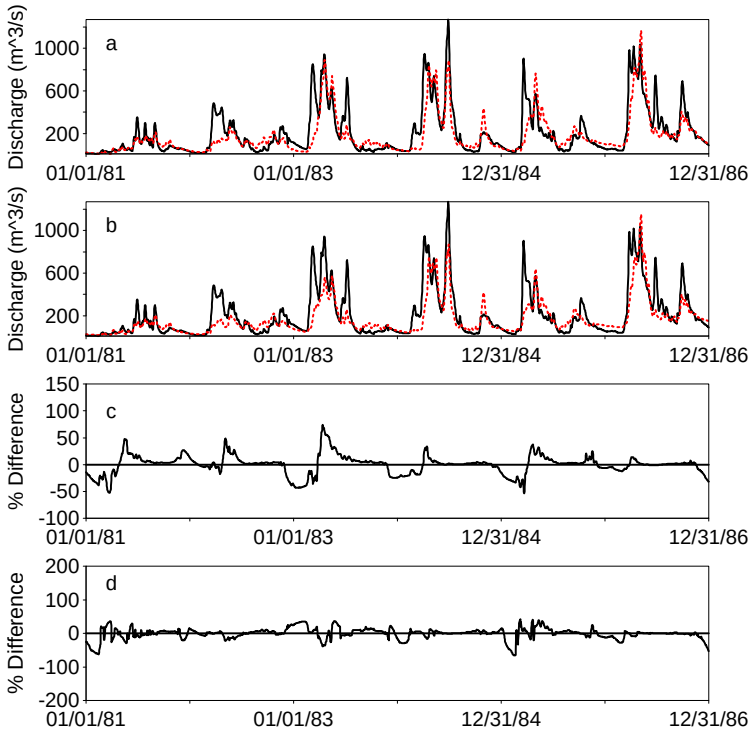

Figure 7. Comparison of simulated (dashed) and observed (solid) flow for the Minnesota River during the calibration period of 1981-1986.

Table 1. Summary Climate and Hydrologic Statistics for the Illinois and Minnesota River Basins, 1981-1993

	Illinois River	Minnesota River
Mean annual air temperature	10.6°C	6.9°C
Mean annual snow depth	2.1 cm	5.2 cm
Average maximum snow depth	20.5 cm	28.1 cm
Mean annual days of snow cover	121	159
Mean annual frost depth	5.8 cm	20.7 cm
Average maximum frost depth	31.9 cm	65.2 cm
Mean annual days of frozen ground	141	192

greater than for the Illinois basin in this period, although the flood in 1992 dominates the discharge plot.

One measure of model accuracy is the Nash-Sutcliffe R^2 coefficient [*Leaf et al.*, 1993],

$$R^2 = 1 - \frac{\sum \left(Q^i_{ob} - Q^i\right)^2}{\left(Q^i_{ob} - Q^i_m\right)^2} \tag{19}$$

where Q_{ob} and Q are the observed and simulated discharge for the ith day, respectively, and Q_m is the mean observed discharge. The R^2 values in Table 2 for the simulations described above are quite similar for the model with and without the frozen soil algorithm. It should be noted that the calculated R^2 value is highly sensitive to the overestimation of peaks. Therefore while the volume of the spring peaks is generally better represented with the frozen soil model, the decrease in R^2 is due primarily to overestimation of the peak flow event.

To further analyze the model simulations, plots were prepared of the percent difference between the absolute errors in the simulated flows:

$$PD_{abs} = \left[abs\left(\frac{Q^i_f - Q^i_{ob}}{Q^i_{ob}}\right) - abs\left(\frac{Q^i_{uf} - Q^i_{ob}}{Q^i_{ob}}\right)\right] 100. \tag{20}$$

Negative differences indicate times when the simulation with frozen soil is closer to observations than the unfrozen simulation. Figures 6d and 7d show the differences for the calibration period discharge in the Illinois and Minnesota River basins, respectively, while Figures 8d and 9d are for the same basins after the calibration

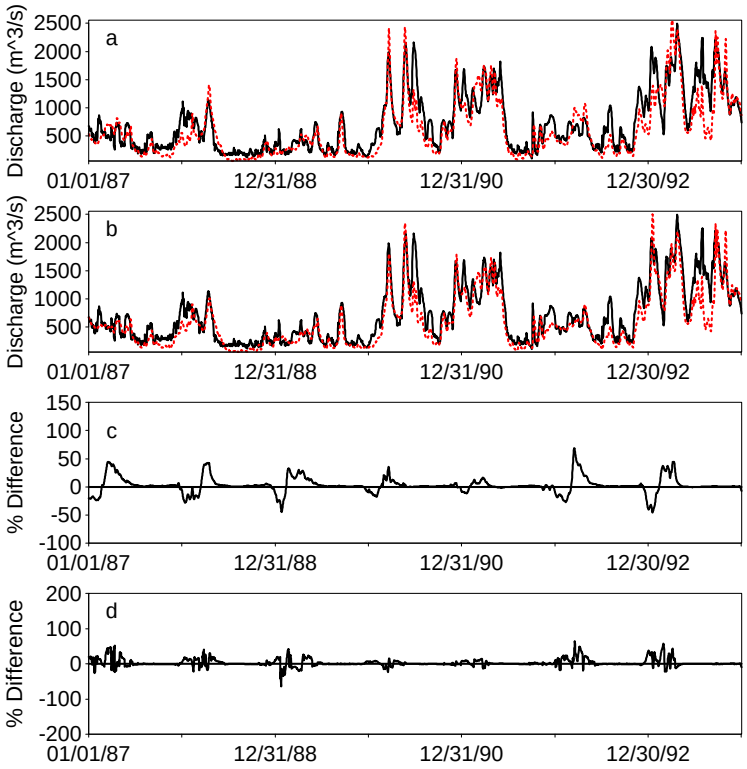

Figure 8. Comparison of simulated (dashed) and observed (solid) flow for the Illinois River during the period of 1987-1993.

Table 2. Tabulated Nash-Sutcliffe R2 Values for the Illinois and Minnesota Rivers

	Illinois River	Minnesota River
Calibration period (1981-1985)		
VIC with frozen soils	0.708	0.635
VIC without frozen soils	0.724	0.624
Post calibration period (1986-1993)		
VIC with frozen soils	0.712	0.739
VIC without frozen soils	0.760	0.722

VIC, variable infiltration capacity hydrologic model.

period. During the summer months the differences are negligible for both basins. The Illinois basin does not show any particularly strong changes, but the sum of the absolute errors is positive (17.60 and 75.30 for the two simulation periods), indicating that on the whole the unfrozen soil model does better. The Minnesota River shows much larger differences, especially in the winter, where the frozen soil model improves overall performance. Sums of the absolute errors for the Minnesota basin (-15.39 and -135.94) show that the frozen soil model does improve the simulation. Improvements are largest in 1987-1990, when the Minnesota River had very low flows. Without the frozen soil algorithm, the model produced too much baseflow through the winter, while with the algorithm, it stored the moisture as ice, decreasing the baseflow. This effect can also be seen in years with more flow, including the winters of 1992 and 1985.

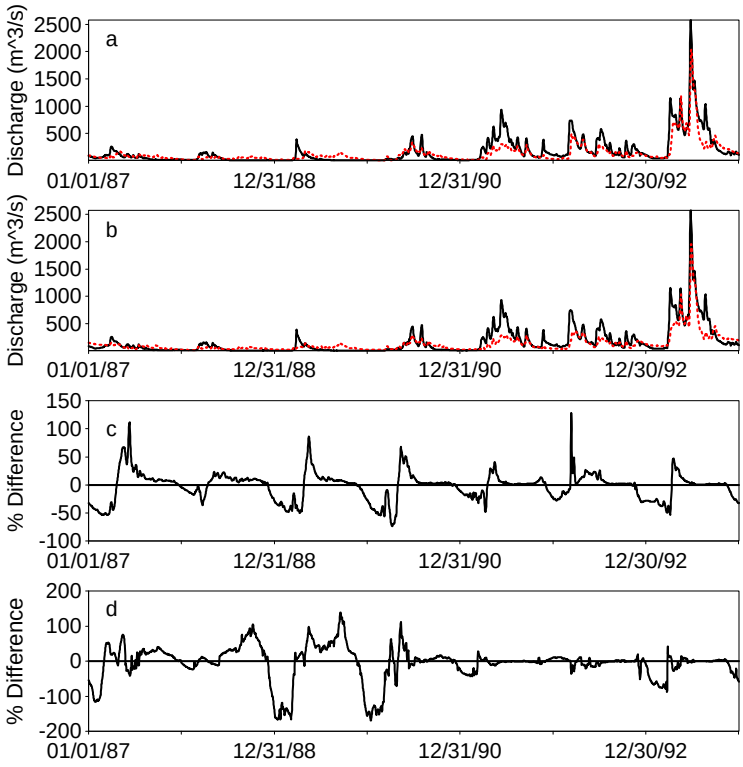

Figure 9. Comparison of simulated (dashed) and observed (solid) flow for the Minnesota River during the period of 1987-1993.

One further measure of model performance is the deviation of seasonal runoff volumes [*Leaf et al.*, 1993]:

$$D_v(\%) = \frac{V_{ob} - V}{V_{ob}} 100 \tag{21}$$

where V_{ob} is the volume of observed discharge, and V is the volume of the simulated discharge. Seasonal deviations for the entire period of model simulations (1981-1993) are shown in Table 3. The deviation differences are computed by subtracting the absolute value of the deviation of the model without frozen soils from the deviation of the simulation with frozen soil. When the deviation difference is negative, it indicates that the model with frozen soil has a smaller deviation from the observed flow volume. The seasonal mean deviations show that the frozen soil algorithm improves simulations of the Illinois River during the winter and spring and the Minnesota River in the fall and winter. Median deviation difference values were included in Table 3 to show the differences between the simulations without the bias of the large floods; since both simulations underpredict these large events for the Minnesota River, the median values may be a fairer comparison. The median differences indicate that the frozen soil algorithm improves the Illinois River simulations during the winter and the Minnesota River simulations during the spring. Since the Illinois basin is farther south, it tends to experience more midwinter melt events when the frozen soil model would have the most impact. It also tends to have less snow cover, which melts earlier in the spring, so there are fewer spring events where frozen soil plays a significant role. The Minnesota basin retains more snow through the winter, so that frozen soil plays more of a role during spring melt events.

Figures 10, 11, and 12 show average simulated snow depth, frost depth, and discharge for the Illinois and Minnesota Rivers during the winters of 1983-1984, 1988-1989, and 1992-1993. The Illinois River simulations

Table 3. Seasonal Discharge and Deviation Statistics for the Illinois and Minnesota Rivers

	Fall	Winter	Spring	Summer
Illinois River				
Mean observed flow ($1e^9$ m^3)	4.222	7.652	5.261	2.628
Mean deviation - frozen soil (%)	29.90	2.06	15.68	34.09
Mean deviation - no frozen soil (%)	24.67	12.42	18.31	34.94
Mean deviation differences (%)	5.23	-4.60	-1.08	-0.84
Median deviation differences (%)	4.63	-5.75	-0.16	-0.89
Minnesota River				
Mean observed flow ($1e^9$ m^3)	0.601	1.742	2.425	1.020
Mean deviation - frozen soil (%)	-61.63	38.46	-2.93	-155.50
Mean deviation - no frozen soil (%)	-77.72	28.80	12.48	-140.31
Mean deviation differences (%)	-10.11	-2.05	0.50	14.33
Median deviation differences (%)	0.78	-0.11	-4.53	4.09

show snow cover depths of 10 to 30 cm (Figures 10a, 11a, and 12a) and frost depths of 20 to 40 cm (Figures 10c, 11c and 12c). Frost depth is shallowest during the winter of 1983-1984, which also had the deepest and most consistent snowpack. The winters of 1988-1989 and 1992-1993 had thin snow covers that experienced melt throughout the winter, resulting in less insulation of the ground surface. Figures 10e, 11e, and 12e show that both model versions produce nearly the same discharge each year prior to the soil freezing. When freezing began, the model with the frozen soil algorithm produced less baseflow. In both Figures 11e and 12e, when the snow melted completely in midwinter, the soil began to thaw from the surface, and baseflow response increased shortly thereafter as the newly thawed water drained through the soil. All three figures show an increase in peak flow after the final thaw as the frozen soil moisture is released. Only Figure 10e shows an increase in peak flow directly related to snowmelt, since a relatively deep snowpack is retained throughout this winter.

The Minnesota River basin has deeper average snow covers than the Illinois River basin. Figures 10b, 11b, and 12b show snowpack depths from 10 to 40 cm. Because of the colder average temperatures, the frost depths are also deeper than in the Illinois basin, with Figures 10d, 11d, and 12d illustrating depths of 20 to 90 cm. The winter of 1988-1989 had the thinnest and most variable snow coverage (Figure 11b) and therefore the deepest penetration of frost. However, because there was almost no snow cover, basin discharge was influenced primarily by the release of ice from the soil, so the frozen soil model predicts a late increase in peak flow. Figures 10b and 12b have maximum snow depths of around 40 and 30 cm, respectively, but the winter of 1992-1993 (Figure 12) had a slower buildup of the snowpack and a related increase in frost penetration. This in turn caused more runoff, so that Figure 12f shows a faster and larger response to the melting snow than in 1983-1984 despite the smaller snowpack.

4. Conclusions

A physically based frozen soil algorithm was developed to represent the effects of frozen soil in a macroscale hydrologic model. Point model simulations compared with observations at the Rosemount, Minnesota, field site show that the frozen soil algorithm is able to predict observed freezing front penetrations, unfrozen soil moisture, and snow cover thickness reasonably well. Differences in the predicted surface temperature through the winter result in differences in the predicted freezing front depth, but by spring melt, the simulated and observed freezing fronts are in good agreement.

Spatial tests showed that the frozen soil algorithm affects model streamflow predictions in cold regions by increasing soil moisture stored through the winter and increasing spring peak flow events. The differences between the model with and without the frozen soil algorithm were apparent in test applications to the Illinois and Minnesota River basins, both of which are tributaries to the upper Mississippi River. Because of its colder climate the Minnesota River simulations show deeper frost depths and thus more of an impact with the frozen soil algorithm than those for the Illinois River simulations. Because of the coarseness of the calibration for these initial test runs it is harder to determine whether the frozen soil algorithm truly improves the simulation of the macroscale hydrologic cycle. The

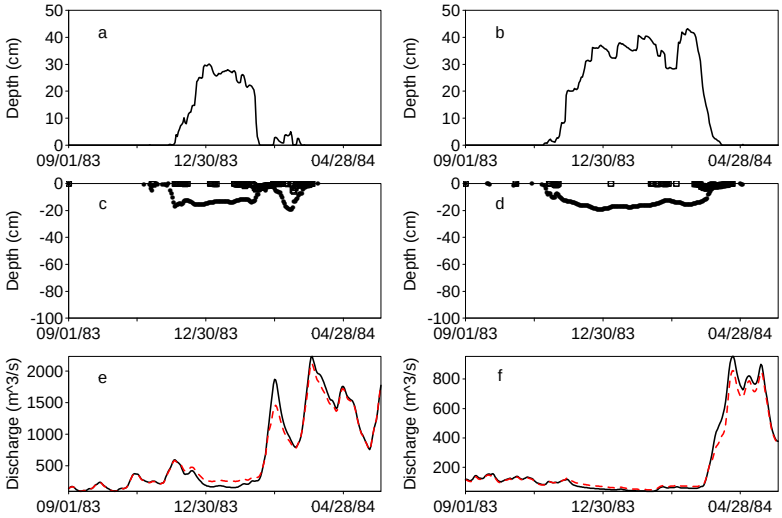

Figure 10. Comparison of simulations with and without the frozen soil algorithm for the winter of 1983-1984. Average simulated snow depth for the (a) Illinois and (b) Minnesota River basins. Average simulated freezing front (dots) and thawing front (squares) depths for the (c) Illinois and (d) Minnesota River basins. Simulated discharge with frozen soils (solid) and without (dashed) for the (e) Illinois and (f) Minnesota River basins.

Minnesota River showed slightly better Nash-Sutcliffe R2 values with the frozen soil algorithm than without, but the opposite was true for the Illinois River. This is partly due to the fact that the Illinois simulations tended to overpredict peak flows, while the Minnesota River peaks tended to be underpredicted. In general, inclusion of the frozen soil algorithm increases peak flows during spring melt, and therefore the Minnesota River simulations improved, while the Illinois River simulations became worse. Median seasonal flow volumes showed improvements for both rivers during the winter and spring, but effects on the mean values were less clear.

The simulations conducted for this paper show that the sensitivity of streamflow predictions to inclusion of the frozen soil algorithm is qualitatively as expected. Further work is needed to determine the sensitivity of the model to the parameters used in the calibration, as well as those derived from the soil database. Once sensitivities have been established the model parameters can be optimized with and without the frozen soil algorithm, which will allow a better understanding of the interactions of the algorithm with runoff production. Future improvements to the frozen soil algorithm, which are under investigation, include the addition of a no-thermal flux bottom boundary and the representation of the subgrid spatial variability of frozen soil. Work has also begun on a lakes and wetlands algorithm, which should improve the simulated results from the northern part of the upper Mississippi watershed (including the Minnesota watershed) where numerous small lakes affect the hydrologic cycle.

Acknowledgments. This is contribution 662 from the Joint Institute for Study of the Atmosphere and Ocean, funded under NOAA Cooperative Agreement NA67RJ0155. John Baker, Egbert Spaans, and Bill Breiter of the University of Minnesota provided the Rosemount Experiment Station data used for the point tests.

References

Abdulla, F. A., D. P. Lettenmaier, E. F. Wood, and J. A. Smith, Application of a macroscale hydrologic model to estimate the water balance of the Arkansas-Red River basin, *J. Geophys. Res.*, *101*, 7449–7459, 1996.

Anderson, E. A., and N. H. Crawford, The systhesis of continuous snowmelt runoff hydrographs on a digital computer, Ph.d., Stanford University, 1964.

Farouki, O. T., *Thermal Properties of Soils*, vol. 11 of *Series on Rock and Soil Mechanics*, Trans Tech Publications, Clausthal-Zellerfeld, Germany, 1986.

Flerchinger, G. N., and K. E. Saxton, Simultaneous heat and water model of a freezing snow-residue-soil system I.

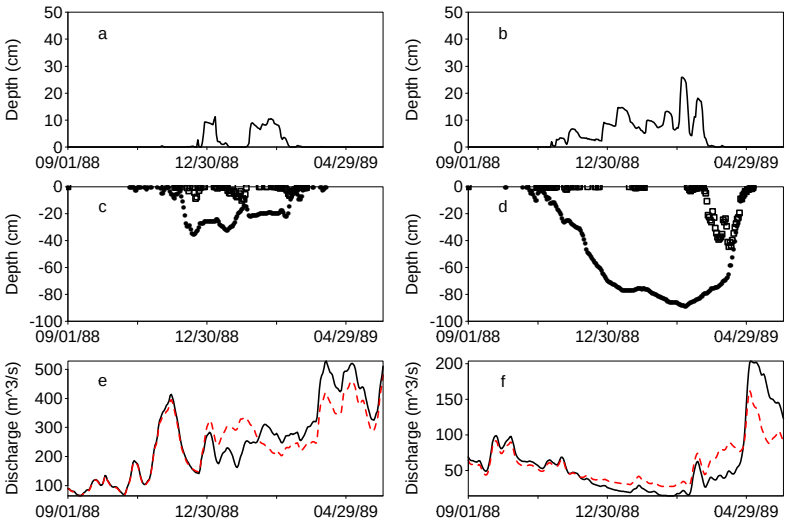

Figure 11. Comparison of simulations with and without the frozen soil algorithm for the winter of 1988-1989.

theory and development, *Trans. A. S. A. E.*, *32*, 565–71, 1989a.

Flerchinger, G. N., and K. E. Saxton, Simultaneous heat and water model of a freezing snow-residue-soil system II. field verification, *Trans. A. S. A. E.*, *32*, 573–8, 1989b.

Fox, J. D., Incorporating freeze-thaw calculations into a water balance model, *Water Resour. Res*, *28*, 2229–2244, 1992.

Garbrecht, J., Effects of spatial accumulation of runoff on watershed response, *J. Environ. Qual.*, *120*, 31–35, 1991.

Gel'fan, A. N., Comparison of two methods of calculating soil freezing depth, *Sov. Meteorol. Hydrol.*, *2*, 78–83, 1989.

Johansen, O., Thermal conductivity of soils, Ph.d., CRREL Draft Trans. 637., Trondheim, Norway, 1975.

Koren, V., J. Schaake, K. Mitchell, Q.-Y. Duan, F. Chen, and J. M. Baker, A parameterization of snowpack and frozen ground intended for NCEP weather and climate models, *J. Geophys. Res.*, *104*, 19,569–19,586, 1999.

Koren, V. I., Modeling of processes of river runoff formation in the forest zone of the european USSR, *Meteorologiya*, *10*, 78–85, 1980.

Leaf, C., T. Engman, E. B. Jones, A. Rango, T. J. Ward, and S. V. Vactor, Criteria for evaluation of watershed models, *J. Irrig. Drain. Eng.*, *119*, 429–42, 1993.

Liang, X., D. P. Lettenmaier, E. F. Wood, and S. J. Burges, A simple hydrologically based model of land surface water and energy fluxes for general circulation models, *J. Geophys. Res.*, *99*, 14,415–28, 1994.

Liang, X., E. F. Wood, and D. P. Lettenmaier, Surface soil moisture parameterization of the VIC-2L model: evaluation and modification, *Global and Planetary Change*, *13*, 195–206, 1996.

Liang, X., E. F. Wood, and D. P. Lettenmaier, Modeling ground heat flux in land surface parameterization schemes, *J. Geophys. Res.*, *104*, 9581–9600, 1999.

Lohmann, D., E. Raschke, B. Nijssen, and D. P. Lettenmaier, Regional scale hydrology; I, formulation of the VIC-2L model coupled to a routing model, *Hydrological Sciences Journal*, *43*, 131–141, 1998a.

Lohmann, D., E. Raschke, B. Nijssen, and D. P. Lettenmaier, Regional scale hydrology; II, application of the VIC-2L model to the weser river, germany, *Hydrological Sciences Journal*, *43*, 143–158, 1998b.

Miller, D. A., and R. A. White, A conterminous United States multilayer soil characteristics dataset for regional climate and hydrology modeling, *Earth Inter.*, *2*, 1998.

Nijssen, B., D. P. Lettenmaier, X. Liang, S. W. Wetzel, and E. F. Wood, Streamflow simulation for continental-scale river basins, *Water Resour. Res.*, *33*, 711–24, 1997.

Schnur, R., and D. P. Lettenmaier, A global gridded data set of soil moisture, in *13th Conference on Hydrology*, AMS, Long Beach, CA, 1997.

Storck, P., and D. P. Lettenmaier, Predicting the effect of a forest canopy on ground snow accumulation and ablation in maritime climates, in *67th Western Snow Conference*, edited by C. Troendle, Colorado State University, 1999.

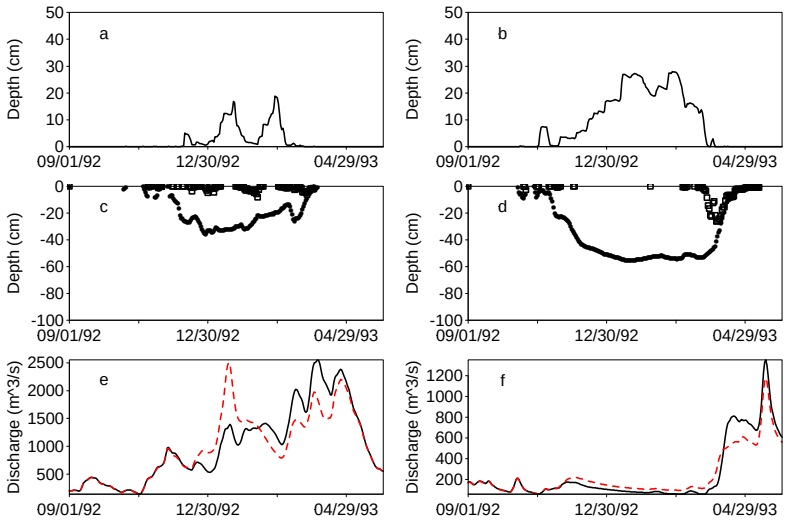

Figure 12. Comparison of simulations with and without the frozen soil algorithm for the winter of 1992-1993.

K. A. Cherkauer and D. P. Lettenmaier, Department of Civil and Environmental Engineering, Box 352700, University of Washington, Seattle, WA 98195-2700. (cherkaue@u.washington.edu)

Received October 2, 1998; revised May 6, 1999; accepted May 17, 1999.

This preprint was prepared with AGU's LaTeX macros v5.01, with the extension package 'AGU++' by P. W. Daly, version 1.6a from 1999/05/21.